SURFACE ROUGHNESS AND TRIP EFFECTS FOR A CIRCULAR CYLINDER AT SUBCRITICAL REYNOLDS NUMBERS

VIDUSHAN RAJAVAROTHAYAM

A THESIS SUBMITTED TO THE FACULTY OF GRADUATE STUDIES
IN PARTIAL FULFILMENT OF THE REQUIREMENTS
FOR THE DEGREE OF
MASTERS OF APPLIED SCIENCE

GRADUATE PROGRAM IN MECHANICAL ENGINEERING
YORK UNIVERSITY
TORONTO, ONTARIO

APRIL 2023

© Vidushan Rajavarothayam, 2023

Abstract

Aerodynamic drag is the major source of resistance experienced by athletes in activities such as road cycling. Over bluff bodies, which is how an athlete is typically modelled, passive flow control methods such as surface roughness and boundary layer tripwires appeared to be particularly relevant in transitioning the local boundary layer at the surfaces to turbulence, resulting in a lower drag at smaller Reynolds numbers. In the experimental study, a cylindrical model equipped with textiles and tripwires that had 2D and zigzag geometries were connected to a custom force balance to understand the effects of these surface modifications on the drag. Fabrics with varied seam positions achieved a maximum drag reduction of 40% relative to a smooth cylinder. Tripwires achieved a maximum drag reduction of 20% relative to a smooth cylinder. It was also found that a combination of fabric seams and tripwires that are placed symmetrically from the stagnation point had a similar flow behaviour to a single tripwire when the thickness of the fabric seam and tripwire are the same regardless of roughness. Moreover, utilizing these flow control methods can provide potential time gains for a cyclist.

Acknowledgements

First of all, I would like to acknowledge my supervisors, Dr. Ronald Hanson and Dr. Philippe Lavoie for giving me the opportunity to pursue my graduate studies at York University in the field of cycling aerodynamics. Their constant support and guidance during meetings helped me to grow as a stronger researcher. I would also like to thank Dr. Vahid Nasr Esfahani for his role as a supportive mentor during my experimental campaign at the University of Toronto Institute for Aerospace Studies (UTIAS) in the Flow Control Experimental Turbulence (FCET) laboratory. They have served as role models during my graduate studies in inspiring me to achieve excellence throughout my career. I would like to express my gratitude to my masters supervisory committee members, Dr. Paul O'Brien and Dr. Dan Palermo for their insights and suggestions to help improve this thesis.

I would also like to thank Kevin Quan Studios for funding the research project and my lab members. My lab members at the Fluid Mechanics and Flow Control (FMFC) lab at York University and FCET lab provided a friendly and encouraging environment to work in. Last but not least, I would like to thank my parents and family for their immense support throughout my academic journey.

Contents

Abstract ii

Acknowledgements iii

Table of Contents iv

List of Tables vii

List of Figures ix

1 Introduction 1

1.1 Motivation and Research Objectives 1

1.2 Modelling the Flow over a Cylinder 2

2 Literature Review 4

2.1 Overview 4

2.2 Flow over a Smooth Circular Cylinder 4

2.3 Flow over a Roughened Cylinder 7

2.3.1 Effect of Different Roughness Methods 7

2.3.2 Effect of Rib Spacings and Rib Heights 11

2.4 Flow over a Tripped Cylinder 13

2.4.1 Flow over a Cylinder with a Single Tripwire 13

2.4.2 Flow over a Cylinder with One and Two Tripwires 14

2.4.3 Effect of Angular Positions of Tripwires 16
2.4.4 Determining Thickness of Tripwires 18
2.4.5 Spatial Wavelengths and Spike Angle of Zigzag Tripwires 21

3 Experimental Setup and Data Acquisition Methods 24
3.1 Experimental Setup 24
3.2 Scanning Roughness Heights of Fabrics 31
3.3 Velocity Measurements 31
3.4 Strouhal Number Measurements 32
3.5 Drag Force Measurements Using Load Cells 32

4 Results and Discussion 34
4.1 Overview 34
4.2 Benchmarking Experimental Setup 35
4.3 Effects of Fabric Roughness and Seams 36
4.3.1 Effects of Fabric Patterns and Roughness 36
4.3.2 Effect of Seam Locations for Fabrics with Multiple Seams 40
4.4 Effect of a Single Spanwise Tripwire 63
4.4.1 Thickness Comparison for 2D Tripwires 64
4.4.2 Thickness Comparison for Zigzag Tripwires 64
4.4.3 Wavelength Comparison for Zigzag Tripwires 69
4.4.4 Optimal Tripwire Cases 71
4.5 Effect of Single Tripwire on Fabric 77
4.5.1 Single Tripwire on a Smooth Fabric 78
4.5.2 Fabric and Tripwire Combinations for Medium and Rough Fabrics . . 81
4.5.3 Comparison of Fabrics and Tripwires Arranged in a Symmetric Orientation 90
4.6 Potential Time Gains for Cyclists 96

5 Conclusions and Future Work **97**

5.1 Benchmarking Experimental Setup 97

5.2 Effects of Fabric Roughness and Seams 98

5.3 Effects of 2D and Zigzag Tripwires 98

5.4 Effect of Single Tripwire on a Fabric 99

5.5 Recommendations for Future Work 100

6 Appendix **106**

6.1 Uncertainty Analysis of Drag Coefficient 106

List of Tables

4.1 Fabrics with relative roughness ratios between arithmetic average roughness heights and cylinder diameter in ascending order where fabric 7 (F7) has the lowest roughness and fabric 3 (F3) is the roughest. 38

4.2 Average C_D values for the smoothest fabric (F7), roughest fabric (F3) and medium roughness fabric (F5) with one seam placed 50^o from the stagnation point at a range of Reynolds numbers. 61

4.3 Average C_D values for the smoothest fabric (fabric 7), roughest fabric (fabric 3) and medium roughness fabric (fabric 5) with three seams placed 60^o from the stagnation point at a range of Reynolds numbers. 63

4.4 Average C_D values for optimal tripwire cases with 2D and zigzag geometry at a range of Reynolds numbers. 77

4.5 Average C_D values for smoothest fabric (fabric 7), roughest fabric (fabric 3) and fabric with medium roughness (fabric 5) with tripwires arranged in a symmetric orientation at a range of Reynolds numbers when placed 30^o from the stagnation point. 92

4.6 Average C_D values for smoothest fabric (fabric 7), roughest fabric (fabric 3) and fabric with medium roughness (fabric 5) with tripwires arranged in a symmetric orientation at a range of Reynolds numbers when placed 40^o from the stagnation point. 92

4.7 Average C_D values for smoothest fabric (fabric 7), roughest fabric (fabric 3) and fabric with medium roughness (fabric 5) with tripwires arranged in a symmetric orientation at a range of Reynolds numbers when placed 50^o from the stagnation point. 93
4.8 Average C_D values for smoothest fabric (fabric 7), roughest fabric (fabric 3) and fabric with medium roughness (fabric 5) with tripwires arranged in a symmetric orientation at a range of Reynolds numbers when placed 60^o from the stagnation point. 93

List of Figures

1.1 Cylinder representation of a cyclist for 1) forearms, 2) upper arms, 3) lower back and 4) thigh regions. 3

2.1 Variation of the drag coefficient with Reynolds number for a smooth circular cylinder. 6

2.2 Variation of pressure, drag and lift coefficients with Reynolds number for a smooth circular cylinder. 8

2.3 Variation of the drag coefficient with Reynolds number for a roughened cylinder with different relative roughness values where $\triangle$, $k_s/D = 110 \times 10^{-5}$; $\bigcirc$, $k_s/D = 450 \times 10^{-5}$; $\square$, $k_s/D = 900 \times 10^{-5}$. 9

2.4 Relationship between relative roughness and drag coefficient. 10

2.5 Relationship between relative roughness and pressure coefficient. 10

2.6 Variation of drag coefficient and Strouhal number with Reynolds number for textiles with $h/d = 0.067$ and $\triangle/h = 20$ where d is 75 mm. 12

2.7 Two stage drag crisis behaviour for a cylinder mounted with a tripwire that has a wake behaviour state for (a) first drag crisis and (b) second stage drag crisis. 14

2.8 Diagram of (a) one wired and (b) two wired cylinders. 15

2.9 Variation of (a) drag coefficient at given angles from stagnation point for different Reynolds numbers and (b) Strouhal number at given angles from stagnation point at a constant Reynolds number of 6.0×10^4 in a two wired fitted case where the drag crisis occurs from $35^o < \alpha < 40^o$ and the bistable flow occurs from $40^o < \alpha < 45^o$. 17
2.10 Variation of drag coefficient with Reynolds number for a two wired cylinder that has two tripwires of different aspect ratios placed 40.5° from the stagnation point. 18
2.11 Velocity profiles at different angles from the stagnation point for a circular cylinder. 20
2.12 Ratios of boundary layer thickness relative to the cylinder diameter, (δ/D), for various Reynolds numbers and angles from stagnation point. 20
2.13 Spatial wavelengths and spike angle of 60^o for a zigzag tripwire where λ_{SL} is the streamwise wavelength and λ_{ZSL} is the spanwise wavelength. 23
2.14 Vortex formation length for different Reynolds numbers for a circular cylinder. 23

3.1 Free body diagram of the active cylinder model. 26
3.2 CAD model showing the dimensions of the experimental setup inside UTIAS wind tunnel test section. 26
3.3 CAD model of front view of experimental setup where the top aluminum extrusion is removed to show the detail of the top load cell. Half of the dummy cylinders are also removed to show the details of the worm drive clamps and flexible shaft couplings. 27
3.4 CAD model of isometric view of experimental setup. 27
3.5 Experimental setup inside UTIAS closed loop wind tunnel. 28
3.6 Fabric covered on a cylinder inside UTIAS wind tunnel. 29
3.7 Angular variations of fabrics with one, two, three and four seams relative to the incoming flow direction. 30

3.8 Zigzag tripwires that consist of (a) ZZ60K with $\lambda_{Re_D=60k}$ and (b) ZZ80K with $\lambda_{Re_D=80k}$. 30
3.9 Location of constant temperature anemometer (CTA) probe relative to the center of the cylinder inside UTIAS wind tunnel. 32
3.10 Comparison of the averaged dynamic drag measurements with static drag measurements for a smooth cylinder. 33

4.1 Comparison of (a) drag coefficient and (b) Strouhal number at given Reynolds numbers for a smooth cylinder and literature. 36
4.2 Seven tested fabrics in order from smoothest (F7) to roughest (F3) where each image has dimensions of $1\frac{1}{3}$ Inches x $1\frac{5}{8}$ Inches given that the width scale is 1:3 and the length scale is 1:20 relative to the actual fabric. 37
4.3 Roughness profile of fabric 3 along the evaluation length, l_r. 38
4.4 Variation of the drag coefficient with Reynolds number for all seven tested fabrics with one seam placed 180^o from the stagnation point. 40
4.5 Variation of the drag coefficient and Strouhal number at given Reynolds numbers and angular locations of fabric 1 with one seam (a), (b) and two seams (c), (d). 42
4.6 Variation of the drag coefficient and Strouhal number at given Reynolds numbers and angular locations of fabric 1 with three seams (a), (b) and four seams (c), (d). 43
4.7 Variation of the drag coefficient and Strouhal number at given Reynolds numbers and angular locations of fabric 2 with one seam (a), (b) and two seams (c), (d). 44
4.8 Variation of the drag coefficient and Strouhal number at given Reynolds numbers and angular locations of fabric 2 with three seams (a), (b) and four seams (c), (d). 45

4.9 Variation of the drag coefficient and Strouhal number at given Reynolds numbers and angular locations of fabric 3 with one seam (a), (b) and two seams (c), (d). 46
4.10 Variation of the drag coefficient and Strouhal number at given Reynolds numbers and angular locations of fabric 3 with three seams (a), (b) and four seams (c), (d). 47
4.11 Variation of the drag coefficient and Strouhal number at given Reynolds numbers and angular locations of fabric 4 with one seam (a), (b) and two seams (c), (d). 48
4.12 Variation of the drag coefficient and Strouhal number at given Reynolds numbers and angular locations of fabric 4 with three seams (a), (b) and four seams (c), (d). 49
4.13 Variation of the drag coefficient and Strouhal number at given Reynolds numbers and angular locations of fabric 5 with one seam (a), (b) and two seams (c), (d). 50
4.14 Variation of the drag coefficient and Strouhal number at given Reynolds numbers and angular locations of fabric 5 with three seams (a), (b) and four seams (c), (d). 52
4.15 Variation of the drag coefficient and Strouhal number at given Reynolds numbers and angular locations of fabric 6 with one seam (a), (b) and two seams (c), (d). 54
4.16 Variation of the drag coefficient and Strouhal number at given Reynolds numbers and angular locations of fabric 6 with three seams (a), (b) and four seams (c), (d). 55
4.17 Variation of the drag coefficient and Strouhal number at given Reynolds numbers and angular locations of fabric 7 with one seam (a), (b) and two seams (c), (d). 56

4.18 Variation of the drag coefficient and Strouhal number at given Reynolds numbers and angular locations of fabric 7 with three seams (a), (b) and four seams (c), (d). 57
4.19 Variation of the drag coefficient at given Reynolds numbers for all tested fabrics placed 30^o from the stagnation point for (a) one seam, (b) two seams, (c) three seams and (d) four seams. 59
4.20 Variation of the drag coefficient at given Reynolds numbers for all tested fabrics placed 45^o from the stagnation point for (a) one seam, (b) two seams, (c) three seams and (d) four seams. 60
4.21 Variation of the drag coefficient at given Reynolds numbers for roughest fabric (fabric 3), smoothest fabric (fabric 7) and fabric with medium roughness (fabric 5) with one seam placed 50^o from the stagnation point. 62
4.22 Comparison of drastic drag reduction for roughest fabric (fabric 3), smoothest fabric (fabric 7) and fabric with medium roughness (fabric 5) with three seams placed 60^o from the stagnation point. 62
4.23 Variation of the drag coefficient at given Reynolds numbers for 2D tripwires with thicknesses of (a) 0.5 mm, (b) 1 mm and (c) 2 mm at angles of 30^o to 70^o from the stagnation point. 65
4.24 Variation of the drag coefficient at given Reynolds numbers for zigzag tripwires with $\lambda_{Re_D=60k}$ for (a) 0.5 and (b) 1 mm thickness at angles of 30^o to 70^o from the stagnation point. 65
4.25 Variation of the drag coefficient at given Reynolds numbers for zigzag tripwires with $\lambda_{Re_D=60k}$ for 0.5 and 1 mm thickness at angles of 30^o, 40^o and 50^o from the stagnation point. 66
4.26 Variation of the drag coefficient at given Reynolds numbers for zigzag tripwires with $\lambda_{Re_D=60k}$ for 0.5 and 1 mm thickness at angles of 60^o and 70^o from the stagnation point. 66

4.27 Variation of the drag coefficient at given Reynolds numbers for zigzag tripwires with $\lambda_{Re_D=80k}$ for (a) 1 and (b) 2 mm thickness at angles of 30^o to 70^o from the stagnation point. 67
4.28 Variation of the drag coefficient at given Reynolds numbers for zigzag tripwires with $\lambda_{Re_D=80k}$ for 1 and 2 mm thickness at angles of 30^o, 40^o and 50^o from the stagnation point. 68
4.29 Variation of the drag coefficient at given Reynolds numbers for zigzag tripwires with $\lambda_{Re_D=80k}$ for 1 and 2 mm thickness at angles of 60^o and 70^o from the stagnation point. 68
4.30 Variation of the drag coefficient at given Reynolds numbers for 1mm thick zigzag tripwires with (a) $\lambda_{Re_D=60k}$ and (b) $\lambda_{Re_D=80k}$ for angles of 30° to 70° from the stagnation point. 69
4.31 Variation of the drag coefficient at given Reynolds numbers for 1mm thick zigzag tripwires with $\lambda_{Re_D=60k}$ and $\lambda_{Re_D=80k}$ for angles of 30^o, 40^o and 50^o from the stagnation point. 70
4.32 Variation of the drag coefficient at given Reynolds numbers for 1mm thick zigzag tripwires with $\lambda_{Re_D=60k}$ and $\lambda_{Re_D=80k}$ for angles of 60^o and 70^o from the stagnation point. 70
4.33 Variation of the drag coefficient with Reynolds numbers for all tripwires at angles of (a) 30^o, (b) 40^o, (c) 50^o, (d) 60^o and (e) 70^o from the stagnation point. 72
4.34 Variation of the drag coefficient and Strouhal number at given Reynolds numbers for 2D tripwires with thickness values of 1 mm (a), (b) and 2 mm (c), (d) at angles of 30^o to 50^o from the stagnation point. 73
4.35 Variation of the drag coefficient and Strouhal number at given Reynolds numbers for 0.5 mm thick tripwires with 2D geometry (a), (b) and zigzag geometry with $\lambda_{Re_D=60k}$ (c), (d) at angles of 50^o to 70^o from the stagnation point. 73

4.36 Variation of the drag coefficient and Strouhal number at given Reynolds numbers for 1 mm thick zigzag tripwires with $\lambda_{Re_D=60k}$, (a), (b) and $\lambda_{Re_D=80k}$ (c), (d) at angles of 30^o to 50^o from the stagnation point. 74
4.37 Variation of (a) drag coefficient and (b) Strouhal number at given Reynolds numbers for 2 mm thick zigzag tripwire with $\lambda_{Re_D=80k}$ for angles of 30^o to 50^o from the stagnation point. 74
4.38 Variation of the drag coefficient with Reynolds number for the tripwire cases producing the lowest drag as previously identified. 76
4.39 Schematic of a tripwire and a fabric seam placed symmetrically from the stagnation point. 78
4.40 Variation of drag coefficient with Reynolds number at angles of 30^o to 60^o from the stagnation point for (a) fabric 7 with one seam, (b) 1 mm thick zigzag tripwire with $\lambda_{Re_D=60k}$, (c) fabric 7 with one seam and 1 mm thick zigzag tripwire with $\lambda_{Re_D=60k}$ that are placed symmetrically from the stagnation point. 79
4.41 Variation of drag coefficient with Reynolds number for fabric 7 with one seam, a 1 mm thick zigzag tripwire with $\lambda_{Re_D=60k}$ and a combination where both are placed symmetrically at angles of (a) $\theta = 30^o$, (b) $\theta = 40^o$, (c) $\theta = 50^o$ and (d) $\theta = 60^o$ from the stagnation point. 80
4.42 Fabric seam and tripwire that are (a) placed symmetrically from the stagnation point, (b) 180^o apart where the tripwire is facing the incoming flow direction before the seam in a T-S orientation and (c) 180^o apart where the seam of the fabric is facing the incoming flow direction before the tripwire in a S-T orientation. 81
4.43 Variation of drag coefficient with Reynolds number at angles of 30^o to 60^o from the stagnation point for (a) fabric 5 with one seam, (b) 2 mm thick 2D tripwire (c) fabric 5 with one seam and 2 mm thick 2D tripwire that are placed symmetrically from the stagnation point. 82

4.44 Variation of drag coefficient with Reynolds number at angles of 30^o to 50^o from the stagnation point for fabric 5 with one seam that is 180^o apart from a 2 mm thick 2D tripwire in (a) T-S orientation where the tripwire is facing the incoming flow direction before the fabric seam and (b) S-T orientation where the fabric seam is facing the incoming flow direction before the tripwire. . . . 83

4.45 Variation of drag coefficient with Reynolds number for fabric 5 with one seam, a 2 mm thick 2D tripwire and a combination where both are placed symmetrically at angles of (a) $\theta = 30^o$, (b) $\theta = 40^o$, (c) $\theta = 50^o$ and (d) $\theta = 60^o$ from the stagnation point. 83

4.46 Variation of drag coefficient with Reynolds number at angles of 30^o to 60^o from the stagnation point for (a) fabric 5 with one seam, (b) 2 mm thick zigzag tripwire with $\lambda_{Re_D=80k}$, (c) fabric 5 with one seam and 2 mm thick zigzag tripwire with $\lambda_{Re_D=80k}$ that are placed symmetrically from the stagnation point. 85

4.47 Variation of drag coefficient with Reynolds number at angles of 30^o to 50^o from the stagnation point for fabric 5 with one seam that is 180^o apart from the 2 mm thick zigzag tripwire with $\lambda_{Re_D=80k}$ in (a) T-S orientation where the tripwire is facing the incoming flow direction before the fabric seam and (b) S-T orientation where the fabric seam is facing the incoming flow direction before the tripwire. 86

4.48 Variation of drag coefficient with Reynolds number for fabric 5 with one seam, a 2 mm thick zigzag tripwire with $\lambda_{Re_D=80k}$ and a combination where both are symmetrically placed at (a) $\theta = 30^o$, (b) $\theta = 40^o$, (c) $\theta = 50^o$ and (d) $\theta = 60^o$ from the stagnation point. 86

4.49 Variation of drag coefficient with Reynolds number at angles of 30^o to 60^o from the stagnation point for (a) fabric 3 with one seam, (b) 1 mm thick zigzag tripwire with $\lambda_{Re_D=60k}$, (c) fabric 3 with one seam and 1 mm thick zigzag tripwire with $\lambda_{Re_D=60k}$ arranged in a symmetric orientation, (d) fabric 3 with one seam that is 180^o apart from the 1 mm thick zigzag tripwire with $\lambda_{Re_D=60k}$ where the tripwire is facing the incoming flow direction first (T-S) and (e) fabric 3 with one seam that is 180^o apart from the 1 mm thick zigzag tripwire with $\lambda_{Re_D=60k}$ where the seam is facing the incoming flow direction first (S-T). 89

4.50 Variation of drag coefficient with Reynolds number for fabric 3 with one seam, a 1 mm thick zigzag tripwire with $\lambda_{Re_D=60k}$ and a combination where both are placed symmetrically at angles of (a) $\theta = 30^o$, (b) $\theta = 40^o$, (c) $\theta = 50^o$ and (d) $\theta = 60^o$ from the stagnation point. 90

4.51 Variation of drag coefficient with Reynolds number for roughest fabric (fabric 3), smoothest fabric (fabric 7) and fabric with medium roughness (fabric 5) with tripwires arranged in a symmetric orientation at angles of (a) $\theta = 30^o$, (b) $\theta = 40^o$, (c) $\theta = 50^o$ and (d) $\theta = 60^o$ from the stagnation point. 91

4.52 Variation of potential time gains when drag reduction is applied up to 50% for the upper arms and lower legs of cyclists with an hourly record in 2022. . . . 96

Chapter 1

Introduction

1.1 Motivation and Research Objectives

In the late 1970's, skinsuits gained popularity to reduce drag relative to previous loose-fitting garments and improve cooling for cycling applications [1]. Aerodynamic drag accounts for approximately 90% of the resistance experienced by cyclists when travelling at racing speeds on a flat surface [2]. Pressure drag mainly contributes to the aerodynamic resistance of bluff bodies such as cyclists compared to viscous drag that causes skin friction in the boundary layer on the cyclist's surface [3]. The magnitude of the pressure drag is proportional to the pressure difference between the windward and leeward side of a cyclist. Flow separation around cyclists occurs from the formation of a turbulent wake and the presence of large scale low pressure vortices [2]. Pressure drag can be reduced by decreasing the frontal area of the cyclist or wearing an aerodynamic skinsuit. The cyclist body and wearable components such as helmets and skinsuits contribute from 64% to 82% of the total drag [3]. In sports such as cycling, the design of skinsuits can be optimized where combinations of smooth and rough fabrics can affect the flow around the body and decrease aerodynamic drag [4]. Seams are also included in the design of skinsuits where they behave as tripwires. Tripwires work as a row of vortex generators by adding momentum to the lower part of the boundary layer to transition flow to turbulence.

In the past, previous researchers have investigated the effects of fabric roughness on the drag of a cylinder without the influence of seams. Although there was discussion in the past on cylinders fitted with tripwires, there was limited experimental testing on attaching a tripwire to a fabric at different angles relative to the incoming flow direction. In the present work, the research objective is to explore the effects of drag reduction when fabrics with multiple number of seams are wrapped on a cylinder. The impact of drag reduction is also investigated when tripwires with 2D and zigzag geometry are attached on a cylinder at specific angles relative to the incoming flow direction. Lastly, recommendations for skinsuit design are made by comparing the drag reduction performance when a tripwire is attached to a fabric with different levels of roughness. A hypothesis is that textile roughness can influence the performance of tripwires created by seams. Flow control methods such as surface roughness of fabrics and tripwires promote turbulence in the boundary layer. This delays flow separation for a cyclist by allowing the turbulent boundary layers to overcome adverse pressure gradients in the flow due to having larger momentum [5]. Furthermore, this decreases the width of the wake and ultimately decrease the drag which can improve the performance of cyclists.

1.2 Modelling the Flow over a Cylinder

The flow around a cyclist is known to exhibit large regions of separated flow such that the flow problem is modelled as a bluff body [2]. A circular cylinder is a type of bluff body that has been often used to model the limbs of an athlete [6]. Cylindrical geometry has been used in the past to evaluate aerodynamic properties of textile features such as stitch position and surface morphology to understand the flow behaviour when subject to moderate Reynolds numbers experienced by a cyclist [5, 7]. The flow separation around a cylinder is dependent on the Reynolds number in identifying flow regimes where laminar and turbulent separation patterns occur [8]. The Reynolds number, Re_D, is the ratio of inertial to viscous forces for a

circular cylinder as shown in Equation 1.1 where U_∞ is the flow velocity, D is the cylinder diameter and v is the kinematic viscosity.

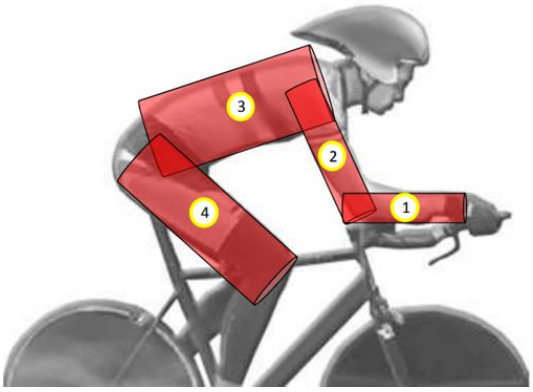


Figure 1.1: Cylinder representation of a cyclist for 1) forearms, 2) upper arms, 3) lower back and 4) thigh regions. Reprinted with permission from Chowdhury [6].

$$Re_D = \frac{U_\infty D}{v} \tag{1.1}$$

The most significant changes in flow topology for the limbs of a cyclist generally occur at speeds ranging from 10 to 15 m/s [8]. The critical flow condition can be achieved on all limbs of a cyclist if the roughness on the upper arm and lower leg is utilized for effective drag reduction [8]. That is why the diameter, D found in Equation 1.1 represents the upper arm width of a cyclist in cross flow. In the work of Malizia and Blocken, a cylinder with a diameter of 0.11 m represented the upper arm of a cyclist in reaching a Reynolds number of 1.10×10^5 at an airspeed of 15 m/s [9]. In addition, the characteristic length scale, D considered for the present work is 4 inches or 0.1016 m. The Reynolds numbers of a cylinder with a diameter of 4 inches would range from 6.0×10^4 to 1.0×10^5 when subject to cycling speeds that vary from 10 to 15 m/s. At these Reynolds numbers, the boundary layer over the cylinder must be tripped using methods such as surface roughness and tripwires to cause a drop in drag found over bluff bodies such as the circular cylinder at greater Reynolds numbers.

Chapter 2

Literature Review

2.1 Overview

In this chapter, the flow regimes of a single smooth cylinder was discussed from previous literature. The flow behaviour of a roughened cylinder was also explored to understand how surface roughness affects the drag at different flow regimes. It was compared with other variables such as pressure, lift and Strouhal number which will be discussed further in this chapter. The flow behaviour of tripped cylinders was analyzed to understand the main parameters in producing a tripwire such as thickness, spatial wavelengths and angular location relative to the stagnation point of a cylinder.

2.2 Flow over a Smooth Circular Cylinder

The drag coefficient, C_D, is usually dependent on the shape, surface roughness (texture) and Reynolds numbers for bluff bodies such as a cylinder [10]. It is determined from Equation 2.1 where F_D is the drag force, p_∞ is density, A is frontal area and U_∞ is the flow velocity.

$$C_D = \frac{F_D}{\frac{1}{2} p_\infty {U_\infty}^2 A} \tag{2.1}$$

In Figure 2.1, there are 4 distinct regions in the variation of the drag coefficient with Reynolds number curve which divide into subcritical, critical, supercritical, and transcritical flow regimes for a single isolated circular cylinder. At low subcritical Reynolds numbers of less than 1.0×10^5, the boundary layer for a smooth cylinder remains laminar with a separation angle of approximately 82^o from the forward stagnation point [8]. In the subcritical flow regime, the boundary layer over the cylinder is laminar where early flow separation occurs resulting in a wake with a high pressure drag [11]. In the critical flow regime, the boundary layer that develops on the surface of the cylinder is initially laminar at separation but eventually transitions to turbulence. In the turbulent state, external fluid can be efficiently entrained into the separated shear layer [12]. This allows for the flow to reattach onto the surface of the cylinder within a short distance and separate further downstream near the rear end of the cylinder. A separation bubble forms in the critical regime which is the region between laminar separation and turbulent reattachment. First, a one bubble state behaviour occurs when the bubble initially forms on one side of the cylinder bi-stably. Asymmetry in the pressure distribution occurs when a single bubble appears on one side of the cylinder, leading to a large lift coefficient. Flow acceleration occurs on the bubble side of the cylinder while experiencing flow deceleration on the opposite side. Accelerated flow found on the bubble side of the cylinder is more favourable for flow reattachment while decelerated flow found on the opposite side of the bubble delays transition to turbulence [13]. The drag crisis phenomenon where maximum drag reduction occurs in the critical flow regime happens after having laminar separation bubbles form on each side of the cylinder as the Reynolds numbers increase. In the supercritical flow regime, the boundary layer over the surface of the cylinder is turbulent on both sides of the cylinder. However, it is not fully turbulent since the transition to turbulence is located somewhere between the stagnation point and separation point [14]. The wake of a bluff body narrows when transitioning from the subcritical to

supercritical flow regime where there is a lower velocity deficit. The velocity deficit is the difference between the mean streamwise velocity and the free stream velocity. Finally, there is a transcritical flow regime where the boundary layer is virtually turbulent everywhere [14].

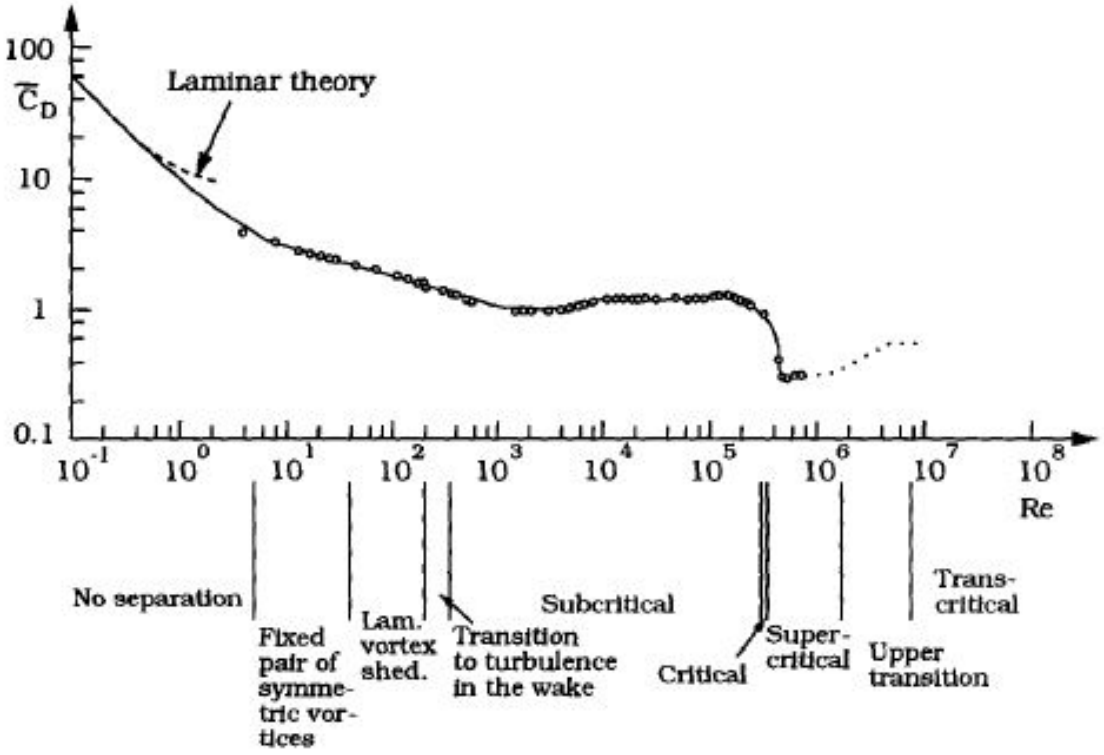


Figure 2.1: Variation of the drag coefficient with Reynolds number for a smooth circular cylinder. Reprinted with permission from Fredsoe *et al.* [14].

2.3 Flow over a Roughened Cylinder

2.3.1 Effect of Different Roughness Methods

Surface roughness does not only promote boundary layer transition from laminar to turbulence but can affect the subsequent flow behaviour at Reynolds numbers beyond the critical flow regime [15]. Roughened cylinders prematurely transition the boundary layer to turbulence by shifting the separation point downstream from the leading edge of the cylinder. At the critical flow regime, surface roughness disturbs the separation bubble by limiting its presence to a narrow range of Reynolds numbers to form the one and two bubble regime shown in Figure 2.2 [16]. A stable two bubble state forms at the Reynolds number where the minimum drag occurs for a smooth cylinder as shown in Figure 2.2.

Earlier flow separation occurs for roughened cylinders compared to a smooth cylinder due to the thickening of the boundary layer induced by roughness [17]. Increasing the surface roughness of a fabric would cause the minimum drag coefficient to increase at a lower critical Reynolds number as shown in Figure 2.3. Figure 2.3 illustrates the drag coefficient as a function of Reynolds numbers for roughened cylinders with different relative roughness values. The relative roughness is a dimensionless parameter that is found by dividing the roughness heights, k or k_s of a surface by the cylinder diameter, D to obtain k/D or k_s/D. For example, a cylinder with a high relative roughness, k_s/D of 2000×10^{-5} achieves a minimum drag coefficient at the smallest critical Reynolds number of approximately 5.0×10^4. However, the drag coefficient would increase in the supercritical flow regime when there is a higher roughness on the surface of the cylinder. In the transcritical flow regime, the drag coefficient becomes constant. This shows that the wall shear stresses are independent of the Reynolds number and are only a function of the roughness parameter in the transcritical flow regime. A relative Nikuradse's sand grained roughness of $400 \times 10^{-5} < k_s/D < 700 \times 10^{-5}$ is a suitable range in achieving the drag crisis at a Reynolds number range experienced by the upper arm

region of a cyclist of 6.0×10^4 to 1.0×10^5. The Nikuradse's sand grain roughness method was used in finding the average diameter of the sand grains on the surface of a cylinder through which friction of the flow was measured [18].

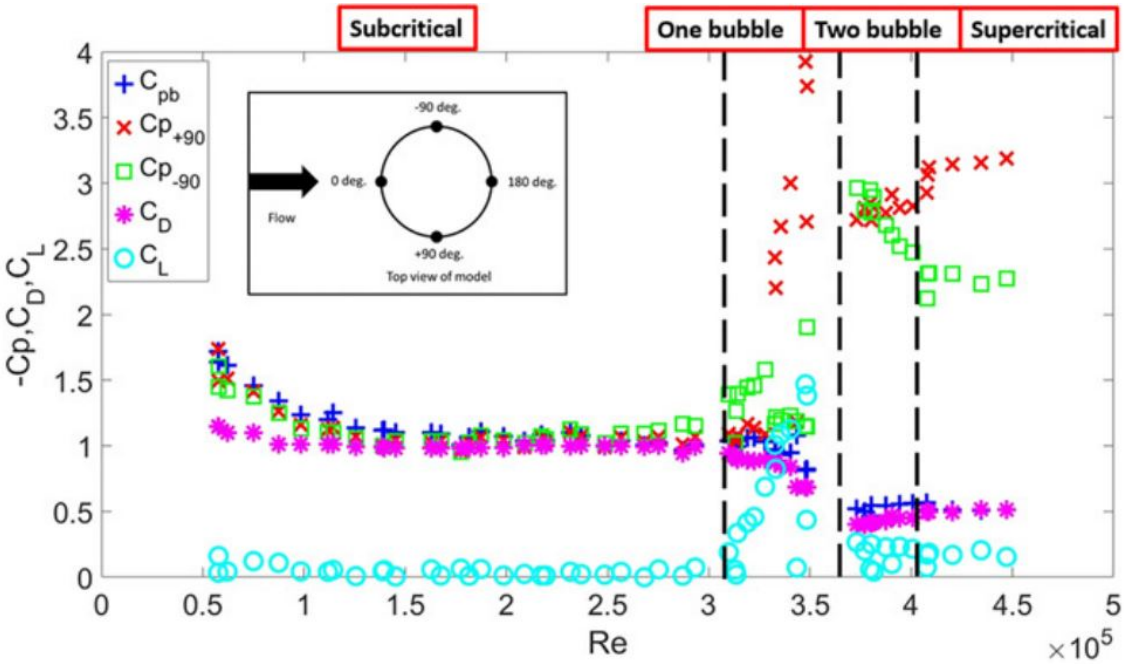


Figure 2.2: Variation of pressure, drag and lift coefficients with Reynolds number for a smooth circular cylinder. Reprinted with permission from Hsu *et al.* [12].

In the work done by Zheng *et al.*, a grooved fabric was wrapped on a cylinder with a diameter of 0.064 m [20]. The arithmetic average roughness height, k was used to quantify the surface roughness of the grooved fabric by taking the average of the absolute value of the roughness profile along the sampling length. The arithmetic roughness height, k of the grooved fabric was approximately 0.159 mm with a relative roughness, k/D of 2.49×10^{-3}. The longitudinal grooved fabric achieves a minimum drag coefficient of less than 0.60 at a critical Reynolds number of approximately 8.0×10^4.

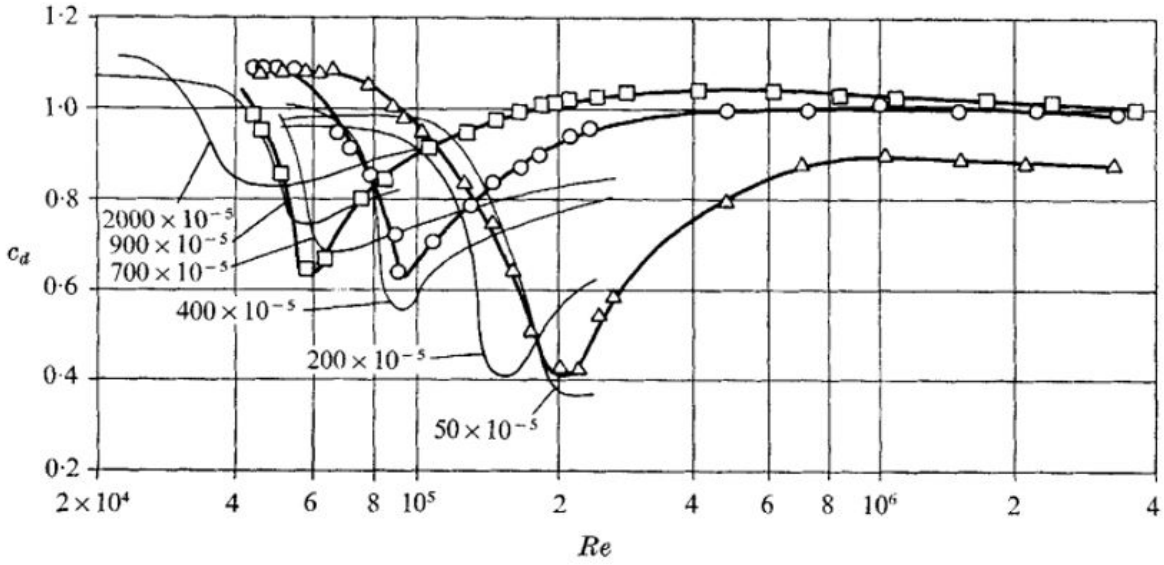


Figure 2.3: Variation of the drag coefficient with Reynolds number for a roughened cylinder with different relative roughness values where △, $k_s/D = 110 \times 10^{-5}$; ◯, $k_s/D = 450 \times 10^{-5}$; □, $k_s/D = 900 \times 10^{-5}$. Reprinted with permission from Cambridge University Press [18, 19].

In Figures 2.4 to 2.5 found below, the variation of the relative roughness with drag and pressure coefficients were illustrated. The geometric roughness height of fabrics, k_s were determined from taking the sum of the five highest peaks and five deepest valleys within the fabric surface area [12]. The Reynolds number where the drag crisis for Nikuradse's sand grained roughness, k_s occurs can be calculated from Equation 2.2 [12]. The minimum drag coefficient increases for fabrics with a larger relative roughness. The pressure coefficient becomes less negative for fabrics with larger relative roughness values from Figure 2.5. As the relative roughness increases, two separation bubbles forming at the given Reynolds number become less significant [12]. A symmetric state occurs in the flow where there are no separation bubbles on either side of the cylinder [21]. This causes a larger drag to occur in the supercritical flow regime for fabrics with a larger relative roughness as it approaches a symmetric state condition. Furthermore, the drag crisis phenomenon becomes less significant for fabrics with a larger surface roughness.

$$\mathrm{Re}_c = \frac{6000}{\sqrt{\frac{k_s}{D}}} \tag{2.2}$$

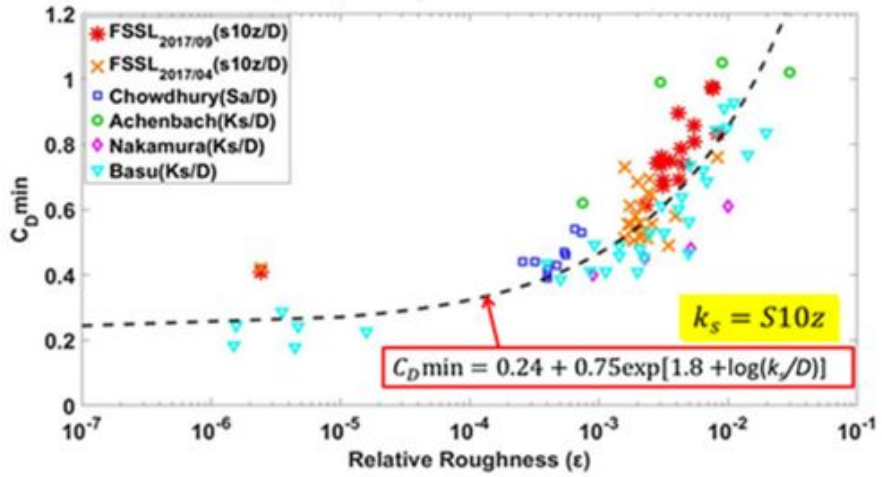


Figure 2.4: Relationship between relative roughness and drag coefficient. Reprinted with permission from Hsu *et al.* [12].

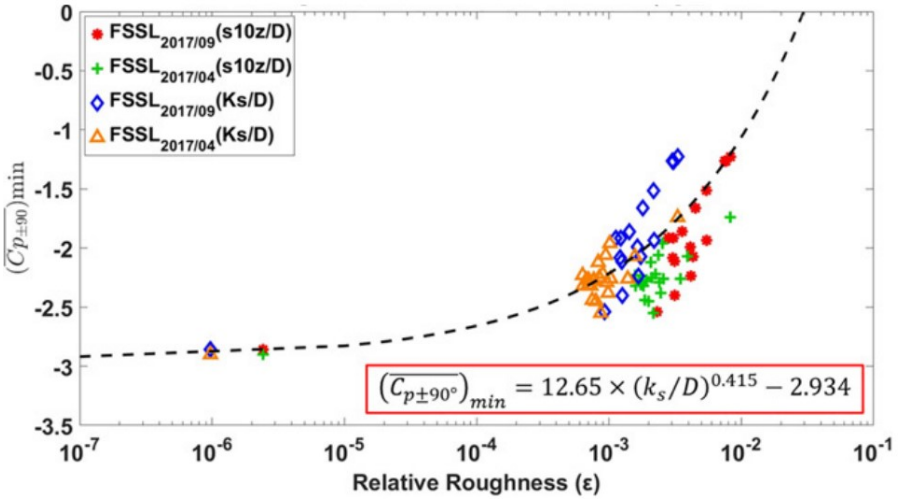


Figure 2.5: Relationship between relative roughness and pressure coefficient. Reprinted with permission from Hsu *et al.* [12].

2.3.2 Effect of Rib Spacings and Rib Heights

Ribs found in athletic garments were commonly used to reduce the drag at a smaller critical Reynolds number because separation always occurred upstream of the last rib [5]. The aerodynamic properties found in [5] was explored for equally distributed semicircular ribs attached on a cylinder that were normal to the incoming flow direction when placed inside a wind tunnel. Surface coatings were covered on a cylinder and consisted of two layers of fabric with 3D printed ribs laminated between the two layers [5]. The size and spacing of the ribs were altered for three different micro roughness coatings that have maximum roughness heights, k_s^{max} of 0.10, 0.20 and 0.42 mm. The Strouhal number variation with Reynolds number was also illustrated for all surface coatings with different rib heights and spacings. The Strouhal number, St is a function of the vortex shedding frequency f, diameter of the cylinder D and flow velocity, U_∞ as shown in Equation 2.3.

$$St = \frac{fD}{U_\infty} \tag{2.3}$$

When a fabric's relative spacing exceeds the critical spacing, the addition of ribs would act to increase the surface area rather than to reduce the drag. This would subsequently cause the Strouhal number to decrease for fabrics with large rib spacings and rib heights. In the curve that illustrates the variation of the drag coefficient with Reynolds number shown in Figure 2.6, a minimum drag coefficient of 0.57 was achieved at a critical Reynolds number of 7.5×10^4 when there is a small rib height h, of 0.5 mm and maximum roughness height of 0.42 mm for a ribbed surface fabric, $S_c\ h_{0.5}\ \triangle_{10}$. A minimum drag coefficient of 0.52 was achieved at a large critical Reynolds number of 9.7×10^4 when there is a small rib height of 0.5 mm and maximum roughness height of 0.2 mm for a ribbed surface fabric, $S_B\ h_{0.5}\ \triangle_{10}$. These two surface coatings reaches the drag crisis at critical Reynolds numbers of 7.5×10^4 to 1.0×10^5 which occurs at the Reynolds numbers experienced by the upper arm region of a cyclist. It is also noticed that a lower drag coefficient corresponds to a larger Strouhal

number as shown in Figure 2.6 because the vortices detach downstream from the wake of the cylinder. This delays flow separation and increase the vortex shedding peak, promoting effective drag reduction relative to a smooth cylinder. Moreover, a smaller rib height and rib spacing causes a vortex shedding peak to occur at a higher Reynolds number where flow reattachment occurs downstream of the cylinder surface.

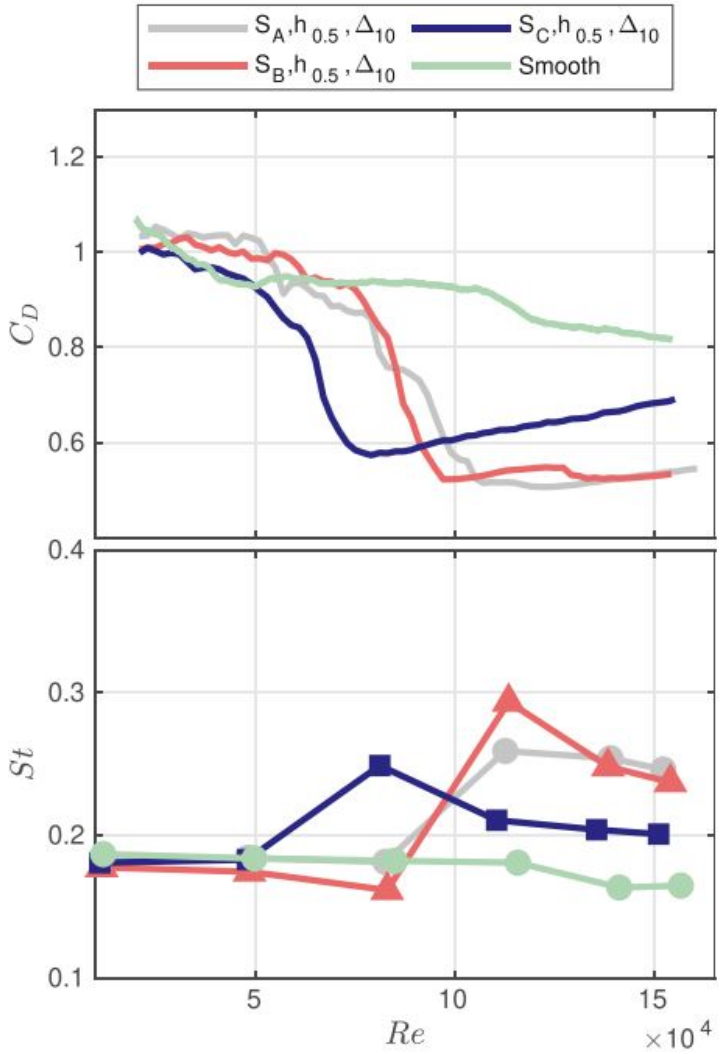


Figure 2.6: Variation of drag coefficient and Strouhal number with Reynolds number for textiles with $h/d = 0.067$ and $\triangle/h = 20$ where d is 75 mm. Reprinted with permission from Skeide *et al.* [5].

2.4 Flow over a Tripped Cylinder

2.4.1 Flow over a Cylinder with a Single Tripwire

Tripwires may be used as a passive flow control method that can influence the drag of a circular cylinder by transitioning the boundary layer to turbulence. The important geometric parameters for 2D cylindrical tripwires are the relative height compared to the cylinder diameter, d/D and the location from the stagnation point. For circular cylinders with a zigzag tripwire, the spatial wavelength of the zigzag tripwire is an additional parameter that is required to characterize the flow behaviour past the cylinder. The tripwires affect the boundary layer occurring over the cylinder surface and modify the reattachment and separation patterns of the wake [22]. For a smooth circular cylinder without a tripwire installed, a single drag crisis occurs as was shown previously in Figure 2.1. On the other hand, a two stage drag crisis may occur for a cylinder with a tripwire as shown in Figures 2.7(a) and 2.7(b). In the first stage drag crisis of a tripped cylinder, the flow becomes asymmetric with respect to the incoming flow direction in having the upper half of the cylinder reach a critical state while the bottom state reaches a subcritical state when a tripwire is mounted. Transitioning the boundary layer on the upper half of the cylinder with a tripwire causes the flow to achieve turbulence and reach a critical state at a lower Reynolds number. This allows for the flow to reattach to the cylinder where the near wake becomes narrower, leading to a rapid drag reduction. However, the boundary layer in the bottom half of the cylinder is in a subcritical state as shown in Figure 2.7(a). It experiences laminar separation since the tripwire does not significantly influence the flow in the bottom half of the cylinder in the first stage of the drag crisis [23]. In the second stage drag crisis, the flow regains symmetry with respect to the free stream in achieving a critical state on the upper and lower halves of the cylinder as shown in Figure 2.7(b).

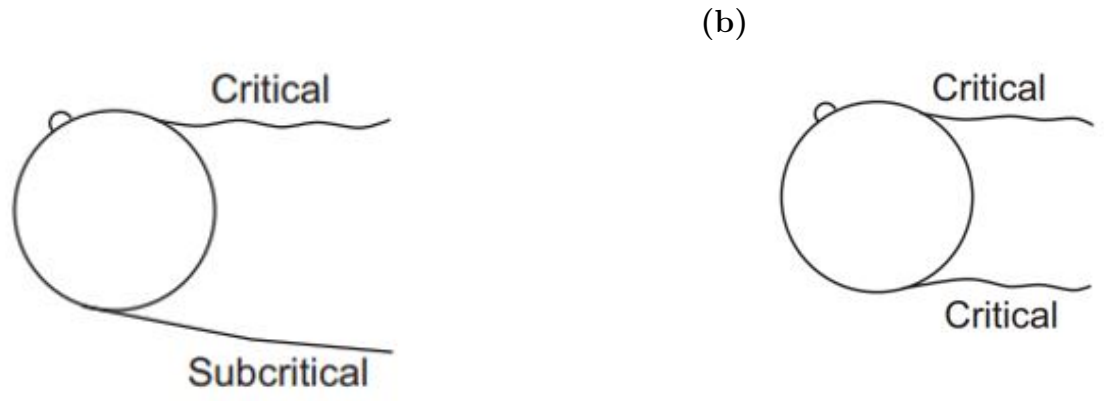


Figure 2.7: Two stage drag crisis behaviour for a cylinder mounted with a tripwire that has a wake behaviour state for (a) first drag crisis and (b) second stage drag crisis. Reprinted with permission from Behara *et al.* [23].

Thicker tripwires would cause the drag crisis to occur at a smaller angle from the stagnation point of the cylinder surface for a given Reynolds number. For example, a zigzag tape with a thickness of 0.93 mm causes the drag crisis to occur at a critical Reynolds number of 1.0×10^5 when placed 45° from the stagnation point of a cylinder [24]. On the other hand, the drag crisis occurs at the same critical Reynolds number when a zigzag tape with a larger thickness of 2 mm is placed 30° from the stagnation point of a cylinder surface.

2.4.2 Flow over a Cylinder with One and Two Tripwires

A one wired cylinder has an angular location with respect to the time averaged forward stagnation point as shown in Figure 2.8(a). The angular location of the tripwire from the stagnation point influences the mean recirculation bubble acting on the cylinder. The mean recirculation bubble length is the distance between the center of the cylinder to the point of zero velocity at the rear of a wake [25]. Maximum bubble extension promotes flow attachment due to asymmetry of the near wake. Critical angles are angles from the stagnation point where the maximum bubble extension occur at the rear wake of the cylinder. The range of the critical angle for maximum bubble extension are affected by the Reynolds number and



Figure 2.8: Diagram of (a) one wired and (b) two wired cylinders.

wire aspect ratio which can be expressed as the diameter of the wire over the diameter of the cylinder, d/D. An increase in the wire size at a critical Reynolds number leads to a decrease in the angular location of the first critical angle for maximum bubble extension. Bistable instability also occurs at the first critical angle of a tripped cylinder where the flow switches between shear layer reattachment and early flow separation [26]. On the other hand, the second critical location which usually occurs 10^o after the first critical angle cause maximum bubble contraction to occur. Maximum bubble contraction causes the boundary layer of the tripwire to permanently separate from the surface of the cylinder. It occurs from having a lack of fluid that can satisfy the entrainment demands of the shear layers in the wake [25].

When both of the tripwires in a two wired case are located in the same angular range where a single tripwire promotes a peak in the Strouhal number, there would be a delay of approximately 5^o to 7^o of the first critical angle in a two wired case compared to its value found in a one wired case. At the critical location, the single tripwire has a large mean recirculation bubble length in the near wake. However, two tripwires would have an opposite effect of a significant reduction in the mean recirculation bubble length when placed at the same angular range as a single tripwire. The near wake asymmetry and bubble extension found in the one wired case has an early transition in one of the separating shear layers, specifically the wired side shear layer [25]. Meanwhile, the symmetric near wake condition associated with the bubble contraction of a two wired case is caused by the early transition of both shear layers when placed in the same angular range as a single tripwire. Furthermore,

this would cause a delay in the first critical angle of a two wired case due to the shortage in the amount of fluid to satisfy the entrainment demands from the two shear layers.

2.4.3 Effect of Angular Positions of Tripwires

The drag crisis for a two wired case with small wire aspect ratios of $d/D < 0.003$ effectively reduce drag from 65^o to 70^o from the stagnation point [19, 27]. Large wire aspect ratios of $0.011 < d/D < 0.045$ would effectively reduce drag from 35^o to 50^o from the stagnation point [28, 29]. In Figure 2.9(a), there is a plot that depicts the variation of the drag coefficient at different angles from the stagnation point for a two wired fitted case where the wire aspect ratio is $d/D = 0.045$. In regime A where two tripwires are placed at angles less than 20° from the stagnation point, laminar flow occurs where there is a slight effect on the wake. In regime B where the tripwire is placed at angles between 20° to 35° from the stagnation point, the boundary layer separating from the tripwire begins to reattach onto the cylinder surface due to the transition to turbulence. This caused an increase in the Strouhal number and a decrease in the drag coefficient. In regime C, a turbulent reattachment occurs when the tripwire is placed at angles ranging from 35° to 40° from the stagnation point. This allows for the drag coefficient to reach its minimum value while the Strouhal number reaches its maximum value as shown in Figures 2.9(a) and 2.9(b). In regime D, the boundary layer is in a critical condition where two tripwires that are placed at angles ranging from 40° to 45° from the stagnation point experience bistable flow where it alternates between states of reattachment and flow separation as shown in Figure 2.9(b). In mode I, the boundary layer separating from the tripwire reattaches onto the cylinder surface. In mode II, the boundary layer separating from the tripwire does not reattach due to having a wider wake or a reduced vortex shedding frequency [28]. In regime E, the drag coefficient increases for the angular range of 45° to 70° from the stagnation point because the boundary layer of the cylinder surface separates from the tripwire due to having a wider wake.

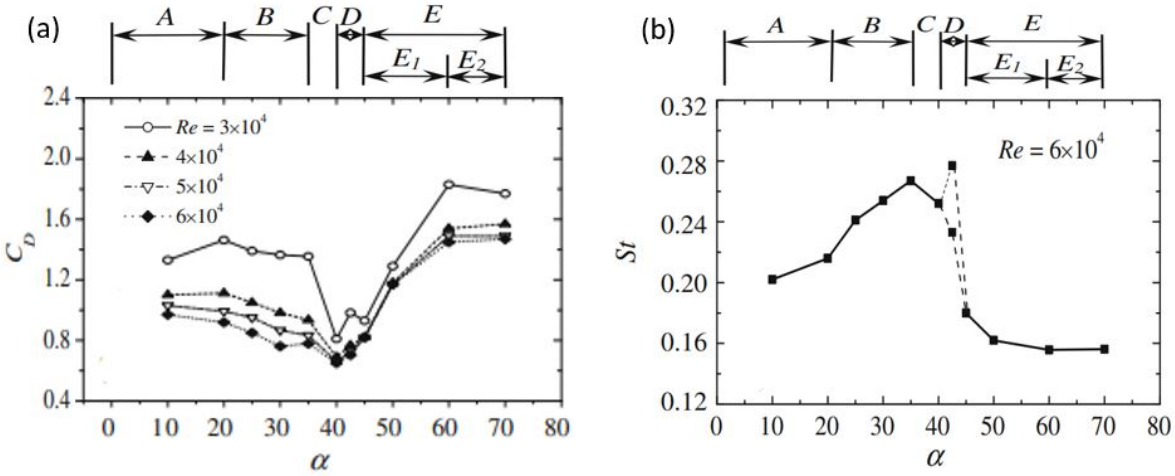


Figure 2.9: Variation of (a) drag coefficient at given angles from stagnation point for different Reynolds numbers and (b) Strouhal number at given angles from stagnation point at a constant Reynolds number of 6.0×10^4 in a two wired fitted case where the drag crisis occurs from $35^o < \alpha < 40^o$ and the bistable flow occurs from $40^o < \alpha < 45^o$. Edited with permission from Alam *et al.* [28].

In another case, two tripwires that have a wire aspect ratio of $d/D = 0.011$ achieve a minimum drag coefficient of approximately 0.65 at a critical Reynolds number of 1.10×10^5 when placed 40.5° from the stagnation point as shown in Figure 2.10 [30]. The boundary layer reattaches downstream and can transition to turbulence when placing two tripwires at angles of 20° to 40° from the stagnation point. The tripwires with large wire aspect ratios such as $d/D = 0.045$ cause the boundary layer to permanently separate when placed at angles larger than 45° from the stagnation point [28]. On the other hand, flow separation of the reattached boundary layer can be delayed at large angles up to 70° for tripwires with a smaller wire aspect ratio. Overall, tripwires have a considerable effect on the wake of a cylinder when placed at angles of 20° to 70° from the stagnation point for a two wired case [28].

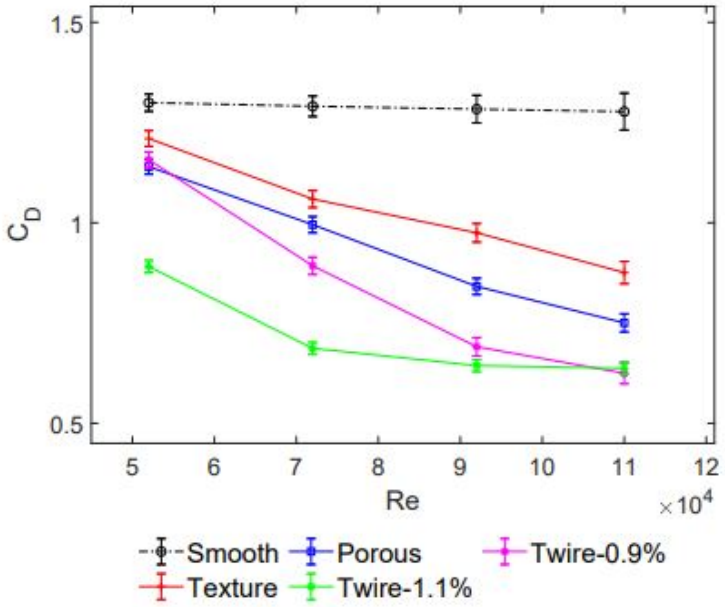


Figure 2.10: Variation of drag coefficient with Reynolds number for a two wired cylinder that has two tripwires of different aspect ratios placed 40.5° from the stagnation point. Reprinted with permission from Pelacci *et al.* [30].

2.4.4 Determining Thickness of Tripwires

The variation of the boundary layer thickness at given Reynolds numbers of a circular cylinder is determined using the Blasius method [31]. The pressure coefficient around a cylinder is first obtained using Equation 2.4 where θ is expressed in radians. The circumferential distribution of the streamwise velocity at the boundary layer edge is expressed using Equation 2.5 as a function of the pressure coefficient derived from Equation 2.4. The coefficients of the velocity distribution of u_1, u_3, u_5 found from Equation 2.6 is obtained using a curve of fit [32]. At each angular location of θ, Equation 2.7 is used to construct the velocity profiles found in Figure 2.11 using similarity parameters, n defined from Equation 2.8. This helped to determine the similarity parameter at the boundary layer edge, n_{BL} where the velocity distribution, $\frac{U(\theta,n)}{U_\infty}$ reaches 99% of the free stream velocity, using Equation 2.7 for each angular location from the stagnation point of the cylinder.

Lastly, the boundary layer thickness, δ can be obtained from Figure 2.12 at different angular positions along the cylinder at a given Reynolds number using Equation 2.9.

$$C_P = 1 - 4\sin^2(\theta) \tag{2.4}$$

$$\frac{U(\theta)}{U_\infty} = \sqrt{1 - C_P} \tag{2.5}$$

$$\frac{U(\theta)}{U_\infty} = u_1\theta + u_3\theta^3 + u_5\theta^5 \tag{2.6}$$

$$\frac{U(\theta, n)}{U_\infty} = u_1\theta f_1'(n) + 4u_3\theta^3 f_3'(n) + 6u_5\theta^5 f_5'(n) \tag{2.7}$$

$$n = (y/D)\sqrt{2u_1 Re_D} \tag{2.8}$$

$$\frac{\delta}{D} = \frac{n_{BL}}{\sqrt{2u_1 Re_D}} \tag{2.9}$$

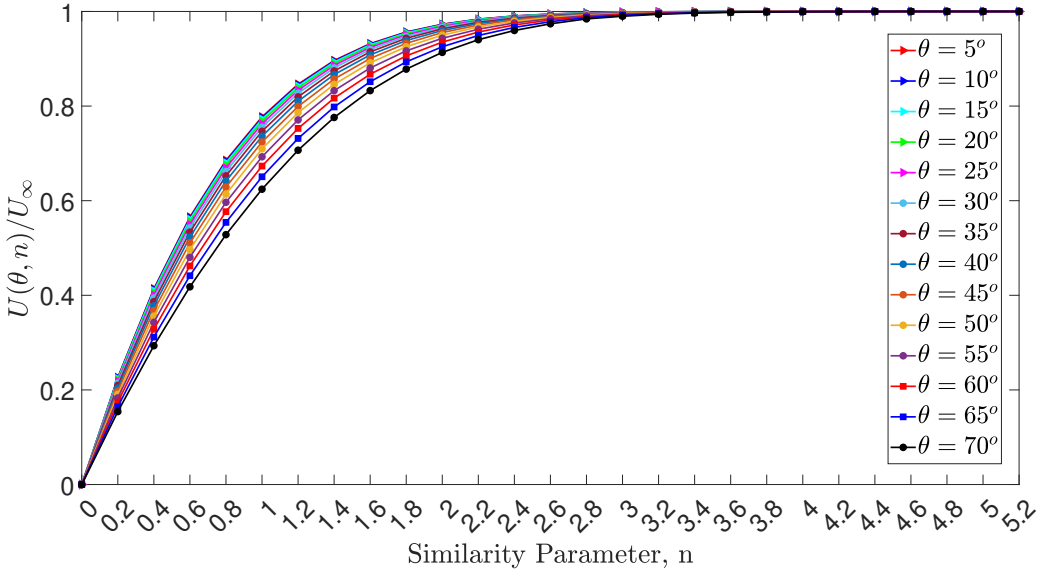


Figure 2.11: Velocity profiles at different angles from the stagnation point for a circular cylinder.

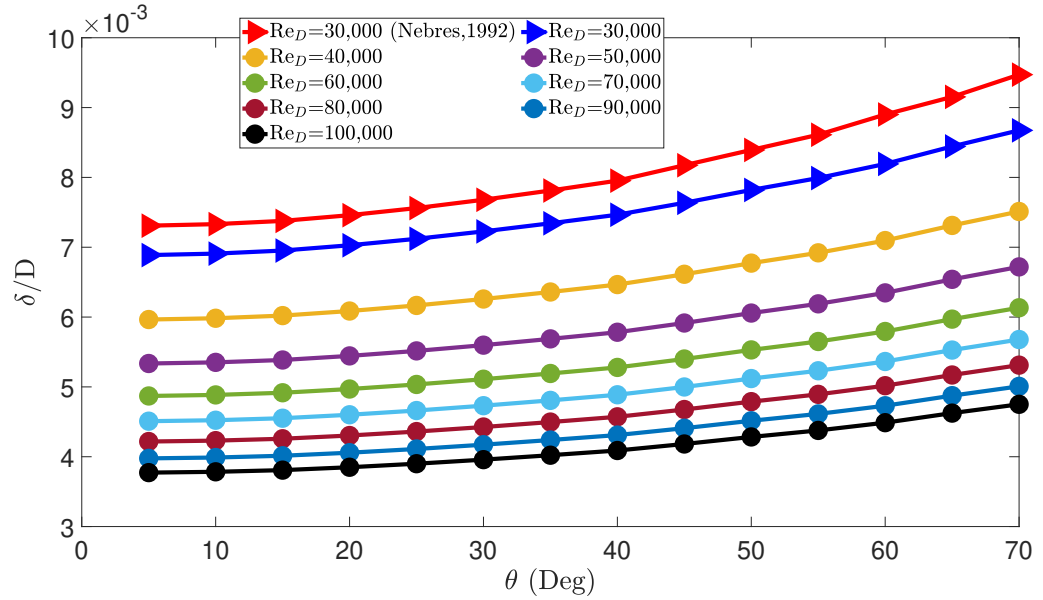


Figure 2.12: Ratios of boundary layer thickness relative to the cylinder diameter, (δ/D), for various Reynolds numbers and angles from stagnation point.

The velocity at the trip height when placed at an angle from the stagnation point for a given Reynolds number is obtained by first finding the similarity parameter shown in Equation 2.8. In Equation 2.8, y represents the tripwire height, k in this application since it is the distance from the cylinder surface. This can help obtain the Reynolds number at the tripwire height location shown in Equation 2.10 where u_k is the velocity at the height of the tripwire location in the undisturbed laminar boundary layer, k is the tripwire height and v is the kinematic viscosity [33]. The height of the tripwires were chosen such that the Reynolds number based on the tripwire, Re_{k,U_k} is greater than the minimum critical Reynolds number to initiate transition to turbulence for a tripwire of 200 [33, 34]. This ensures that the flow becomes turbulent in the nearest downstream location behind the tripwire. The appropriate trip heights are 0.5, 1 and 2 mm because the Reynolds numbers at the respective trip heights are greater than 200 and the values ranged from approximately 400 to 1780.

$$Re_{k,U_k} = \frac{U_k k}{v} \tag{2.10}$$

2.4.5 Spatial Wavelengths and Spike Angle of Zigzag Tripwires

In Figure 2.13, the spatial wavelengths are shown for a zigzag tripwire which consists of the streamwise and spanwise wavelengths. Streamwise wavelength is the spanwise distance between adjacent streamwise vortex pairs in the wake. Spanwise and streamwise wavelengths for a tripwire are determined based on mode instabilities [35]. In mode D-E, a shear layer transition regime forms for Reynolds numbers ranging from 1.0×10^3 to 2.0×10^5 where 2D Reynolds stresses occur [11]. Streamwise wavelength, λ_{SL} is the spanwise distance between adjacent streamwise vortex pairs in the wake which is found using Equation 2.11 [11]. Spanwise wavelength, λ_{ZSL} is the distance between the streamwise vortices in the separating shear layer and is determined from Equation 2.12 [11]. The length of the shear layer is limited by the streamwise extent of the vortex formation region. The vortex formation length, L_F is the streamwise distance between the cylinder surface and the point where the vortex is shedding

from the wake [36]. The vortex formation can be determined by identifying the location of the maximum root mean square (r.m.s.) fluctuation in the streamwise velocity component [11]. A larger vortex formation length, L_F/D indicates lower level of maximum velocity fluctuations and Reynolds stresses. When the Reynolds number increase, more streamwise vortex pairs are found along the cylinder's span, causing a decrease in spanwise wavelength [11]. For instability to occur in the near wake for large Reynolds numbers, the streamwise wavelength should be less than the vortex formation length where $\lambda_{SL} < L_F$. As shown in Figure 2.14 from [37], the vortex formation length would be 127 mm for a cylinder with a diameter of 101.6 mm. The streamwise wavelength values for a tripwire at Reynolds numbers experienced by a cyclist ranging from 6.0×10^4 to 1.0×10^5 occur from 12 to 15 mm using Equation 2.11 [11]. Moreover, the vortex formation length of 127 mm is greater than all streamwise wavelength values of 12 to 15 mm that occurs at Reynolds numbers experienced by the upper arm region of a cyclist ranging from 6.0×10^4 to 1.0×10^5.

The spike angle is the angle between the vertex of the zigzag tripwire section as shown below in Figure 2.13. A spike angle of 60^o is commonly used for a zigzag tripwire because it forms a wide hairpin vortex behind the curved shear layer of a trip to effectively transition to turbulence. A pair of vortices build up along each tooth of the zigzag tripwire and separate at the end of the tooth. Wider hairpin vortices allow for mixing and increase the velocity gradients in the flow and generate turbulence [38]. Increasing the spanwise wavelength can help form broader recirculation regions behind the downstream pointing spikes of a zigzag tripwire [39]. Moreover, this allows for majority of the hairpin vortices to move closer towards the tripwire to promote an effective transition to turbulence.

$$\frac{\lambda_{SL}}{D} \sim \frac{37}{\sqrt{Re_D}} \tag{2.11}$$

$$\frac{\lambda_{ZSL}}{D} \sim \frac{25}{\sqrt{Re_D}} \tag{2.12}$$

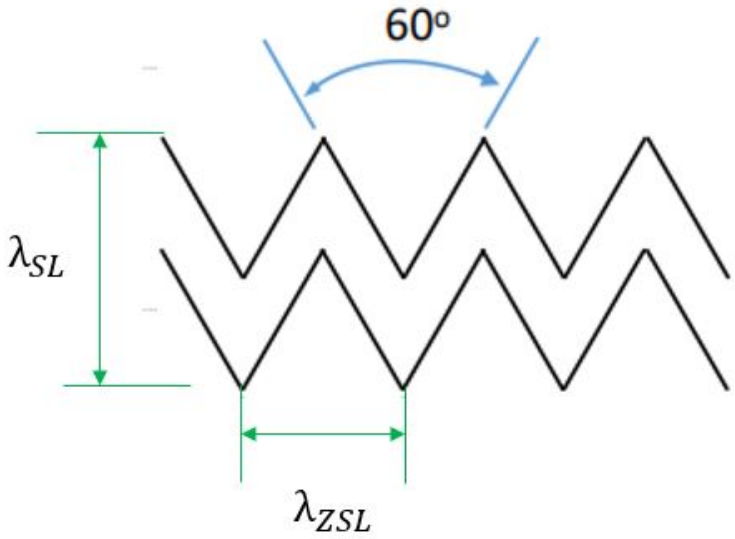


Figure 2.13: Spatial wavelengths and spike angle of 60^o for a zigzag tripwire where λ_{SL} is the streamwise wavelength and λ_{ZSL} is the spanwise wavelength.

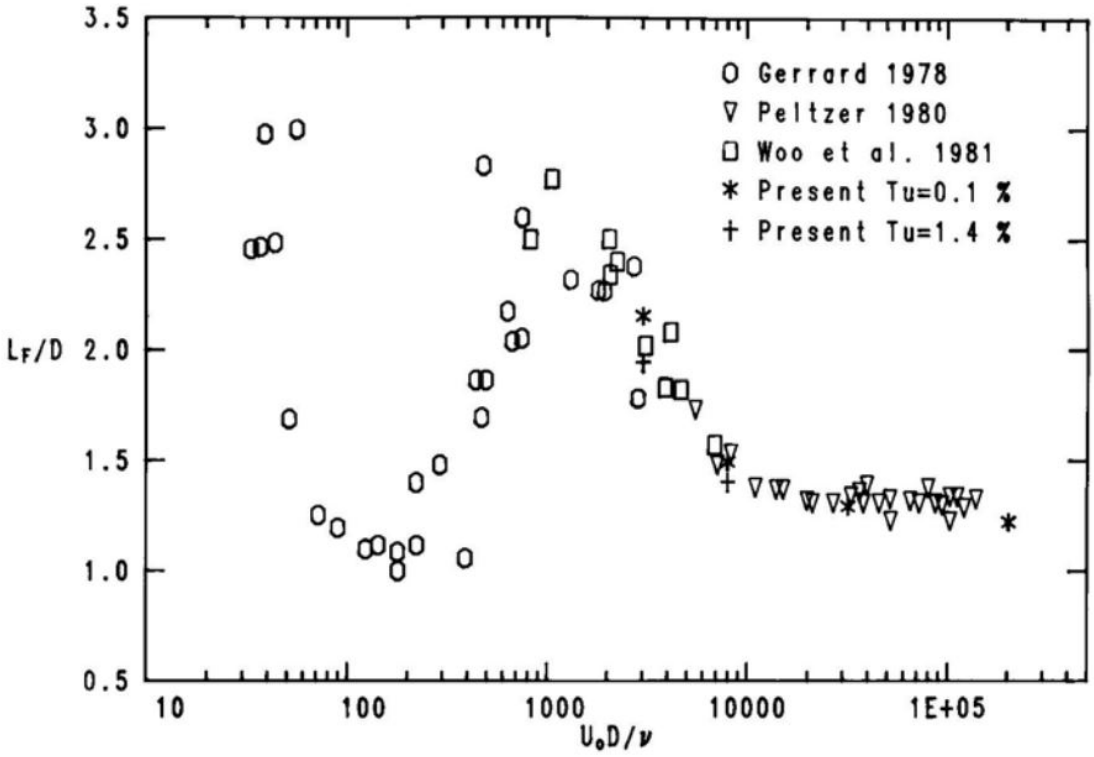


Figure 2.14: Vortex formation length for different Reynolds numbers for a circular cylinder. Reprinted with permission from Norberg [37].

Chapter 3

Experimental Setup and Data Acquisition Methods

All experiments were performed in the Flow Control and Experimental Turbulence (FCET) laboratory at the University of Toronto Institute for Aerospace Studies (UTIAS). The details of the experimental setup and the data acquisition methods are explained in this chapter.

3.1 Experimental Setup

All tests were performed on a cylinder placed in the wind tunnel. Two load cells were used to measure the drag force on an active portion of the cylinder as shown by the free body diagram in Figure 3.1. As shown, the drag force should be linearly distributed across the span of the cylinder in the x direction. Each load cell measured three forces of (F_x, F_y, F_z) and three moments of (M_x, M_y and M_z). A press fit bearing block support was used to ensure that the cylinder rotates at a specified angle while the top load cell remained fixed. Dummy cylinders were used to decouple the boundary layer effects of the wall as shown below in Figures 3.2, 3.3 and 3.5. Four halves of the dummy cylinder were 3D printed to mount at the top and bottom of the wind tunnel test section. Figures 3.1 to 3.4 depicted the experimental

setup mounted in the wind tunnel section. The active cylinder was rotated using a rotary table that is found underneath the wind tunnel test section as shown in Figures 3.2 and 3.3. The tubes from the top load cell and rotary table were connected to the shaft of the active cylinder using flexible shaft couplings to handle misalignments. The cylindrical model was placed inside the wind tunnel with an area blockage ratio of 7% and aspect ratio (length over diameter) of 6. The blockage ratio is the ratio of the projected area of the cylinder on the flow normal plane to the cross-sectional area of the wind tunnel test section [40]. In the work done by Bishop *et al.*, the aspect ratio of the cylinder is 14 for blockage ratios of 5% and 8%. There was a low uncertainty in the Strouhal numbers of +/- 0.005 when the blockage ratios of the cylinder were 5% and 8% regardless of the wall configurations of the wind tunnel having geometrically straight, asymmetrically straight or streamlined walls [40]. Despite the blockage ratio being slightly above the 6% recommendation from [41], the Strouhal numbers were roughly around 0.19 to 0.21 in the subcritical flow regime for a cylinder at a blockage ratio of 8% [40]. Given the maximum height of the UTIAS wind tunnel test section being 800 mm and the cylinder diameter representing the width of an upper arm of a cyclist of 101.6 mm (4 Inches) as shown in Figure 3.2, an aspect ratio of 6 and a blockage ratio of 7% were appropriate testing conditions for the present work.

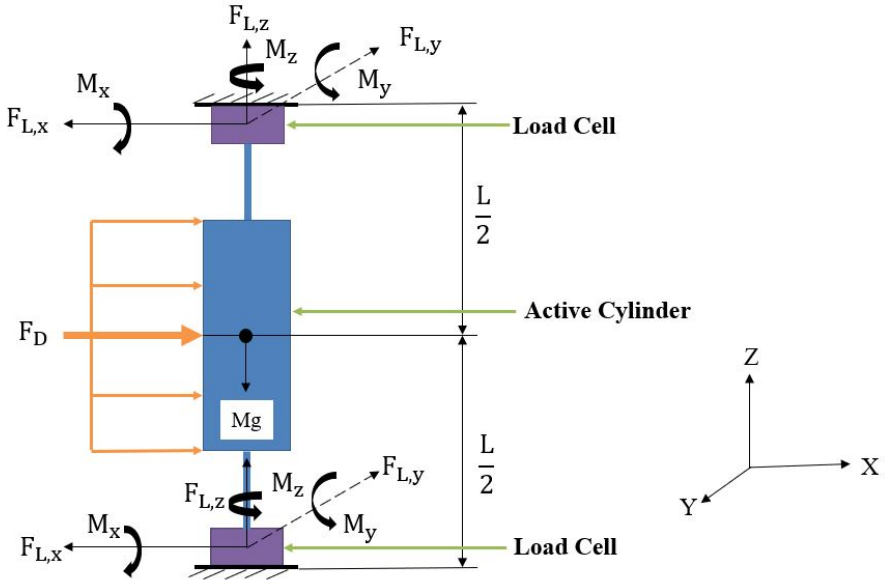


Figure 3.1: Free body diagram of the active cylinder model.

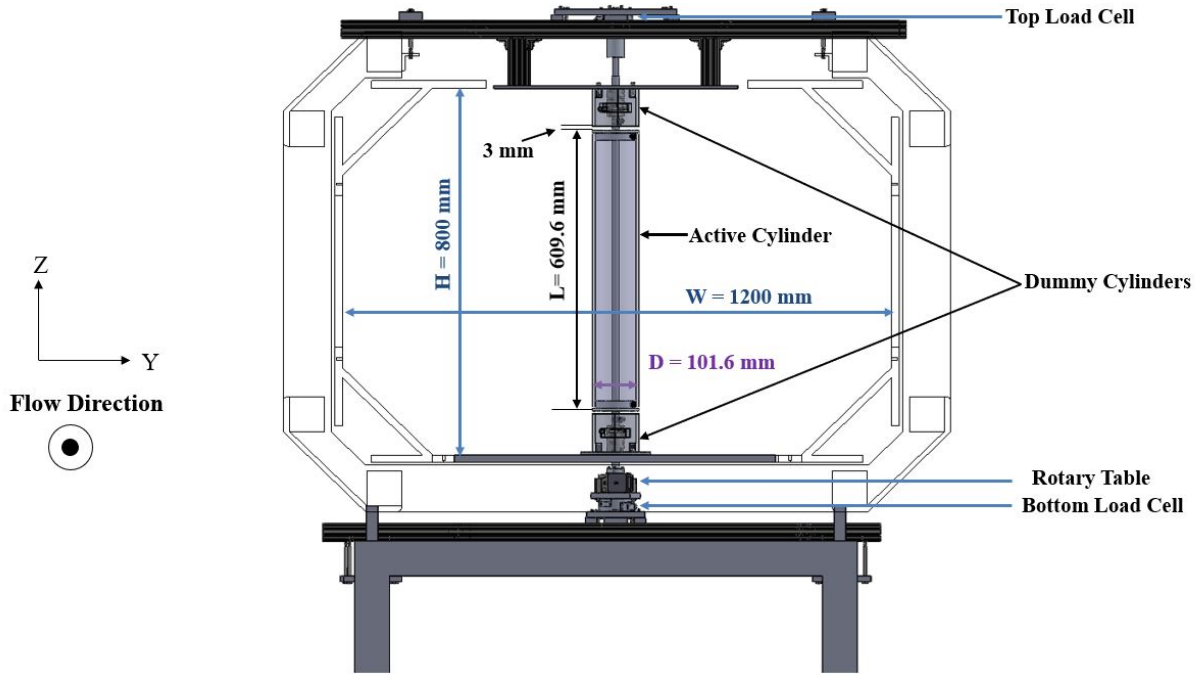


Figure 3.2: CAD model showing the dimensions of the experimental setup inside UTIAS wind tunnel test section.

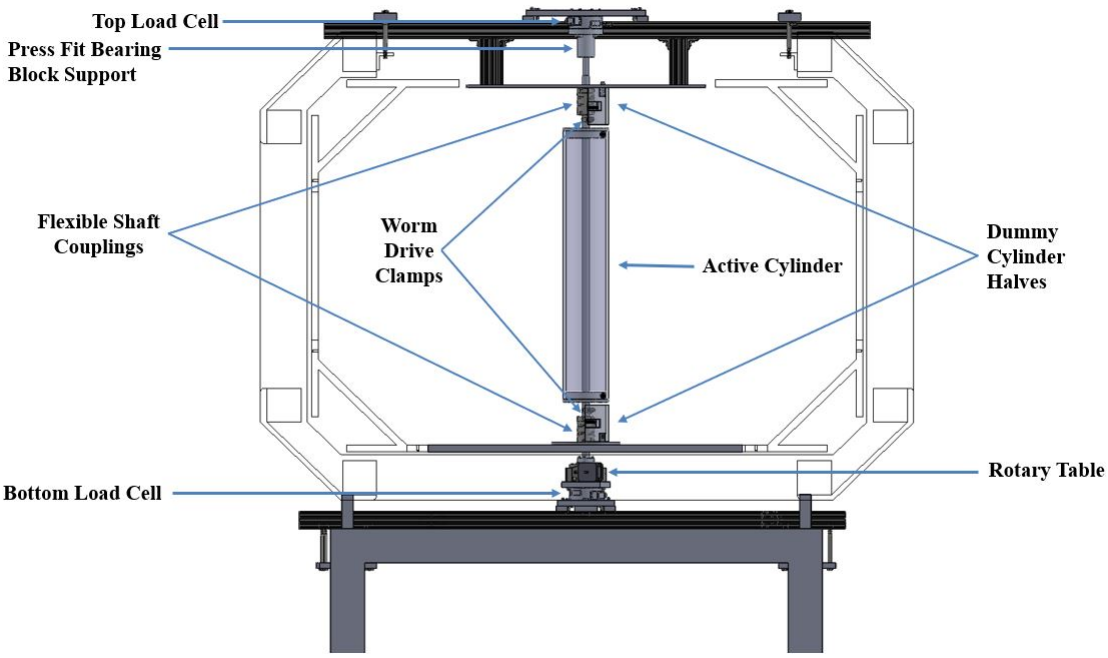


Figure 3.3: CAD model of front view of experimental setup where the top aluminum extrusion is removed to show the detail of the top load cell. Half of the dummy cylinders are also removed to show the details of the worm drive clamps and flexible shaft couplings.

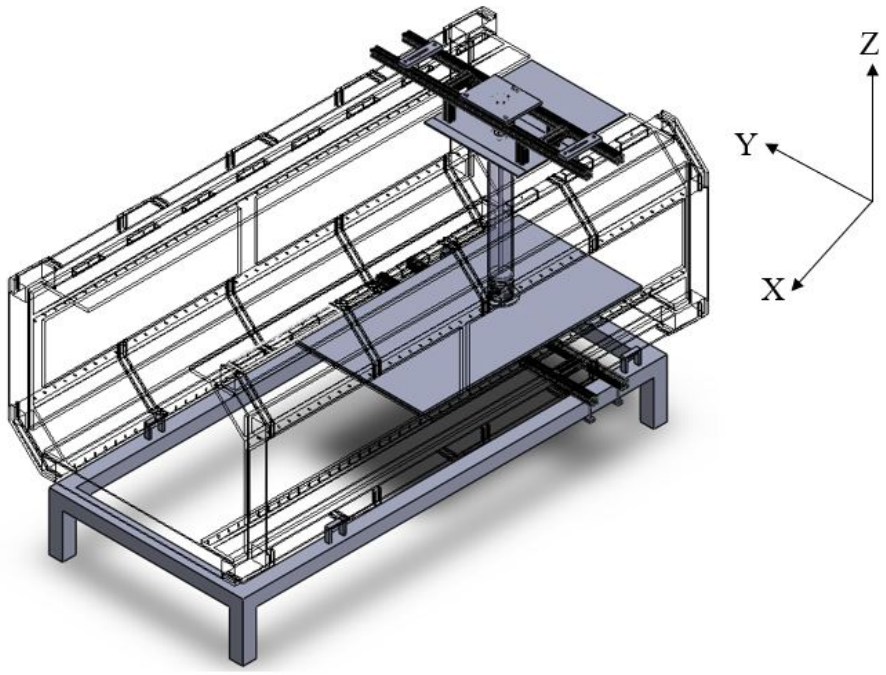


Figure 3.4: CAD model of isometric view of experimental setup.

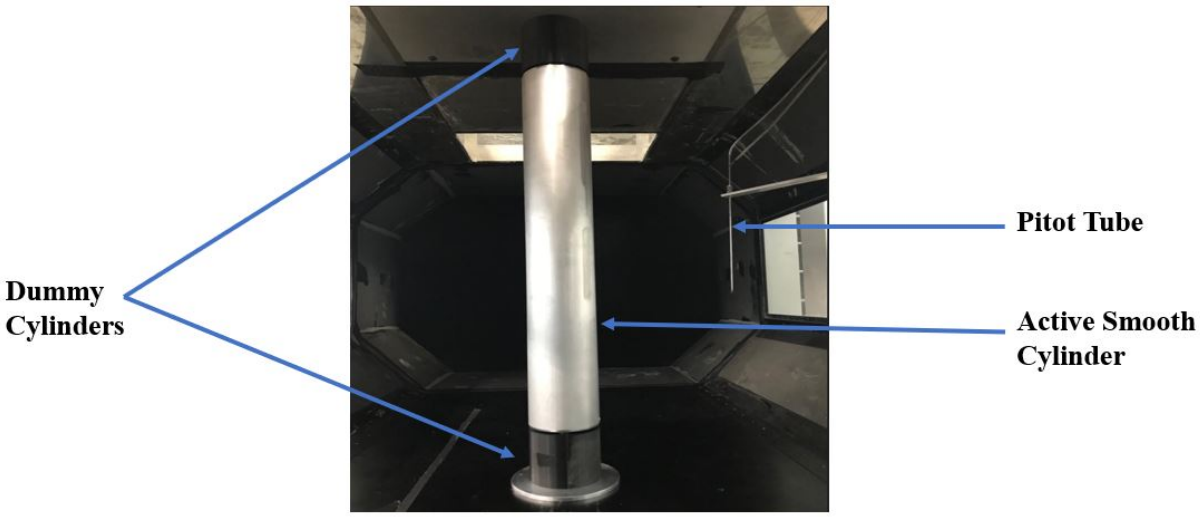


Figure 3.5: Experimental setup inside UTIAS closed loop wind tunnel.

The seams of the fabric shown in Figures 3.6 and 3.7 each had a thickness of 1 mm. They were rotated at different angles from the stagnation point of the cylinder ranging from 30° to 60° for one, two, three and four seam configurations as shown below in Figure 3.7. The 2D and zigzag tripwires with thickness of 0.5, 1 and 2 mm were 3D printed and glued onto the cylinder surface. In Figure 3.8, ZZ60K represents a zigzag tripwire with streamwise and spanwise wavelengths evaluated at $Re_D = 6.0 \times 10^4$ using Equations 2.11 and 2.12. These spatial wavelengths for a ZZ60K tripwire that consist of streamwise and spanwise wavelengths are represented as $\lambda_{Re_D=60k}$. Similarly, ZZ80K represents another zigzag tripwire with streamwise and spanwise wavelengths evaluated at $Re_D = 8.0 \times 10^4$. These spatial wavelengths for a ZZ80K tripwire are represented as $\lambda_{Re_D=80k}$. A single tripwire was attached to the fabric when rotated at angles of 30^o to 60^o from the stagnation point. They were arranged in different orientations which is discussed further in chapter 4.

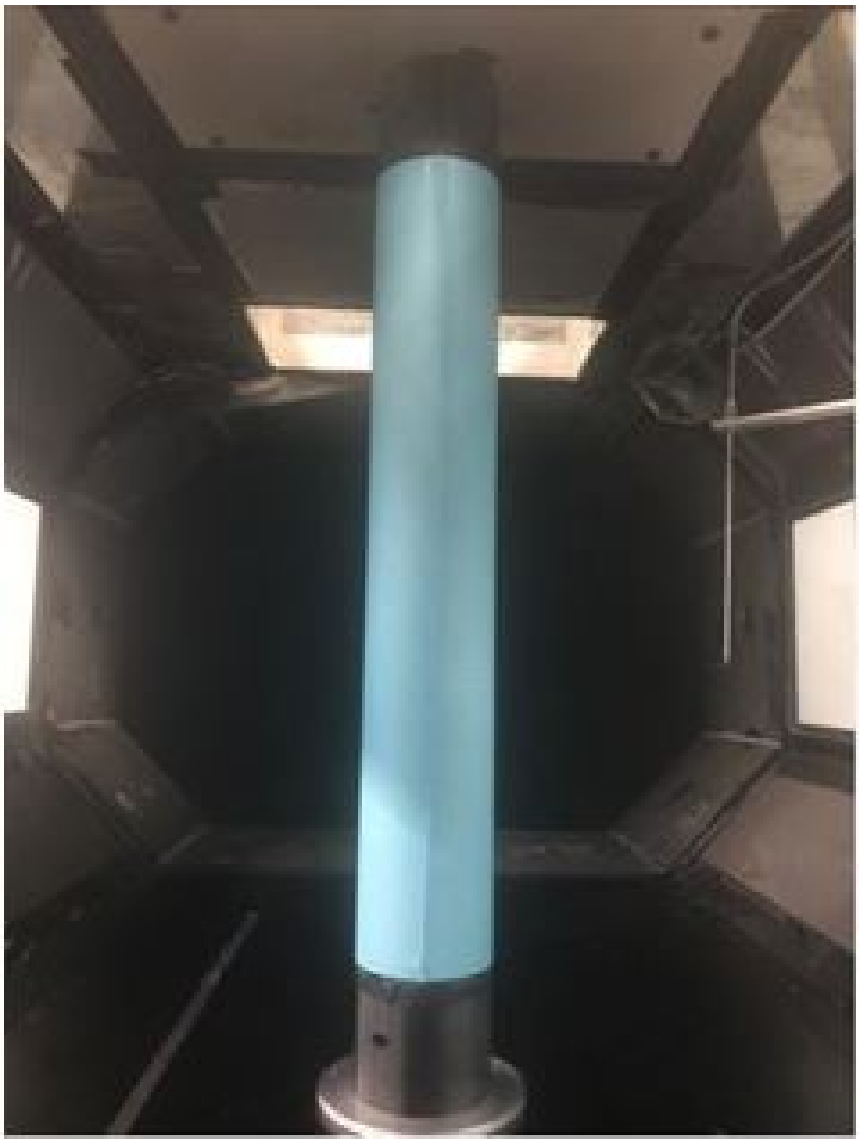


Figure 3.6: Fabric covered on a cylinder inside UTIAS wind tunnel.

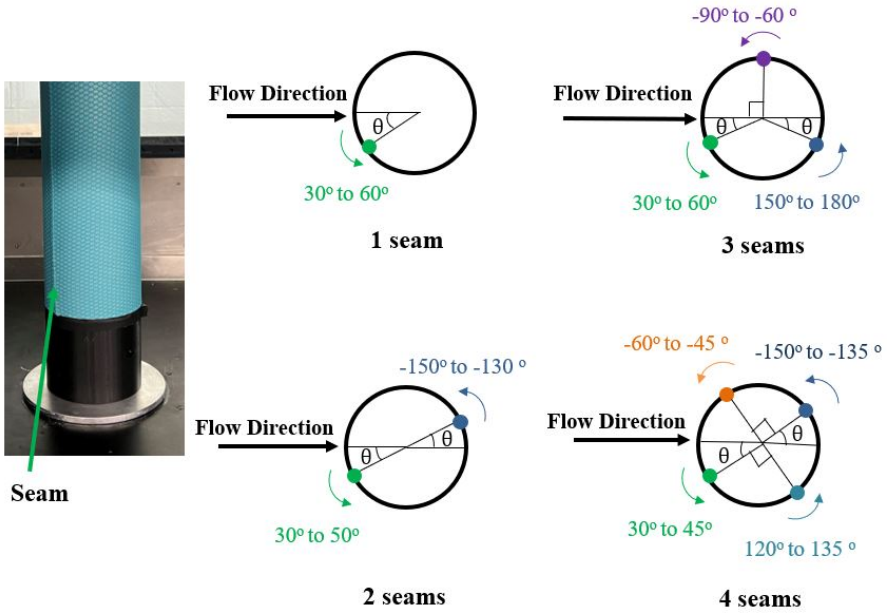


Figure 3.7: Angular variations of fabrics with one, two, three and four seams relative to the incoming flow direction.

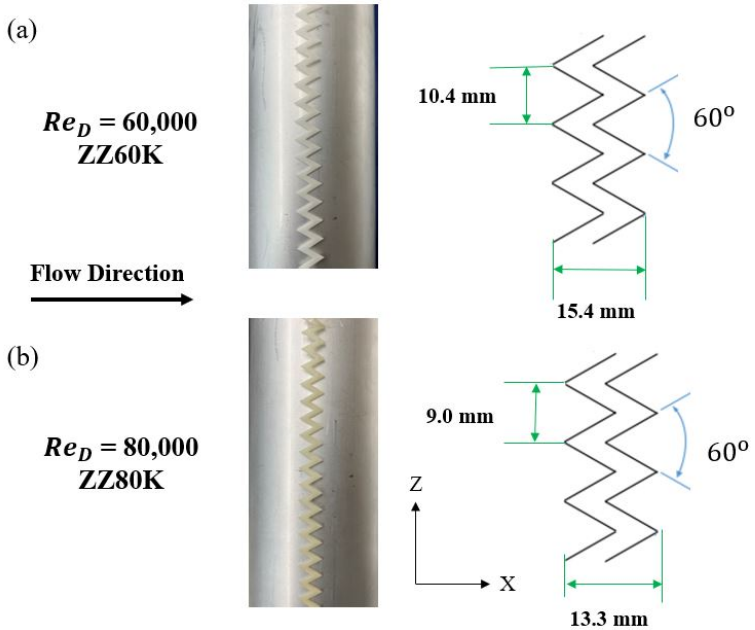


Figure 3.8: Zigzag tripwires that consist of (a) ZZ60K with $\lambda_{Re_D=60k}$ and (b) ZZ80K with $\lambda_{Re_D=80k}$.

3.2 Scanning Roughness Heights of Fabrics

A laser displacement sensor was used to scan the roughness of seven fabrics by finding the relationship between voltage and displacement. The cylinder was spun with a sampling time of 60 seconds at an arc length at 30^o rotation. The arc length at 30^o rotation represented the evaluation length, l_r where surface irregularities occur along the roughness profile of the respective fabric. The arithmetic average roughness height was obtained by taking the integral of the absolute value of the roughness profile, Z(x) of the fabric along the evaluation length and then dividing it by the respective evaluation length as shown in Equation 3.1 [42]. The integral of the roughness profile of the fabric was found by constructing a mean reference line in the profile such that the areas of the profile above and below the mean line were equal in magnitude. The sum of the absolute areas were divided by the evaluation length to obtain the arithmetic average roughness height, R_a of each fabric.

$$R_a = \frac{1}{l_r} \int_0^{l_r} |Z(x)| \, dx \tag{3.1}$$

3.3 Velocity Measurements

The velocity was measured using a pitot tube which was connected to a pressure transducer. The pressure transducer sent a voltage signal to the pitot tube that is proportional to the pressure difference between the static and total pressure. The pressure difference was equal to the dynamic pressure which is a function of density, p_∞ and velocity, U_∞. Furthermore, the velocity was determined using Equation 3.2.

$$U_\infty = \sqrt{\frac{2\Delta P}{p_\infty}} \tag{3.2}$$

3.4 Strouhal Number Measurements

Six velocities were sampled at 3 minutes for each fabric and tripwire to evaluate the vortex shedding phenomena in the wake of the cylinder with a sampling frequency of 2 kHz. The constant temperature anemometer (CTA) probe was placed 7 diameters in the x direction and 2 diameters in the y direction as shown below in Figure 3.9. The vortex shedding frequency, f was obtained using power spectral density. This helped to determine the Strouhal number at a given velocity using Equation 2.3.

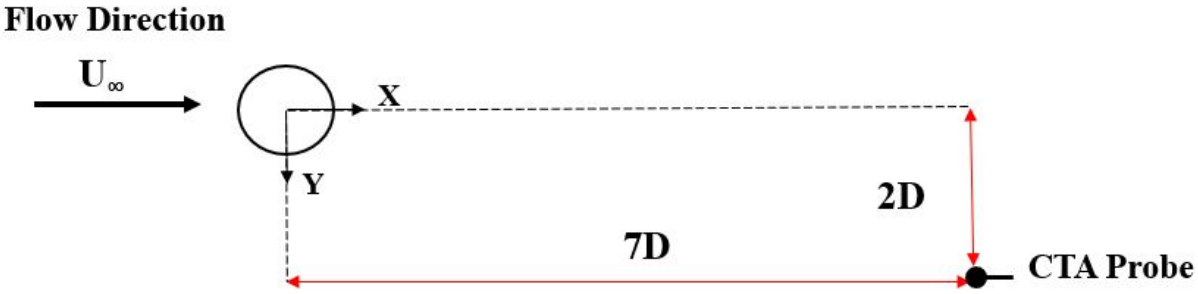


Figure 3.9: Location of constant temperature anemometer (CTA) probe relative to the center of the cylinder inside UTIAS wind tunnel.

3.5 Drag Force Measurements Using Load Cells

The drag force acting on the cylinder was determined while slowly increasing the wind tunnel velocity. This method was also used by Skeide et al. [5] to better capture variations in the C_D versus Re_D curve. Six drag static measurements of the drag coefficient values were obtained at various velocities to validate that the dynamic measurement method did not introduce potential errors. For the dynamic case, the velocity steadily increased from 5 to 20 m/s over a duration of four minutes. Each measurement was repeated five times for each fabric and tripwire case placed on the cylinder, giving 5 independent C_D-Re_D curves. These 5 curves were averaged to yield a continuous curve for each fabric and tripwire case. In Figure 3.10,

the averaged dynamic drag and static drag measurements were in agreement over a large range of Reynolds numbers for a smooth cylinder. The percentage value of uncertainty for the forces, F_x, F_y and F_z is 0.75% for a full scale reading. This helped to obtain the error bars discussed further in the appendix.

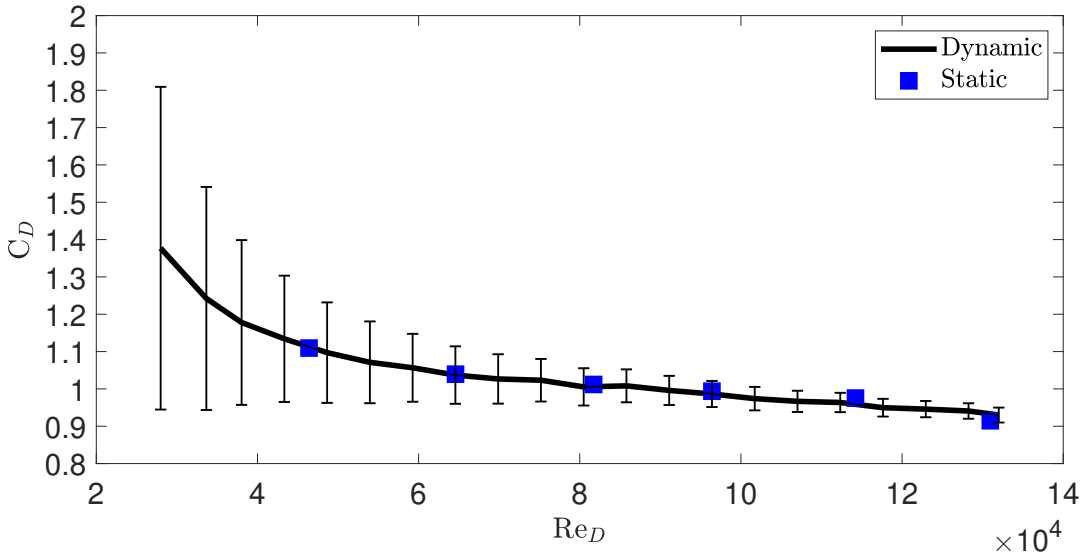


Figure 3.10: Comparison of the averaged dynamic drag measurements with static drag measurements for a smooth cylinder.

Chapter 4

Results and Discussion

4.1 Overview

In this chapter, the effect of fabrics with different arithmetic roughness heights and surface trips on the drag coefficient are presented and discussed. First in Section 4.2, the experimental setup is validated by comparing the drag coefficient and Strouhal numbers of a smooth cylinder to previous literature. After, seam locations are varied at different angles from the stagnation point for seven fabrics with one, two, three and four seams. These variations demonstrate how the drag crisis changes when reaching the Reynolds number range experienced by the upper arm region of a cyclist. In the next section, the effect of tripwires with 2D and zigzag geometry on the drag coefficient and Strouhal number is explored at various angles from the stagnation point. Thickness and spatial wavelengths are compared for the tripwires to determine its effectiveness in reducing drag at specific angles from the stagnation point. In the final section, the variation of the drag coefficient with Reynolds number is explored for tripwires attached to smooth, medium and rough fabrics. The flow behaviour of a combination of fabrics and tripwires are compared to placing only fabrics and tripwires separately on a cylinder to determine its effectiveness in drag reduction at various angles from the stagnation point.

4.2 Benchmarking Experimental Setup

The smooth cylinder is compared to previous literature such as [5] and [43] found in Figure 4.1. The comparison is done to verify that the drag coefficient values of a smooth cylinder range from 0.9 to 1.2 at subcritical Reynolds numbers with orders of magnitude of 10^4 to 10^5 before reaching the critical flow regime at a critical Reynolds number of 3.0×10^5 [43]. In the works of Skeide *et al.* and Kleissl *et al.*, the blockage ratios vary from 7% to 8% which is within the range from the present work. The work from Skeide *et al.* had a cylinder aspect ratio of 5.56 and used dummy cylinders as their end conditions similar to the experimental setup in the present work. No blockage corrections were employed from Skeide *et al.* and the present work. The drag coefficient values from Kleissl *et al.* were similar to the present work despite having a large cylinder aspect ratio greater than 10 and being placed horizontally normal to the flow direction with end plates. The values were corrected using the Maskell III blockage correction method that applies for experimental setups that use normal flat plates as their end conditions [43, 44]. Moreover, the drag coefficients and Strouhal number values obtained with the present setup compare well with the previous literature, lending confidence in the setup.

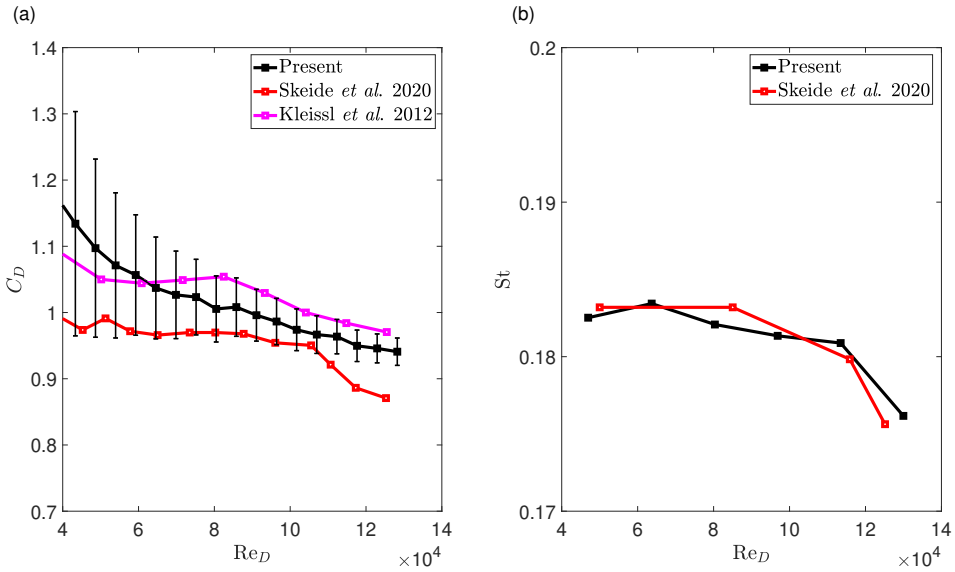


Figure 4.1: Comparison of (a) drag coefficient and (b) Strouhal number at given Reynolds numbers for a smooth cylinder and literature.

4.3 Effects of Fabric Roughness and Seams

4.3.1 Effects of Fabric Patterns and Roughness

The effect of surface roughness associated with different fabrics is considered. A series of textile sleeves were created with a single seam. The seven different fabrics considered are shown in Figure 4.2. Scans of the surface geometry were made to determine the arithmetic average roughness height. An example of the roughness profile is shown for fabric 3 in Figure 4.3. The green and red shaded regions have equal areas. The sum of the areas enclosed between the roughness profile and the mean reference line was divided by the evaluation length which is the arc length of the cylinder at 30^o rotation to obtain the arithmetic average roughness height of a fabric. A summary of the arithmetic average roughness heights for each the fabrics is given in Table 4.1 in order of the smoothest (F7 with $R_a = 0.03$ mm) to roughest (F3 with $R_a = 0.1$ mm).

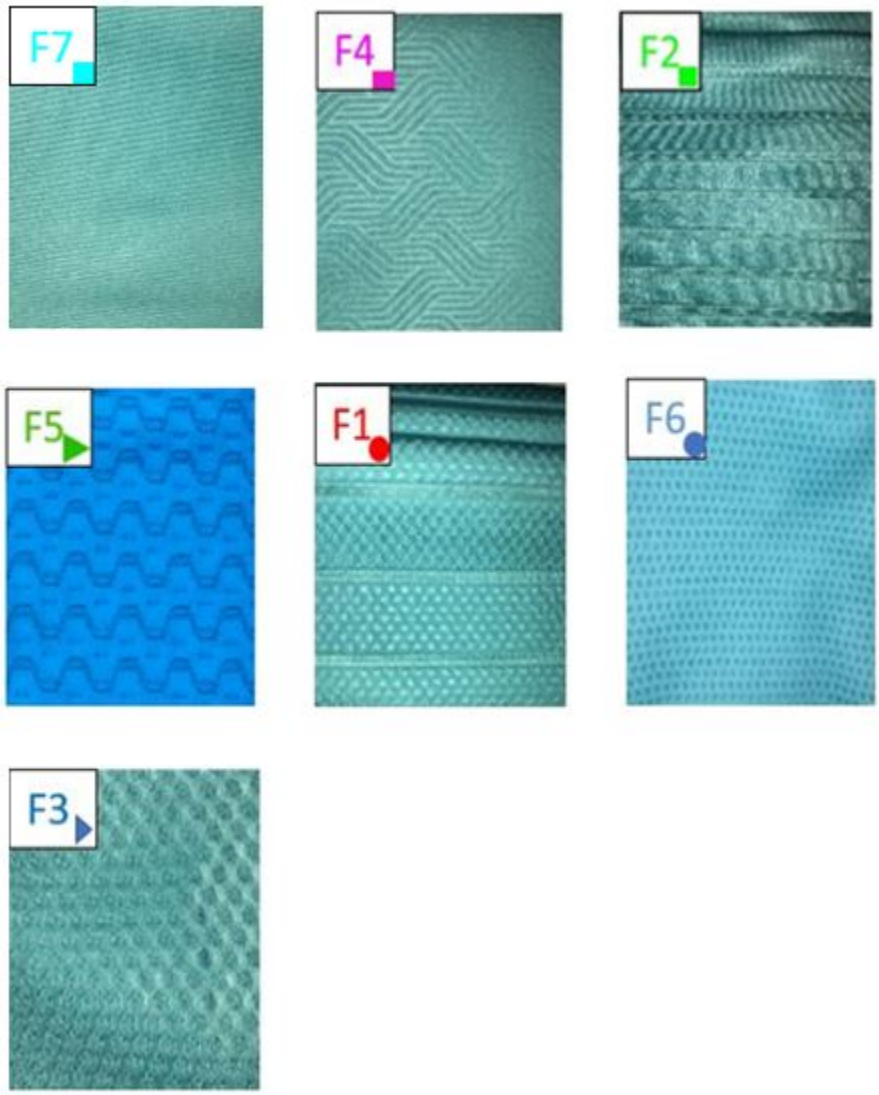


Figure 4.2: Seven tested fabrics in order from smoothest (F7) to roughest (F3) where each image has dimensions of $1\frac{1}{3}$ Inches x $1\frac{5}{8}$ Inches given that the width scale is 1:3 and the length scale is 1:20 relative to the actual fabric.

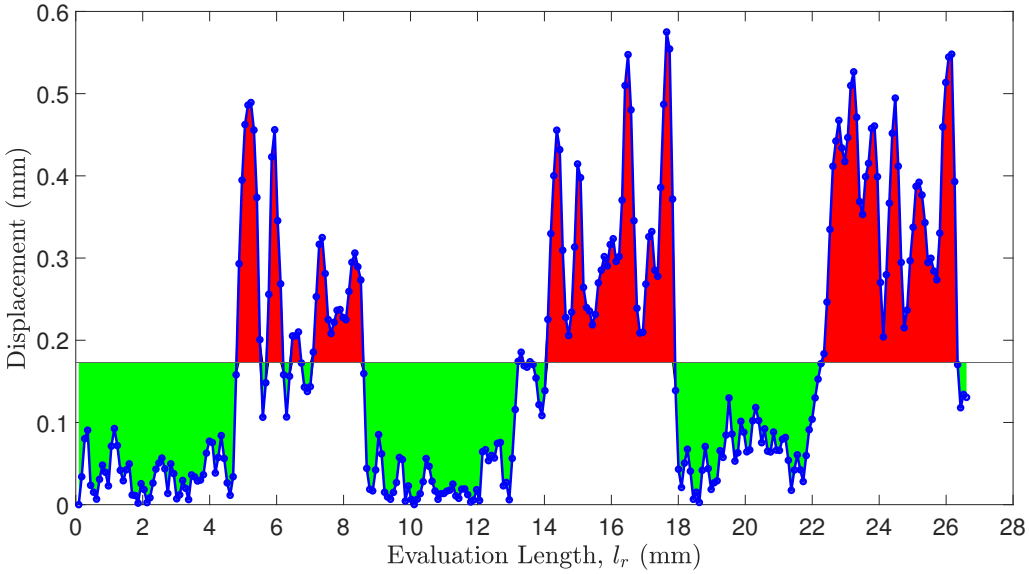


Figure 4.3: Roughness profile of fabric 3 along the evaluation length, l_r.

Table 4.1: Fabrics with relative roughness ratios between arithmetic average roughness heights and cylinder diameter in ascending order where fabric 7 (F7) has the lowest roughness and fabric 3 (F3) is the roughest.

Fabric #	R_a	k/D
F7	0.030 mm	2.95×10^{-4}
F4	0.037 mm	3.64×10^{-4}
F2	0.055 mm	5.41×10^{-4}
F5	0.058 mm	5.71×10^{-4}
F1	0.065 mm	6.40×10^{-4}
F6	0.072 mm	7.09×10^{-4}
F3	0.10 mm	9.84×10^{-4}

Each fabric sample had at least one seam that is required to create the sleeve. The seam was placed at 180^o from the leading edge of the cylinder during aerodynamic testing to prevent any possible trip effect by it. The drag coefficient as a function of Reynolds number is plotted in Figure 4.4 for seven different fabrics. Fabrics 1, 3 and 6 are found to be the roughest in reaching the drag crisis at a smaller critical Reynolds number in the critical flow regime. Fabrics 4 and 7 appeared to be smoother with the least impact on drag reduction as shown in Figure 4.4. Fabrics with a larger arithmetic average roughness height

can reach a minimum drag coefficient at a smaller critical Reynolds number compared to smoother fabrics without the effect of the seam. Rougher fabrics 3 and 6 that have relative roughness ratios, k/D ranging from 7.09×10^{-4} to 9.84×10^{-4} share a similar flow behaviour at Reynolds numbers past 1.0×10^5 in reaching a minimum drag coefficient of approximately 0.57 at a critical Reynolds number of 1.30×10^5. In the work from Zheng *et al.*, a grooved fabric with a higher arithmetic average roughness ratio, k/D of 2.49×10^{-3} achieves a similar minimum drag coefficient as fabrics 3 and 6 from the present work but at a smaller critical Reynolds number of 8.0×10^4 [20]. A minimum drag coefficient that was slightly below the values for fabrics 3 and 6 of 0.53 occurred at a critical Reynolds number of 1.23×10^5 at a relative maximum roughness height ratio, k_s/D of 1.33×10^{-3} from Skeide *et al.* [5]. In the work of Skeide *et al.*, it was observed that the drag coefficient had rapidly decreased from a Reynolds number of 6.0×10^4 to a minimum value of 0.53 at a critical Reynolds number of 1.23×10^5 for the surface coating, $S_A\ h_{0.5}\ \triangle_5$. However in the present work, the drag coefficient values for the roughest fabrics began to decrease at larger Reynolds numbers past 1.0×10^5 before achieving a minimum drag coefficient of 0.57 at a critical Reynolds number of 1.30×10^5.

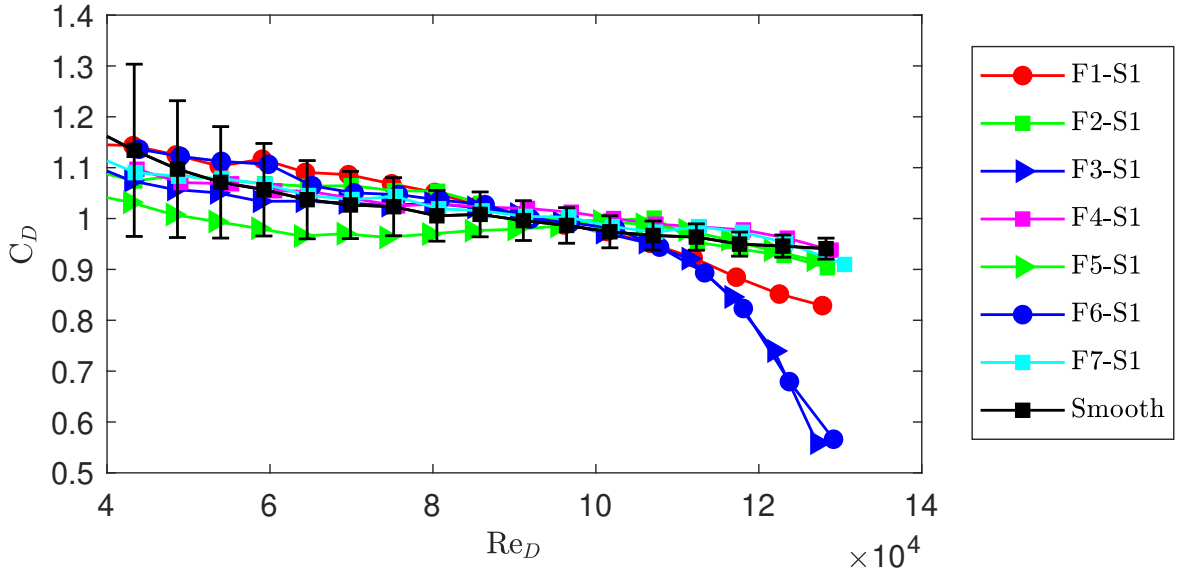


Figure 4.4: Variation of the drag coefficient with Reynolds number for all seven tested fabrics with one seam placed 180^o from the stagnation point.

4.3.2 Effect of Seam Locations for Fabrics with Multiple Seams

The variation of the drag coefficient and Strouhal numbers for all seven fabrics with one, two, three and four seams is evaluated. In the critical flow regime, the drag crisis phenomenon occurs when the minimum drag coefficient is achieved at the critical Reynolds number due to the separation point moving downstream, decreasing the wake width [10, 16]. In plots that illustrate the variation in drag coefficients with Reynolds numbers from the thesis, the drag crisis was shown by selecting the minimum drag coefficient values at the corresponding critical Reynolds numbers for the tested cases. The drag coefficient values are averaged at different Reynolds number ranges. The Reynolds numbers ranging from 6.0×10^4 to 1.0×10^5 have a greater emphasis in the discussion of the results because it is obtained when the cyclist's upper arm that has a width of 4 inches is subject to racing speeds of 10 to 15 m/s. It is observed that a larger Strouhal number occurs at smaller drag coefficients from the tested cases. This is a similar finding from the work of Skeide *et al.,* where the Strouhal number is relatively constant until the drag crisis is achieved at

which point the shedding frequency increases rapidly, before settling back to a supercritical state that resembles the subcritical state based on the Reynolds numbers explored [5]. Fabrics with low, medium and high roughness that have one and three seams placed at an angle from the stagnation point that yield drastic drag reduction were compared to each other.

The drag coefficient and Strouhal number as a function of Reynolds number is plotted in Figures 4.5 and 4.6 for fabric 1 with one, two, three and four seams. In Figure 4.5(a), fabric 1 with one seam placed 60^o from the stagnation point can decrease the drag coefficient to values of roughly 0.8 at Reynolds numbers ranging from 8.0×10^4 to 1.2×10^5 before achieving a minimum drag coefficient of 0.70 at a critical Reynolds number of 1.30×10^5. When fabric 1 with two seams is placed 45^o and 50^o from the stagnation point as shown in Figure 4.5(c), a similar flow behaviour is observed past a Reynolds number of 9.0×10^4. Adding four seams to fabric 1 allows the minimum drag coefficient values to be approximately 0.65 to 0.70 at angles of 35° to 45° from the stagnation point at critical Reynolds numbers ranging from 8.0×10^4 to 9.0×10^4 from Figure 4.6(c). The drag coefficient and Strouhal number values are similar at angles of 35^o to 45^o from the stagnation point in the transcritical flow regime at Reynolds numbers greater than 1.1×10^5.

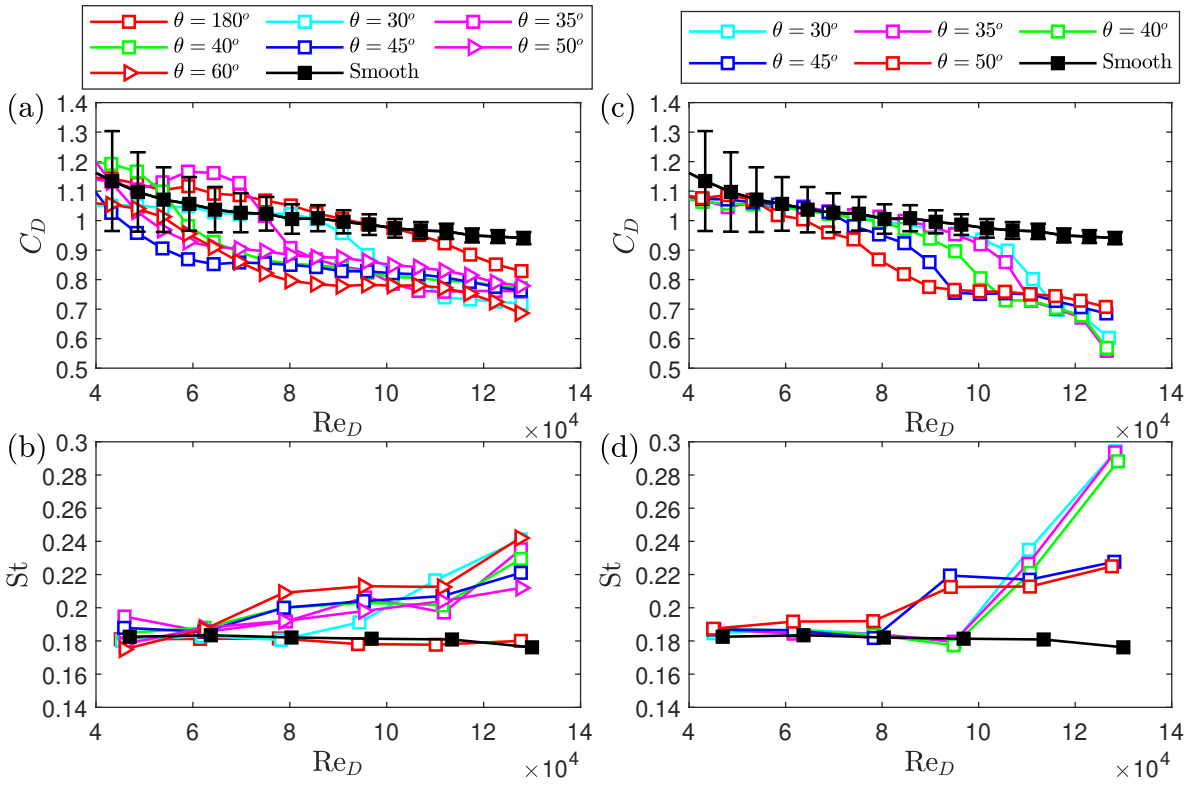


Figure 4.5: Variation of the drag coefficient and Strouhal number at given Reynolds numbers and angular locations of fabric 1 with one seam (a), (b) and two seams (c), (d).

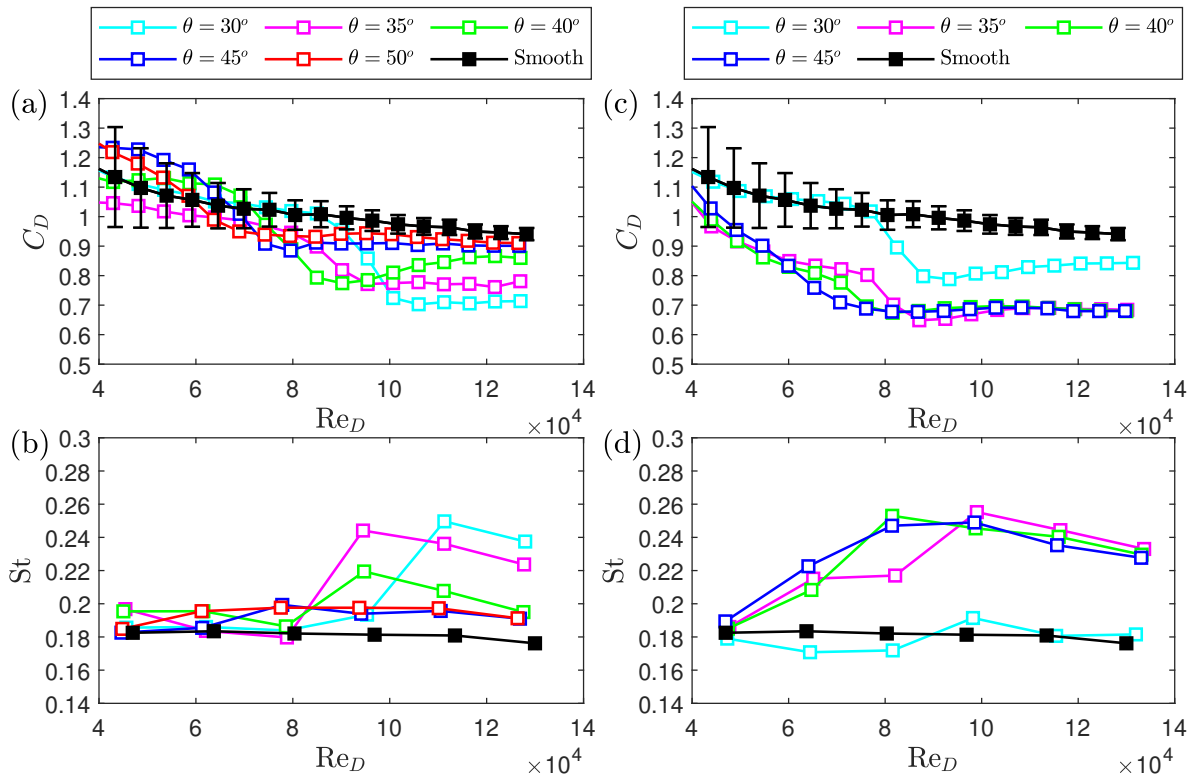


Figure 4.6: Variation of the drag coefficient and Strouhal number at given Reynolds numbers and angular locations of fabric 1 with three seams (a), (b) and four seams (c), (d).

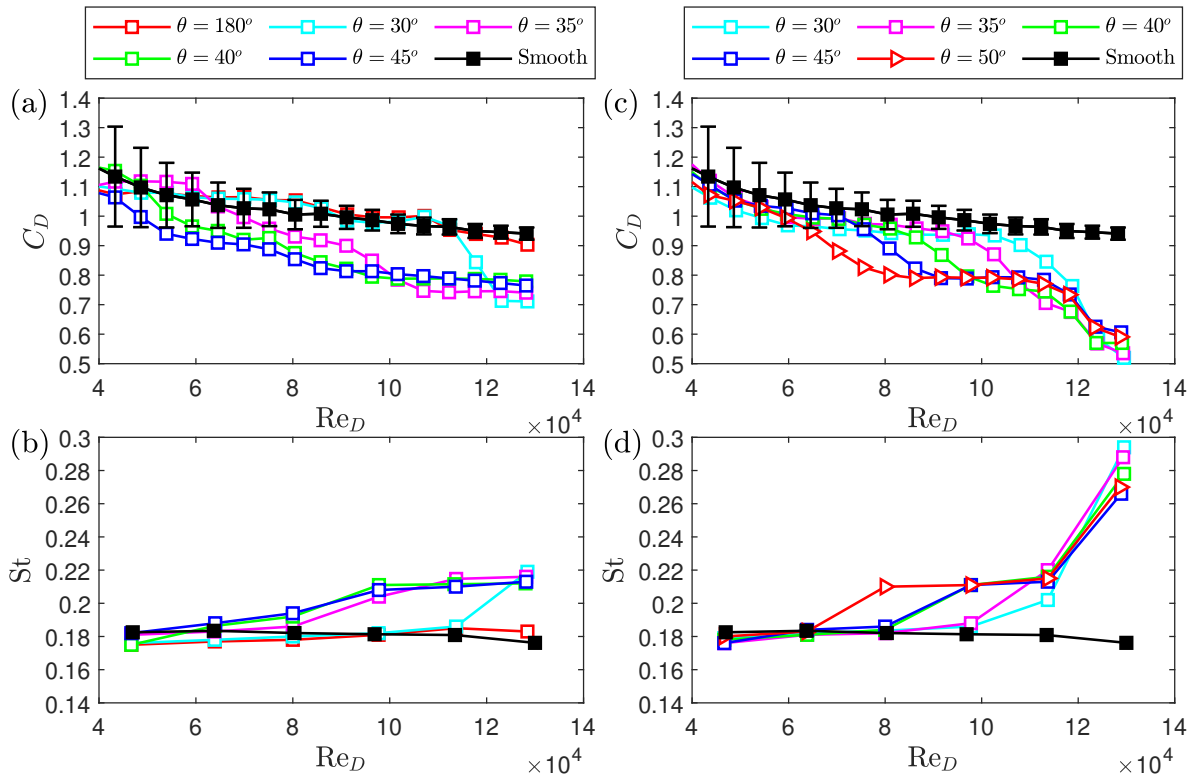


Figure 4.7: Variation of the drag coefficient and Strouhal number at given Reynolds numbers and angular locations of fabric 2 with one seam (a), (b) and two seams (c), (d).

The drag coefficient and Strouhal number as a function of Reynolds number is plotted in Figures 4.7 and 4.8 for fabric 2 with one, two, three and four seams. In Figure 4.7(a), fabric 2 with one seam has maintained an average drag coefficient value of 0.80 from a Reynolds number of 8.0×10^4 and greater when placed at angles of 40^o and 45^o from the stagnation point. Adding the second seam for fabric 2 decreases the drag coefficient to an average value of approximately 0.80 at Reynolds numbers experienced by the upper arm region of a cyclist of 8.5×10^4 to 1.0×10^5 before reaching a minimum drag coefficient of 0.60 at a critical Reynolds number of 1.30×10^5 when placed 45^o and 50^o from the stagnation point. At Reynolds numbers past 1.20×10^5, fabric 2 with two seams have the same flow behaviour at all angles in Figure 4.7(c). At 60°, fabric 2 with three seams has the lowest drag coefficient values at a large range of Reynolds numbers from 6.0×10^4 and greater compared to other angles in Figure 4.8(a). At 30°, fabric 2 with four seams reaches the lowest drag coefficient of

0.58 at the highest critical Reynolds number of 1.3×10^5 compared to other angles in Figure 4.8(c). In Figure 4.8(c), a minimum drag coefficient of 0.63 is achieved at the smallest critical Reynolds number of approximately 9.0×10^4 when four seams of fabric 2 are placed 45^o from the stagnation point compared to other angles.

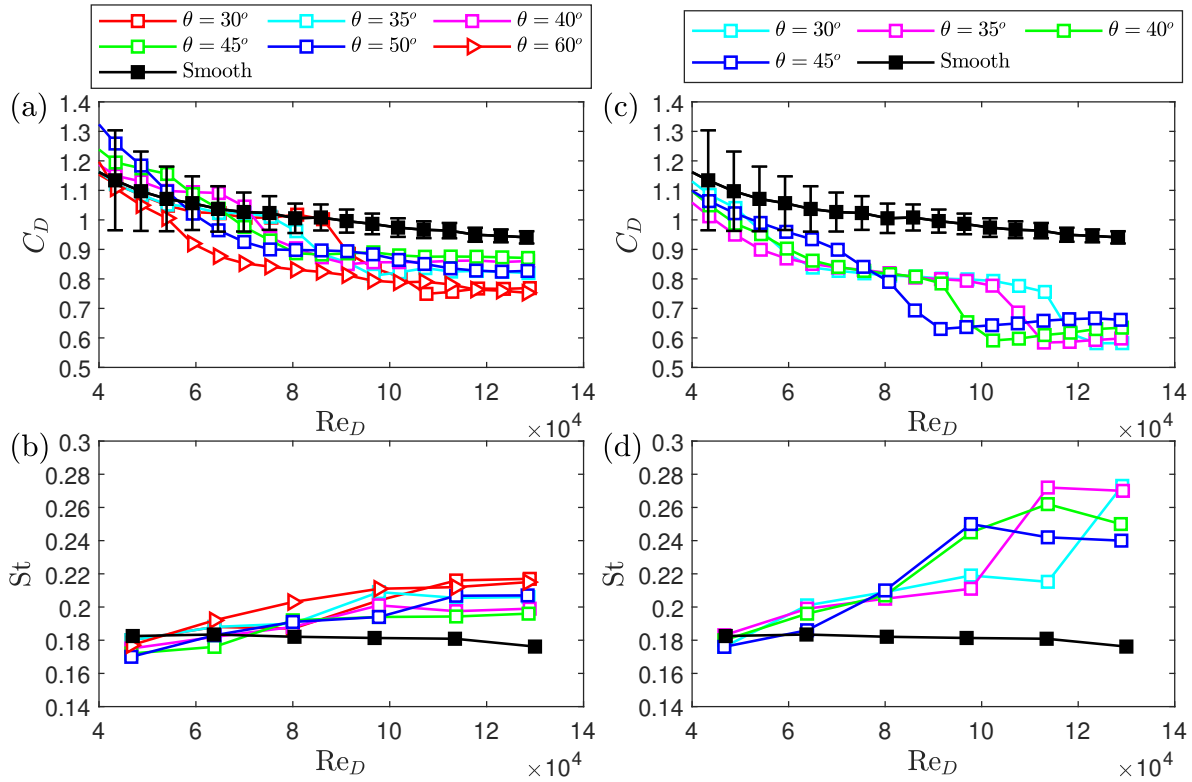


Figure 4.8: Variation of the drag coefficient and Strouhal number at given Reynolds numbers and angular locations of fabric 2 with three seams (a), (b) and four seams (c), (d).

The drag coefficient and Strouhal number as a function of Reynolds number is plotted in Figures 4.9 and 4.10 for fabric 3 with one, two, three and four seams. The critical flow regime for fabric 3 with one seam occurs at a critical Reynolds number of 1.3×10^5 for all angles including 180° where the seam is located at the rear of the incoming flow direction. This shows fabric 3 to be the roughest fabric that decreases the drag coefficient values at the smallest critical Reynolds number compared to other fabrics when one seam is placed 180° from the stagnation point as shown in Figures 4.4 and 4.9(a). In Figure 4.9(c), fabric 3 with

two seams reaches a drag crisis for all angles where the average minimum drag coefficient is approximately 0.65 at a critical Reynolds number of approximately 1.15×10^5. In Figure 4.10 (a), the drag crisis for fabric 3 with three seams placed at angles of 30^o to 50^o from the stagnation point occur at critical Reynolds numbers ranging from approximately 7.0×10^4 to 9.0×10^4. However, the transcritical flow regime at angles of 30^o to 50^o from the stagnation point are close to the drag coefficient values found for a smooth cylinder. When fabric 3 with three seams are placed 60° from the stagnation point from Figure 4.10(a), the drag coefficients are lower than other angles with an average value of approximately 0.68 at Reynolds numbers ranging from 6.0×10^4 to 1.3×10^5. The critical flow regime occurs at critical Reynolds numbers ranging from 7.5×10^4 to 9.0×10^4 when four seams of fabric 3 are placed at angles of 30° to 45° from the stagnation point as shown in Figure 4.10(c) with 30^o yielding the highest minimum drag coefficient of approximately 0.70.

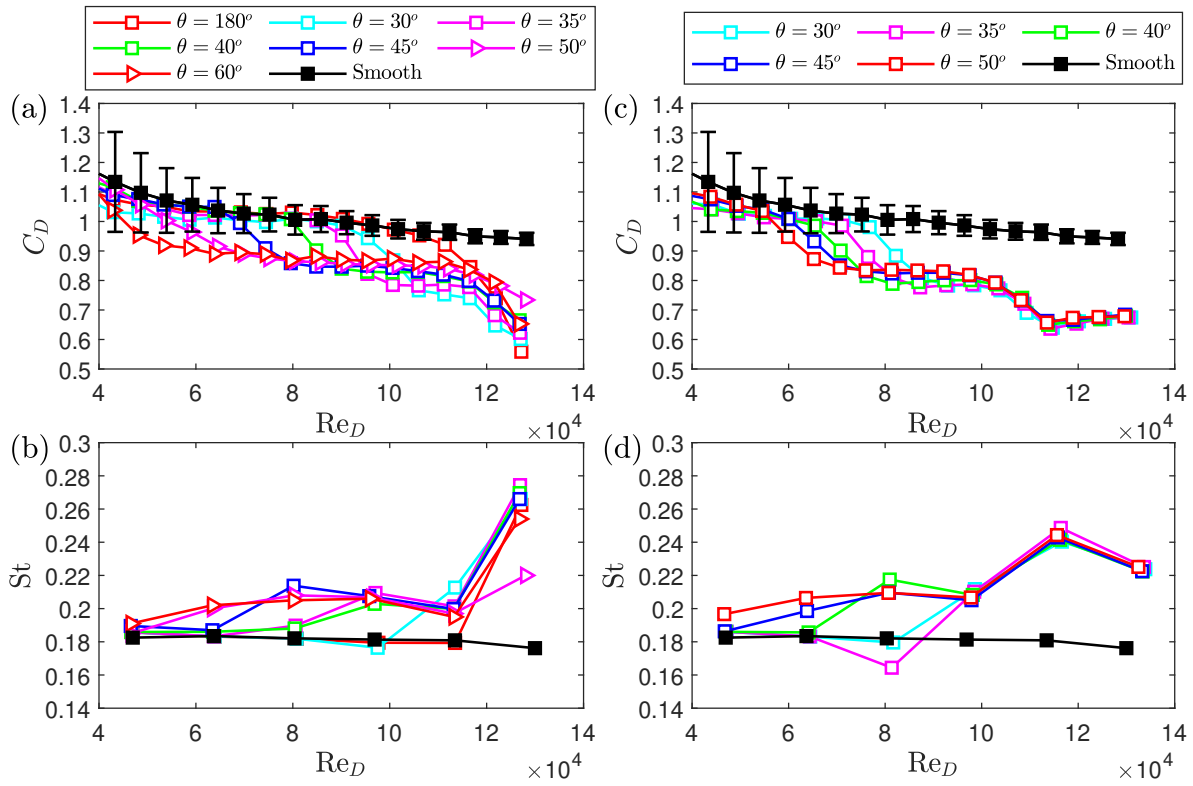


Figure 4.9: Variation of the drag coefficient and Strouhal number at given Reynolds numbers and angular locations of fabric 3 with one seam (a), (b) and two seams (c), (d).

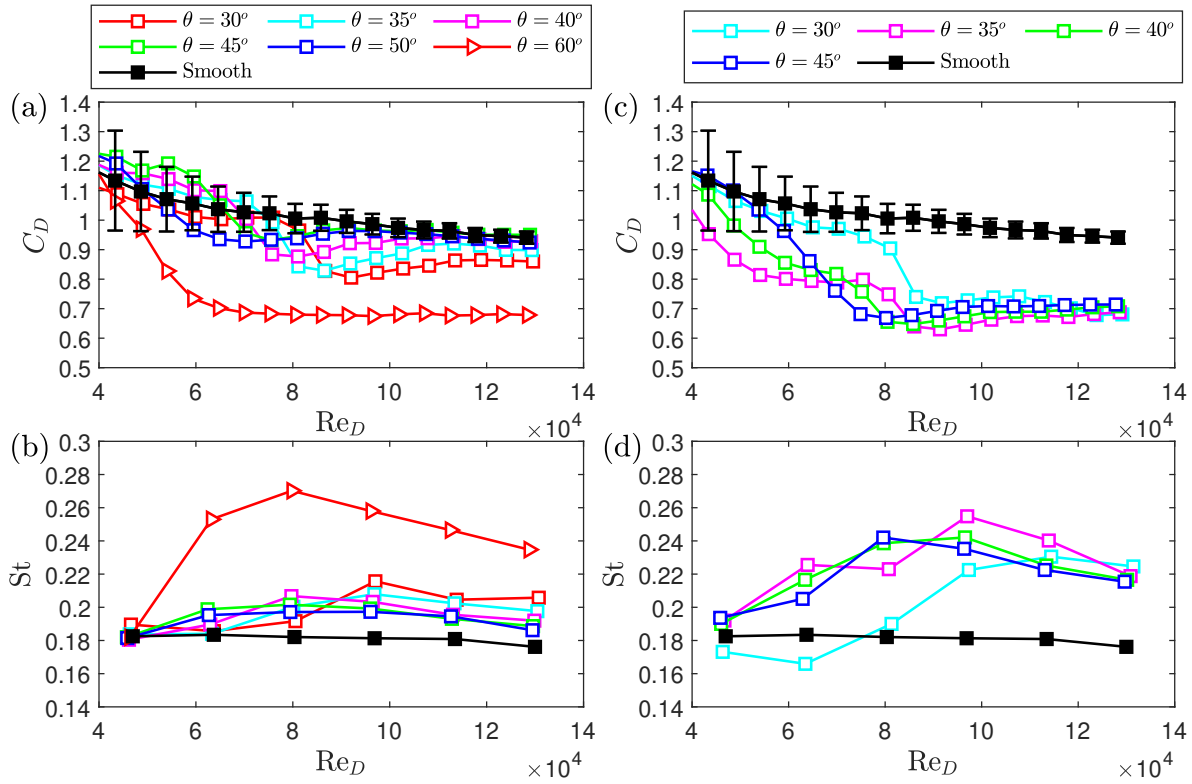


Figure 4.10: Variation of the drag coefficient and Strouhal number at given Reynolds numbers and angular locations of fabric 3 with three seams (a), (b) and four seams (c), (d).

The drag coefficient and Strouhal number as a function of Reynolds number is plotted in Figures 4.11 and 4.12 for fabric 4 with one, two, three and four seams. In Figure 4.11(a), fabric 4 with one seam shares a similar flow behaviour past a Reynolds number of 8.0×10^4 when placed 50^o and 60^o from the stagnation point. It is most effective in reducing the drag coefficient to an average value of 0.80 at Reynolds numbers experienced by the upper arm region of a cyclist ranging from 6.0×10^4 to 1.0×10^5 when fabric 4 with one seam is placed 60^o from the stagnation point compared to other angles. On the other hand, the drag coefficient values are close to the values found for a smooth cylinder at Reynolds numbers ranging from 4.0×10^4 to 1.0×10^5 when a single seam of fabric 4 is placed at angles of 30° and 35° from the stagnation point. When a single seam is placed 180^o from the stagnation point, the drag coefficient values are also close to the values found for a smooth cylinder for all Reynolds numbers. In Figure 4.11(c), fabric 4 with two seams share a similar flow

behaviour past a Reynolds number of 1.0×10^5 when placed 45^o and 50^o from the stagnation point. Fabric 4 with three seams achieves the lowest drag coefficient of approximately 0.66 at a critical Reynolds number of 8.0×10^4 when placed 60^o from the stagnation point in Figure 4.12(a). The drag coefficient values for the supercritical flow regime at 60^o are lower than the drag coefficient values at the critical flow regime for lower angles from the stagnation point for fabric 4 with three seams. At 45^o from the stagnation point in Figure 4.12(c), fabric 4 with four seams decreases the drag coefficient to a minimum value of 0.67 at a critical Reynolds number of approximately 1.0×10^5 and remains relatively constant at higher Reynolds numbers.

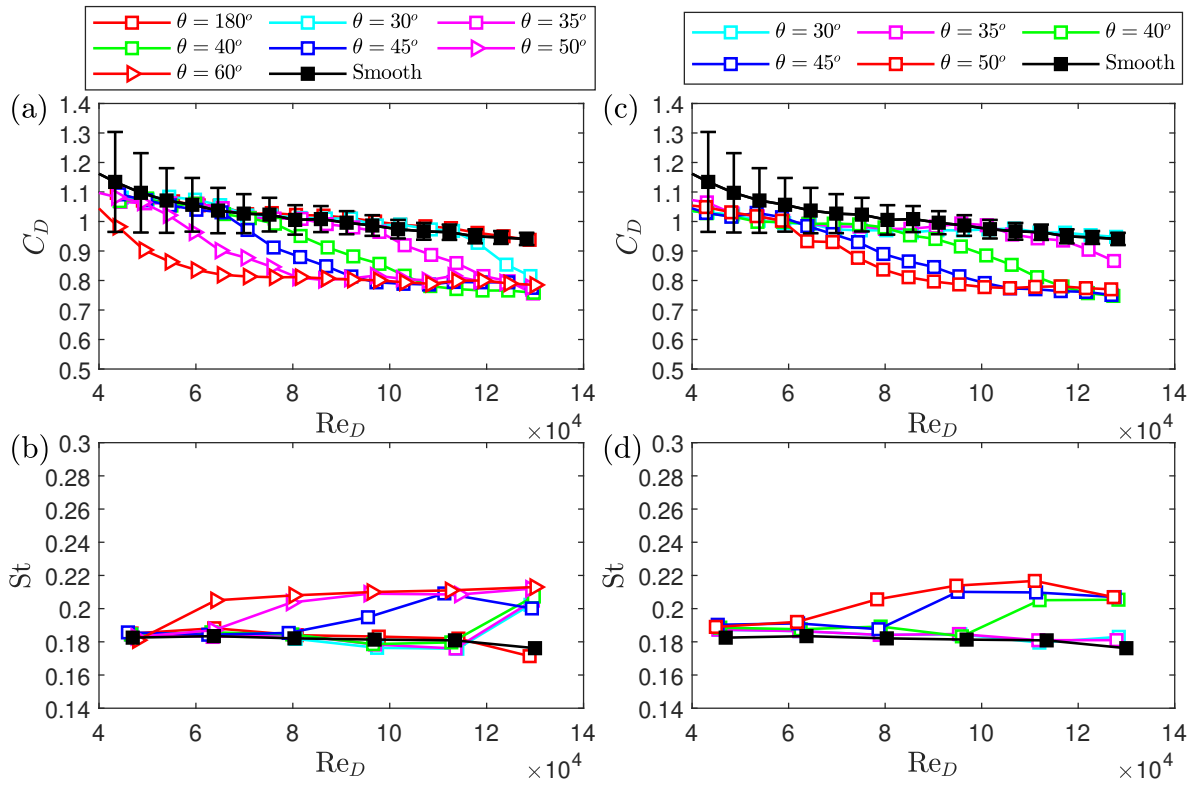


Figure 4.11: Variation of the drag coefficient and Strouhal number at given Reynolds numbers and angular locations of fabric 4 with one seam (a), (b) and two seams (c), (d).

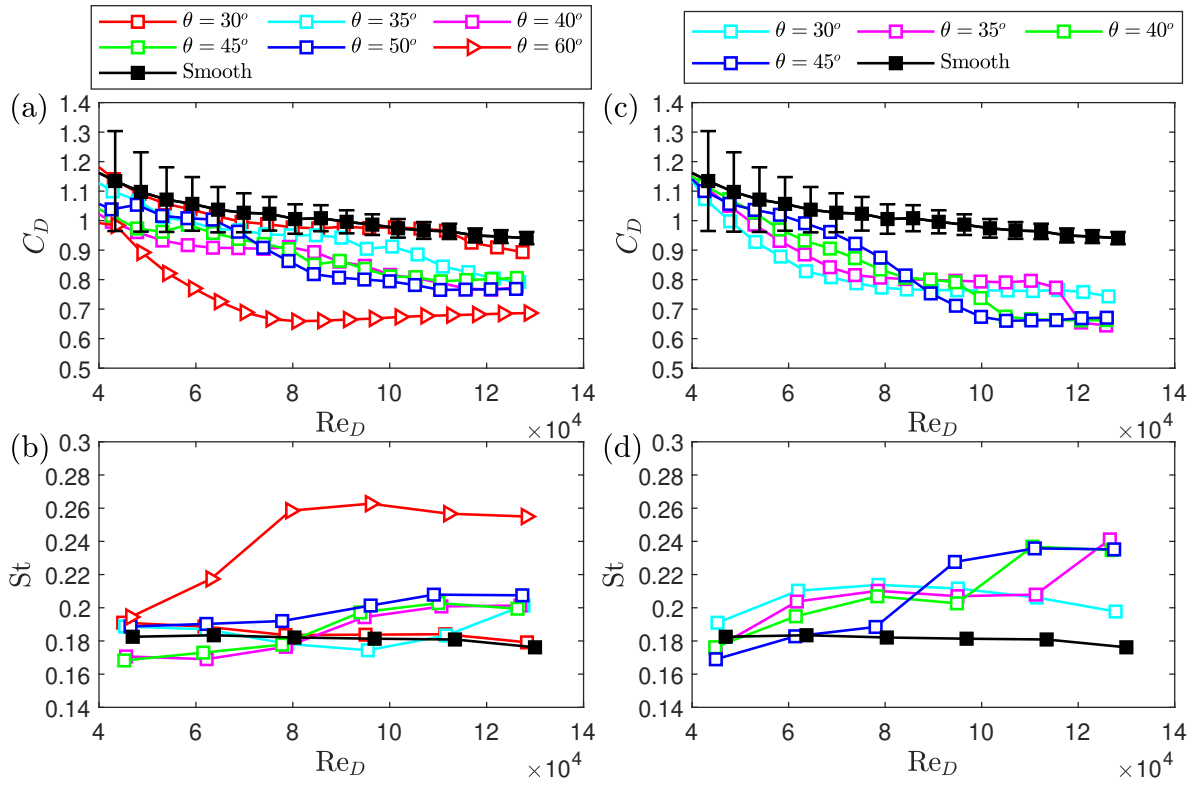


Figure 4.12: Variation of the drag coefficient and Strouhal number at given Reynolds numbers and angular locations of fabric 4 with three seams (a), (b) and four seams (c), (d).

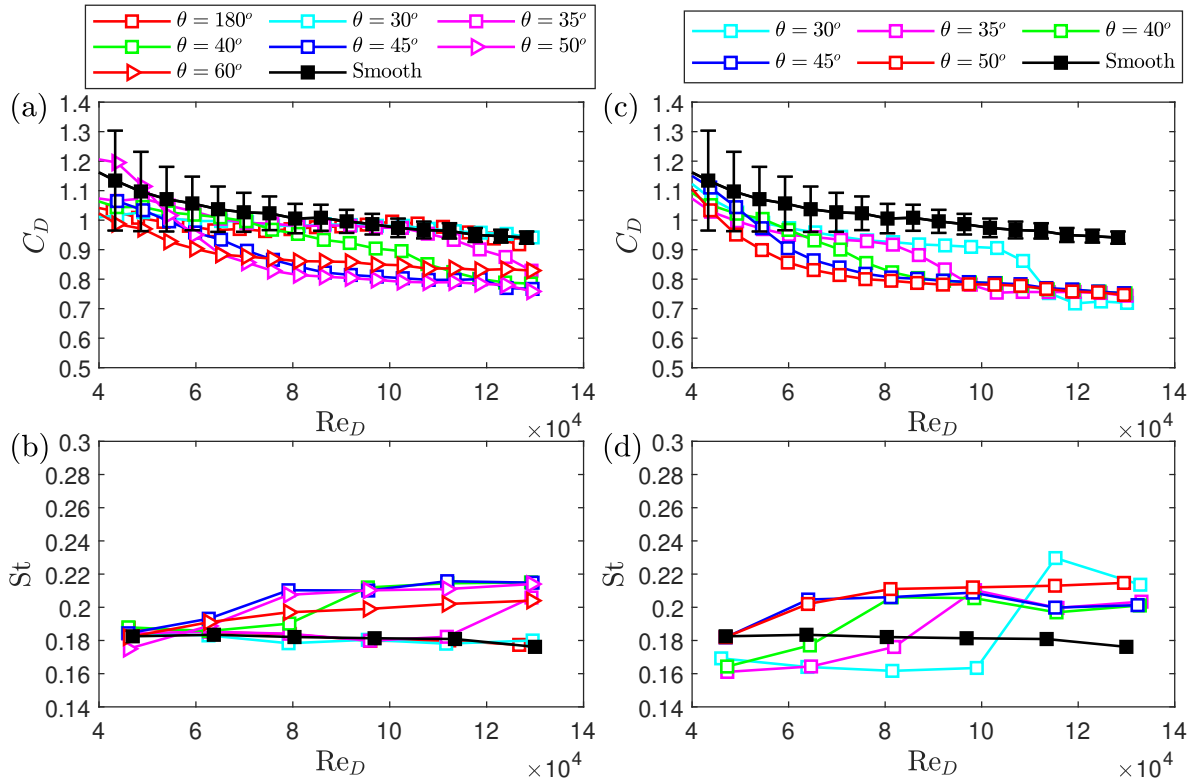


Figure 4.13: Variation of the drag coefficient and Strouhal number at given Reynolds numbers and angular locations of fabric 5 with one seam (a), (b) and two seams (c), (d).

The drag coefficient and Strouhal number as a function of Reynolds number is plotted in Figures 4.13 and 4.14 for fabric 5 with one, two, three and four seams. In Figure 4.13(a), placing a single seam of fabric 5 at angles of 45^o and 50^o from the stagnation point is effective in decreasing the drag at Reynolds numbers experienced by the upper arm region of a cyclist of 8.0×10^4 and greater with a constant average value of approximately 0.80. On the other hand, placing the single seam 30° and 180° from the stagnation point causes the drag coefficient values to be close to the values found for a smooth cylinder at all Reynolds numbers tested. In Figure 4.13(c), the drag coefficient values are relatively constant with an average value of 0.80 when two seams of fabric 5 are placed at angles of 40^o to 50^o from the stagnation point at Reynolds numbers greater than 8.0×10^4. Fabric 5 with two seams reaches the drag crisis at the largest critical Reynolds number past 1.2×10^5 when placed 30^o from the stagnation point compared to other angles in Figure 4.13(c). The drag coefficient

values for fabric 5 with three seams gradually decreases from a value of approximately 0.85 at a Reynolds number of 6.0×10^4 and reaches a lower value of 0.70 at Reynolds numbers past 8.0×10^4 when placed 60° from the stagnation point in Figure 4.14(a). Fabric 5 with three seams placed 60^o from the stagnation point are observed to be the most effective in reducing drag in the Reynolds numbers experienced by the upper arm region of a cyclist of 6.0×10^4 to 1.0×10^5 compared to having one, two and four seams on the same fabric. Fabric 5 with four seams has achieved a drag crisis at the lowest critical Reynolds number of 1.0×10^5 with a minimum drag coefficient value of approximately 0.63 when placed at an angle of 45° from the stagnation point compared to other angles as shown in Figure 4.14(c). At 30^o and 35^o from the stagnation point, the subcritical flow regime have a similar flow behaviour with an average drag coefficient value of approximately 0.80 being achieved at Reynolds numbers ranging from 7.0×10^4 to 1.0×10^5 for fabrics 4 and 5 with four seams.

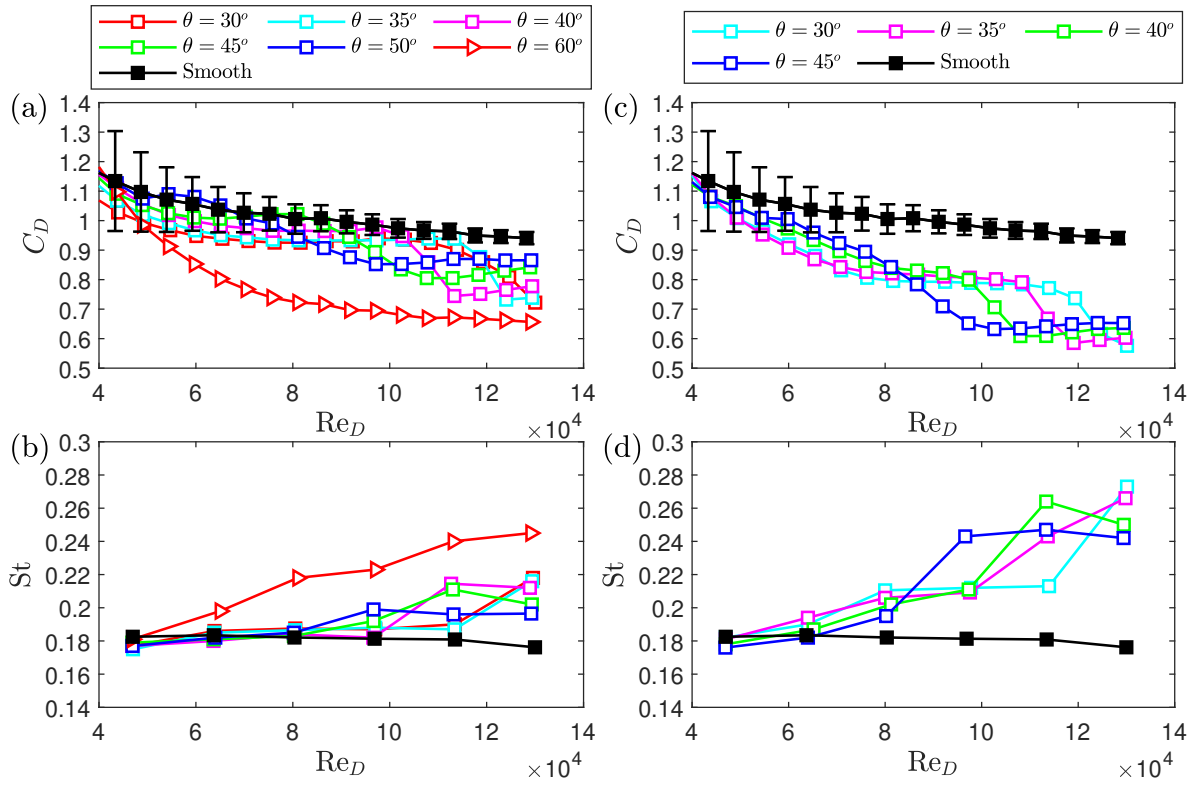


Figure 4.14: Variation of the drag coefficient and Strouhal number at given Reynolds numbers and angular locations of fabric 5 with three seams (a), (b) and four seams (c), (d).

The drag coefficient and Strouhal number as a function of Reynolds number is plotted in Figures 4.15 and 4.16 for fabric 6 with one, two, three and four seams. At all angles including 180° in Figure 4.15(a), fabric 6 with one seam reaches the critical flow regime at a Reynolds number of 1.3×10^5. Angles of 45^o and 55^o has the first drop in the drag coefficient at a Reynolds number of 6.0×10^4 compared to other angles before reaching a lower value past a Reynolds number of 1.20×10^5. In Figure 4.15(c), the drag crisis for fabric 6 with 2 seams occurs at a critical Reynolds number of 1.20×10^5 for all angles where 30° position from the stagnation point achieves the lowest minimum drag coefficient of approximately 0.60. Fabric 6 with two seams is most effective in reducing the drag at Reynolds numbers experienced by the upper arm region of a cyclist of 7.0×10^4 to 1.0×10^5 before reaching the drag crisis at a critical Reynolds number of 1.20×10^5 when placed 45^o and 50^o from the stagnation point. In Figure 4.16(a), placing fabric 6 with three seams at angles ranging from 35° to 50° relative to the stagnation point achieves the drag crisis at critical Reynolds numbers ranging from 7.5×10^4 to 1.0×10^5 with minimum drag coefficient values varying from 0.80 to 0.86. The drag coefficient is relatively constant at a value of 0.70 for Reynolds numbers of 7.0×10^4 and greater when three seams of fabric 6 are placed at an angle of 60^o from the stagnation point. In Figure 4.16(c), fabric 6 with four seams decreases the minimum drag coefficient to values of 0.60 to 0.70 at critical Reynolds numbers ranging from 8.0×10^4 to 1.0×10^5 when placed 30° to 45° from the stagnation point.

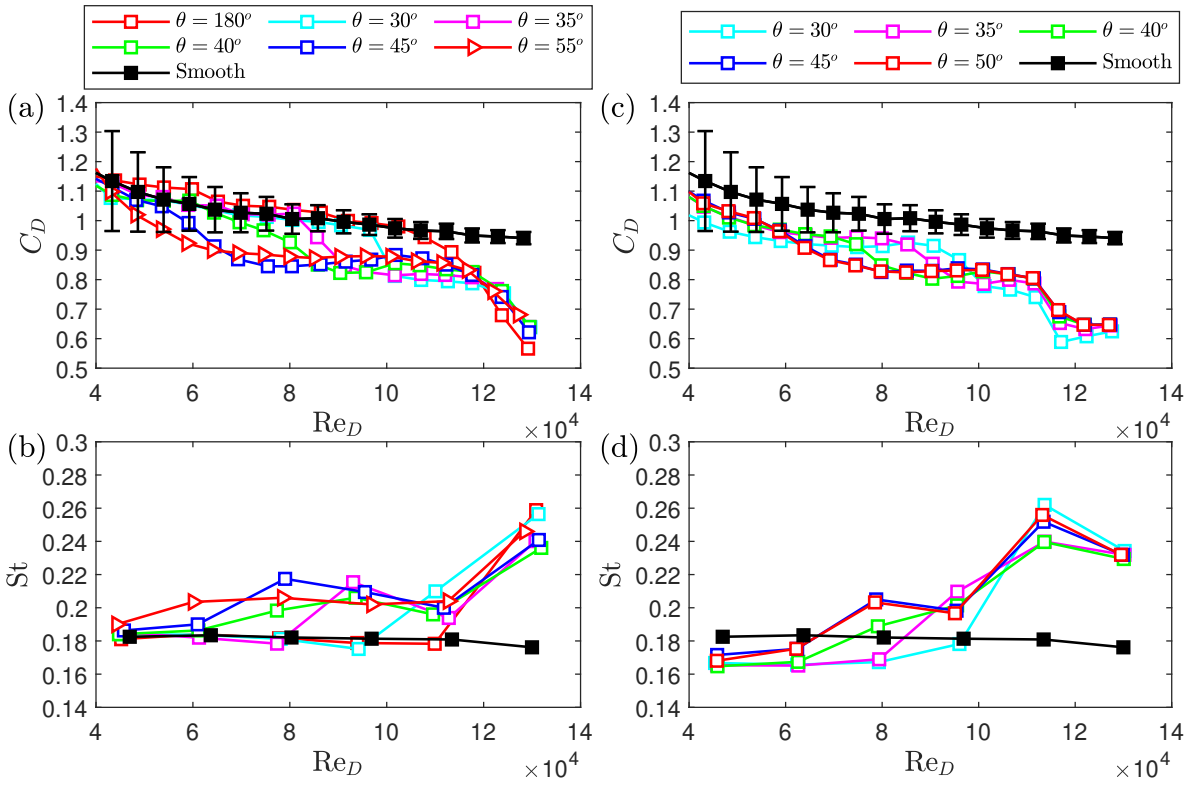


Figure 4.15: Variation of the drag coefficient and Strouhal number at given Reynolds numbers and angular locations of fabric 6 with one seam (a), (b) and two seams (c), (d).

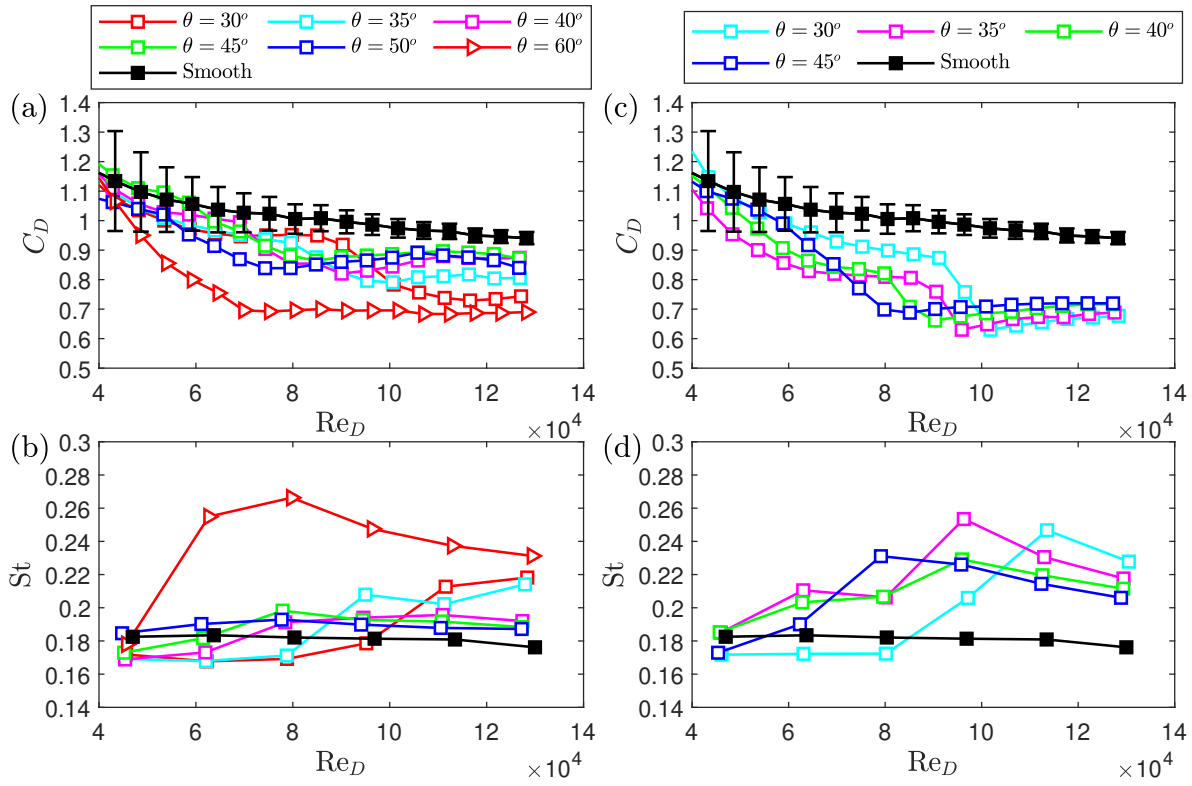


Figure 4.16: Variation of the drag coefficient and Strouhal number at given Reynolds numbers and angular locations of fabric 6 with three seams (a), (b) and four seams (c), (d).

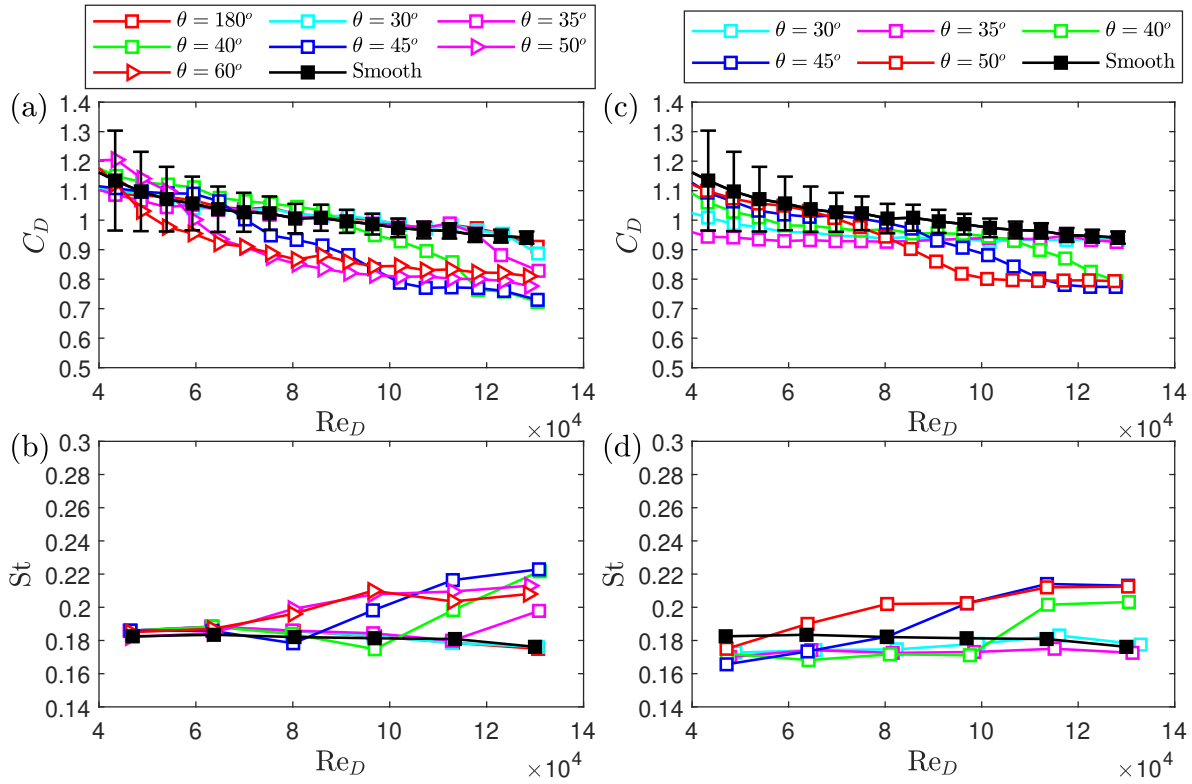


Figure 4.17: Variation of the drag coefficient and Strouhal number at given Reynolds numbers and angular locations of fabric 7 with one seam (a), (b) and two seams (c), (d).

The drag coefficient and Strouhal number as a function of Reynolds number is plotted in Figures 4.17 and 4.18 for fabric 7 with one, two, three and four seams. In Figure 4.17(a), placing fabric 7 with one seam at angles of 180° and 30° from the stagnation point causes the drag coefficient values to be similar to a smooth cylinder. When fabric 7 with one seam is placed 50° from the stagnation point, drag reduction is the most effective for the upper arm region of a cyclist compared to other angles in achieving the lowest average drag coefficient of approximately 0.80 at Reynolds numbers ranging from 8.0×10^4 to 1.0×10^5. At Reynolds numbers greater than 1.0×10^5, the single seam of fabric 7 placed at an angle of 45^o from the stagnation point is shown to be effective in reducing the drag compared to other angles found in Figure 4.17(a). Fabric 7 with two seams has high drag coefficient values close to a smooth cylinder at angles of 30° and 35° from the stagnation point in Figure 4.17(c). This is also evident from having low Strouhal number values shown in Figure 4.17(d). The drag

coefficient reduces to an average value of 0.80 at the lowest critical Reynolds number of approximately 1.0×10^5 and greater when fabric 7 with two seams is placed 50^o from the stagnation point. In Figure 4.18(a), placing fabric 7 with three seams at an angle of 60° from the stagnation point decreases the drag coefficient drastically to a minimum value of approximately 0.65 at Reynolds numbers greater than 1.0×10^5. Fabric 7 with four seams is least effective when placed 30^o from the stagnation point compared to other angles as shown in Figure 4.18(c). Fabric 7 with four seams has the lowest drag coefficient value of approximately 0.80 at Reynolds numbers for the upper arm region of a cyclist that ranges from 6.0×10^4 to 9.0×10^4 when placed 35^o from the stagnation point. However, a minimum drag coefficient of 0.60 is reached at Reynolds numbers greater than 1.0×10^5 when four seams of fabric 7 are placed 45^o from the stagnation point.

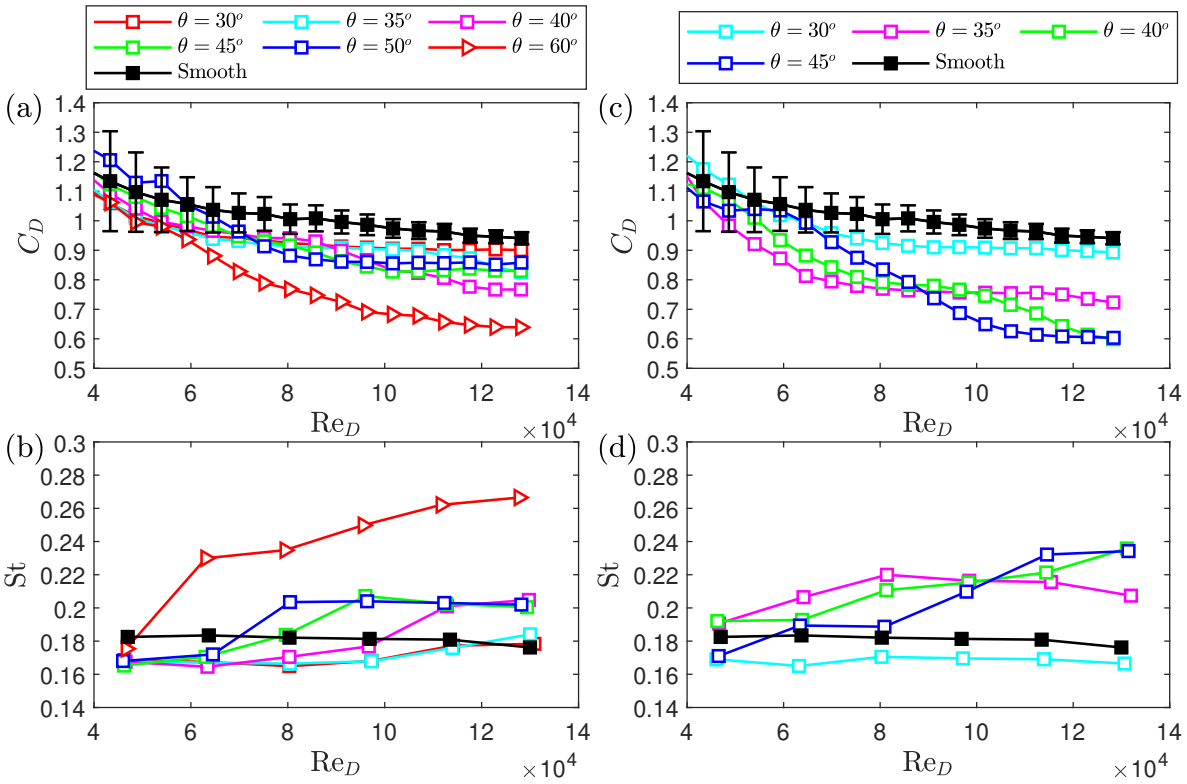


Figure 4.18: Variation of the drag coefficient and Strouhal number at given Reynolds numbers and angular locations of fabric 7 with three seams (a), (b) and four seams (c), (d).

All of the tested fabrics with one, two, three and four seams are compared at angles of 30^o and 45^o from the stagnation point to explore its effect on drag reduction in Figures 4.19 and 4.20. Fabrics with one seam reaches the drag crisis at critical Reynolds numbers greater than 1.2×10^5 when placed 30^o from the stagnation point. In Figure 4.19(b), fabric 3 with two seams has the lowest average drag coefficient value of approximately 0.80 at the Reynolds number range of the upper arm of a cyclist from 8.5×10^4 to 1.0×10^5 compared to other fabrics with two seams before reaching a drag crisis at a critical Reynolds number of 1.15×10^5. Fabric 3 with three seams has achieved a drag crisis at the smallest critical Reynolds number of approximately 9.0×10^4 when placed 30^o from the stagnation point. Fabric 1 with three seams has reached the lowest average drag coefficient of 0.71 at Reynolds numbers past 1.0×10^5 compared to other fabrics with three seams in Figure 4.19(c). Fabric 4 with four seams has fairly constant drag coefficients with an average value of 0.76 at Reynolds numbers greater than 8.0×10^4 when placed 30^o from the stagnation point. Fabrics 2 and 5 with four seams placed 30^o from the stagnation point has a similar flow behaviour in achieving an average drag coefficient of approximately 0.80 for Reynolds numbers ranging from 7.0×10^4 to 1.2×10^5 before reaching the critical flow regime. The drag coefficient decreases rapidly to a minimum value of 0.60 at a critical Reynolds number of approximately 1.30×10^5 when fabrics 2 and 5 with four seams are placed 30^o from the stagnation point.

At 45^o from the stagnation point in Figure 4.20(a), fabrics 2, 4 and 5 with one seam has constant drag coefficients with an average value of roughly 0.80 at Reynolds numbers starting from 8.0×10^4. Fabric 1 with one seam reduces drag at the smallest Reynolds number of approximately 6.0×10^4 with a constant average value of roughly 0.85. Fabrics 3 and 6 with one seam share a similar flow behaviour in having the lowest minimum drag coefficients ranging from 0.62 to 0.65 at a critical Reynolds number of approximately 1.3×10^5. Majority of the fabrics with two seams reach the drag crisis at critical Reynolds numbers greater than 1.20×10^5 when placed 45^o from the stagnation point. Fabric 5 with two seams has the lowest drag coefficient with an average value of 0.80 compared to other fabrics at

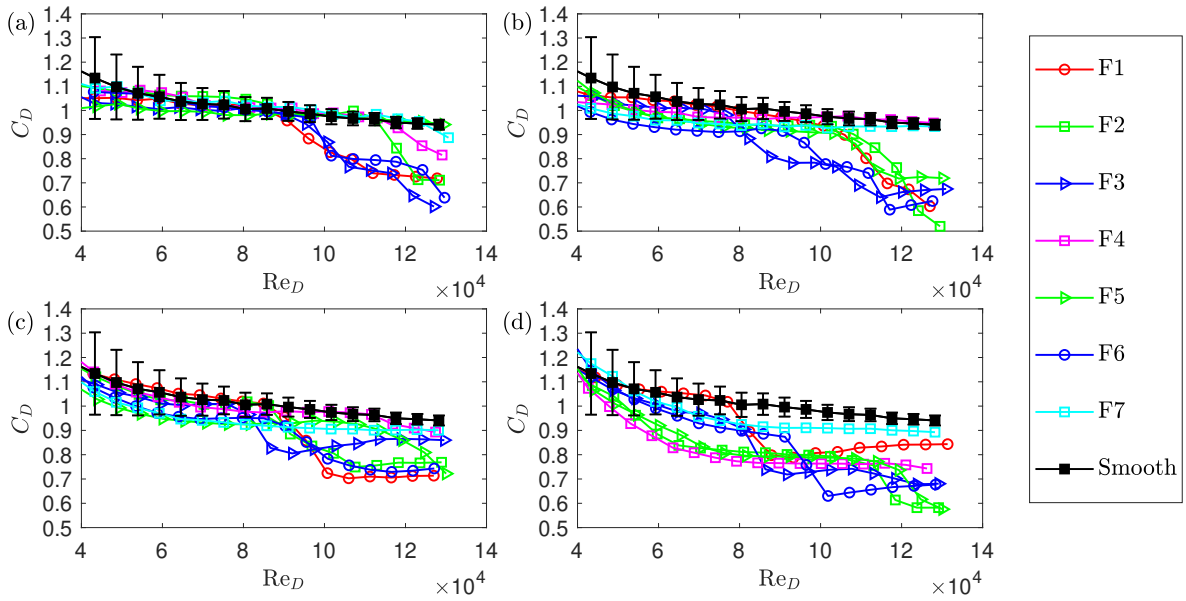


Figure 4.19: Variation of the drag coefficient at given Reynolds numbers for all tested fabrics placed 30^o from the stagnation point for (a) one seam, (b) two seams, (c) three seams and (d) four seams.

a Reynolds number range of 7.5×10^4 to 1.0×10^5 before reaching the critical flow regime at Reynolds numbers past 1.20×10^5 in Figure 4.20(b). Fabric 4 with three seams has a constant drag coefficient past a Reynolds number of 1.0×10^5 with an average value of 0.80 when placed 45^o from the stagnation point as shown in Figure 4.20(c). Fabric 3 with three seams are found to be the least effective at 45^o from the stagnation point since the drag coefficient values for a large range of Reynolds numbers are close to the values found for a smooth cylinder in Figure 4.20(c). In Figure 4.20(d), fabrics 1, 3 and 6 with four seams achieves the drag crisis at the lowest critical Reynolds number of approximately 8.0×10^4 with similar minimum drag coefficient values that have an average value of approximately 0.70.

Fabrics 3, 5 and 7 with one seam placed 50^o from the stagnation point are found to be generally effective in reducing drag at Reynolds numbers ranging from 6.0×10^4 to 1.0×10^5. These cases are compared in Figure 4.21 to find the overall effectiveness of a fabric with one seam that has smoothest (fabric 7), medium (fabric 5) and highest (fabric 3) arithmetic

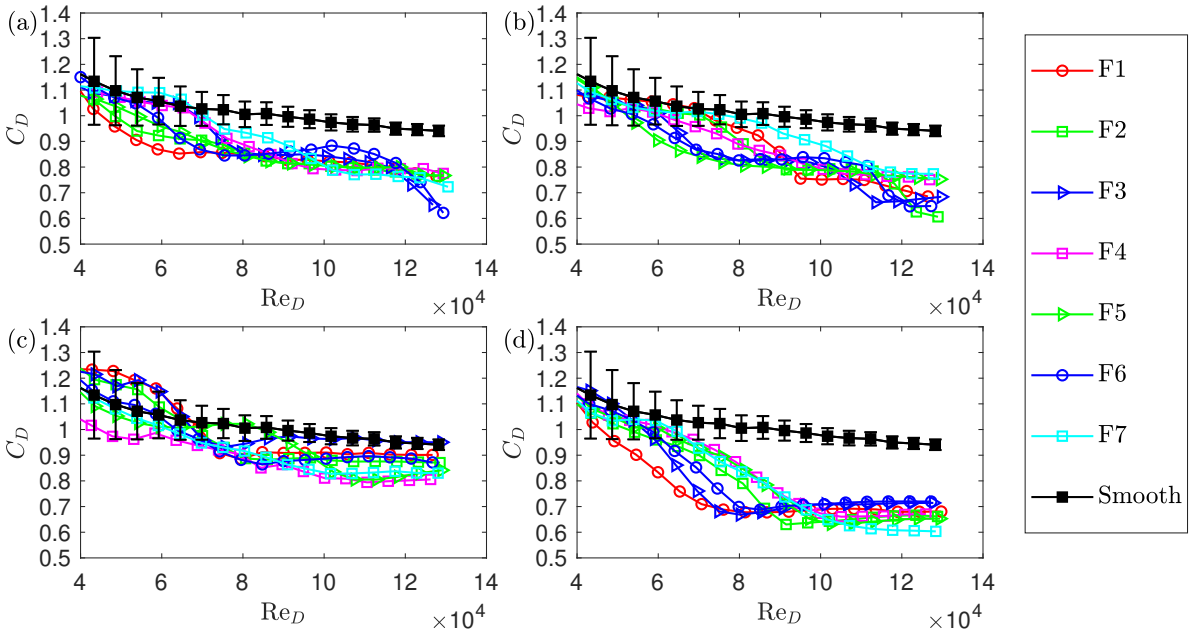


Figure 4.20: Variation of the drag coefficient at given Reynolds numbers for all tested fabrics placed 45^o from the stagnation point for (a) one seam, (b) two seams, (c) three seams and (d) four seams.

roughness heights. They had also been compared when three seams are used and placed at 60^o from the stagnation point because they have yielded the most drastic drag reduction. Fabric 5 is the most effective in reducing the drag in the upper arm region of a cyclist of $6.0 \times 10^4 < Re_D < 1.0 \times 10^5$ with average drag coefficients ranging from 0.81 to 0.86 when one seam is placed at an angle of 50^o from the stagnation point. In Figure 4.21 and Table 4.2, fabric 3 with one seam placed 50^o from the stagnation point has the highest average coefficients past a Reynolds number of 8.0×10^4. However, fabric 3 with one seam has the lowest minimum drag coefficient of 0.73 at a critical Reynolds number of approximately 1.3×10^5 compared to other fabrics when placed 50^o from the stagnation point. Each seam of all fabrics have an aspect ratio, d/D of approximately 0.98% relative to the cylinder diameter. The single seam fabrics with different roughness heights has a lower drag compared to a single tripped cylinder from Truong *et al.* that reached a minimum drag coefficient value of approximately 0.80 when placed with 2D tripwires having aspect ratios, d/D of 0.6%, 1.6%,

3.2% and 6.3% at their respective critical angles [45]. Furthermore, fabrics with a single seam that is 1 mm thick are more effective in reducing drag compared to a single 2D tripwire fitted on a cylinder due to the effects of roughness.

Fabric 3 with three seams is most effective in reducing the drag at a large range of Reynolds numbers when placed at an angle of 60^o compared to other fabric cases. It is observed from Tables 4.2 and 4.3 that smooth, medium and rough fabrics with one and three seams has the smallest variation in drag coefficients at $Re_D > 1.0 \times 10^5$ compared to other Reynolds number ranges. In the work of Ekmekci, a cylinder was fitted with three helical wires that had an aspect ratio, d/D of 1.2% at a Reynolds number of 1.0×10^4 [26]. A significant bubble extension in the near wake occurs when two of the front tripwires are located 60^o from the stagnation point while the third one is located at the base of the cylinder at 180^o from the stagnation point similar to the orientation found when three seams of the fabric are placed 120^o apart from each other. All of the fabrics with three seams achieve a drastic drag reduction and vortex shedding over a large range of Reynolds numbers when placed in this configuration.

Table 4.2: Average C_D values for the smoothest fabric (F7), roughest fabric (F3) and medium roughness fabric (F5) with one seam placed 50^o from the stagnation point at a range of Reynolds numbers.

Type	$4.0 \times 10^4 < Re_D < 6.0 \times 10^4$ (6 - 10 m/s)	$6.0 \times 10^4 < Re_D < 8.0 \times 10^4$ (10 - 13 m/s)	$8.0 \times 10^4 < Re_D < 1.0 \times 10^5$ (13 - 15 m/s)	$Re_D > 1.0 \times 10^5$ (15 - 20 m/s)
F3-S1	1.03	0.89	0.86	0.81
F5-S1	1.07	0.86	0.81	0.78
F7-S1	1.11	0.91	0.83	0.80

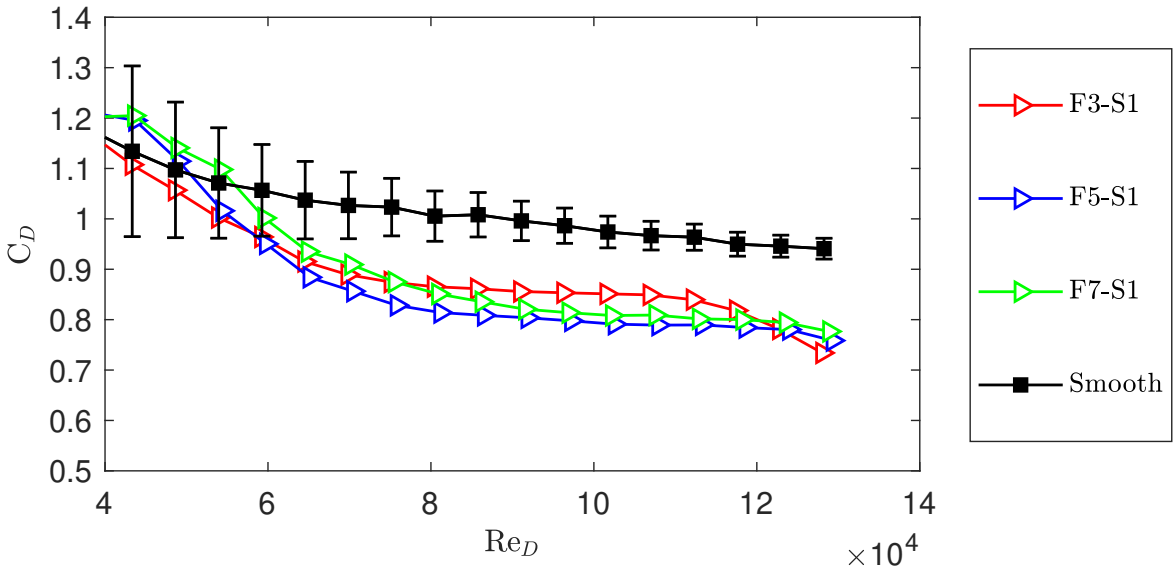


Figure 4.21: Variation of the drag coefficient at given Reynolds numbers for roughest fabric (fabric 3), smoothest fabric (fabric 7) and fabric with medium roughness (fabric 5) with one seam placed 50^o from the stagnation point.

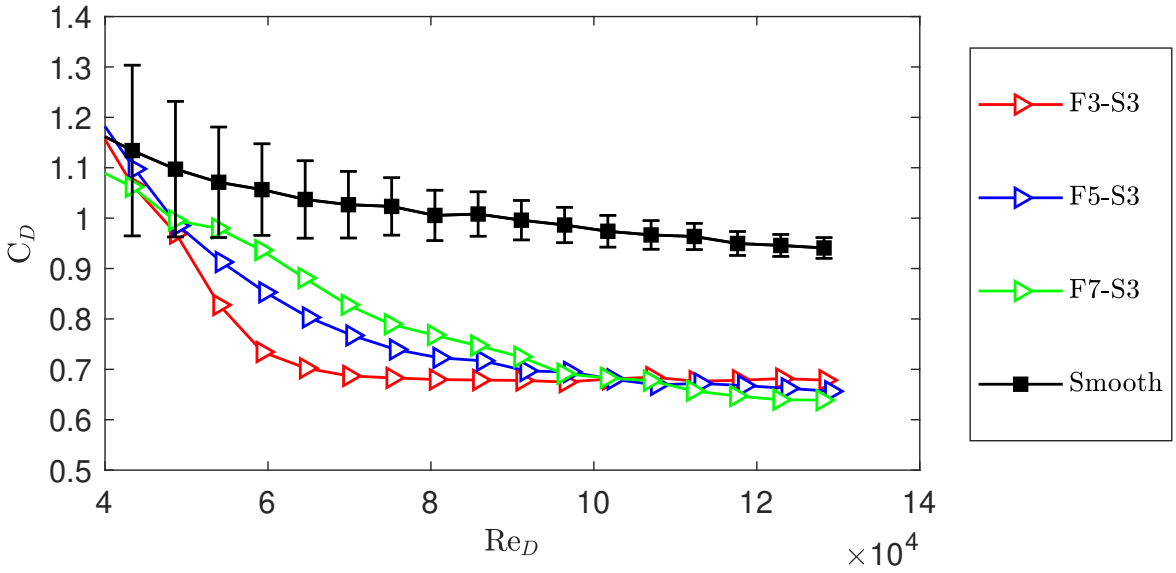


Figure 4.22: Comparison of drastic drag reduction for roughest fabric (fabric 3), smoothest fabric (fabric 7) and fabric with medium roughness (fabric 5) with three seams placed 60^o from the stagnation point.

Table 4.3: Average C_D values for the smoothest fabric (fabric 7), roughest fabric (fabric 3) and medium roughness fabric (fabric 5) with three seams placed 60^o from the stagnation point at a range of Reynolds numbers.

Type	$4.0 \times 10^4 < Re_D < 6.0 \times 10^4$ (6 - 10 m/s)	$6.0 \times 10^4 < Re_D < 8.0 \times 10^4$ (10 - 13 m/s)	$8.0 \times 10^4 < Re_D < 1.0 \times 10^5$ (13 - 15 m/s)	$Re_D > 1.0 \times 10^5$ (15 -20 m/s)
F3-S3	0.90	0.69	0.68	0.68
F5-S3	0.96	0.77	0.71	0.67
F7-S3	0.99	0.83	0.73	0.66

Moreover, adding seams on a fabric are effective in reducing the drag of a cylinder to a smaller critical Reynolds number. Rougher fabrics such as fabrics 1, 3 and 6 with four seams achieve the drag crisis at critical Reynolds numbers ranging from 6.0×10^4 to 1.0×10^5 for angles placed from 30^o to 45^o from the stagnation point. They also have a similar flow behaviour past a critical Reynolds number of 8.0×10^4 when placed 45^o from the stagnation point. The maximum drag reduction for a fabric with multiple seams relative to a smooth cylinder is approximately 40% at the Reynolds numbers experienced by the upper arm region of a cyclist when subject to speeds of 10 to 15 m/s.

4.4 Effect of a Single Spanwise Tripwire

The influence of the tripwire has an effect on the wake at angles greater than 30^o from the stagnation point in a one wired case [46]. That is why the position of all tested tripwires are varied from 30^o to 70^o from the stagnation point with wire aspect ratios ranging from $0.00492 < d/D < 0.0197$ with thickness values of 0.5, 1 and 2 mm. Thickness comparison is explored for 2D and zigzag tripwires at $\lambda_{Re_D=60k}$ and $\lambda_{Re_D=80k}$. Wavelength comparison is also explored for zigzag tripwires with a constant thickness of 1 mm. These comparisons are investigated in this section because thickness and spatial wavelengths are the main characteristics that influence the angular location of the tripwire along the surface of the cylinder in effectively reducing drag. The variation of the drag coefficient and Strouhal number with Reynolds

number is plotted for all tripwires when placed at their respective critical angles. This helped to obtain optimal cases that is most effective in reducing drag.

4.4.1 Thickness Comparison for 2D Tripwires

The drag coefficient as a function of Reynolds numbers is plotted in Figure 4.23 for 2D tripwires with thicknesses of 0.5, 1 and 2 mm. A 2D tripwire with a 0.5 mm thickness decreases the drag coefficient at higher Reynolds numbers at angles of 60° and 70° from the stagnation point in Figure 4.23(a). The 1 mm thick 2D tripwire can reduce drag at higher Reynolds numbers at an angle of 50° from the stagnation point in Figure 4.23(b). In the work of Ekmekci, a cylinder fitted with end plates inside a water channel had a length to diameter ratio, L/D of 8.78 [26]. A single 2D tripwire that had an aspect ratio, d/D of 0.012 relative to the cylinder diameter is placed at a critical angle of 60^o from the stagnation point at a Reynolds number of 1.0×10^4 due to having the greatest extension in the mean recirculation bubble length. In the present work, the 1 mm thick 2D tripwire can effectively reduce drag at a lower critical angle of 50^o from the stagnation point compared to past literature. The 2 mm thick 2D tripwire is effective in reducing drag at angles of 30° and 40° from the stagnation point as shown in Figure 4.23(c).

4.4.2 Thickness Comparison for Zigzag Tripwires

In Figure 4.24, the drag coefficient as a function of Reynolds number is plotted when the thickness of zigzag tripwires are varied from 0.5 mm and 1 mm at $\lambda_{Re_D=60k}$. The 1 mm thick zigzag tripwire with $\lambda_{Re_D=60k}$ is effective in drag reduction at higher Reynolds numbers for angles of 30° and 40° from the stagnation point in achieving a minimum drag coefficient of approximately 0.80 at a critical Reynolds number of 1.3×10^5 in Figures 4.24(b) and 4.25. In Figures 4.25 and 4.26, a zigzag tripwire that is 0.5 mm thick is more effective in drag reduction at angles of 50° to 70° from the stagnation point compared to having a 1 mm thickness.

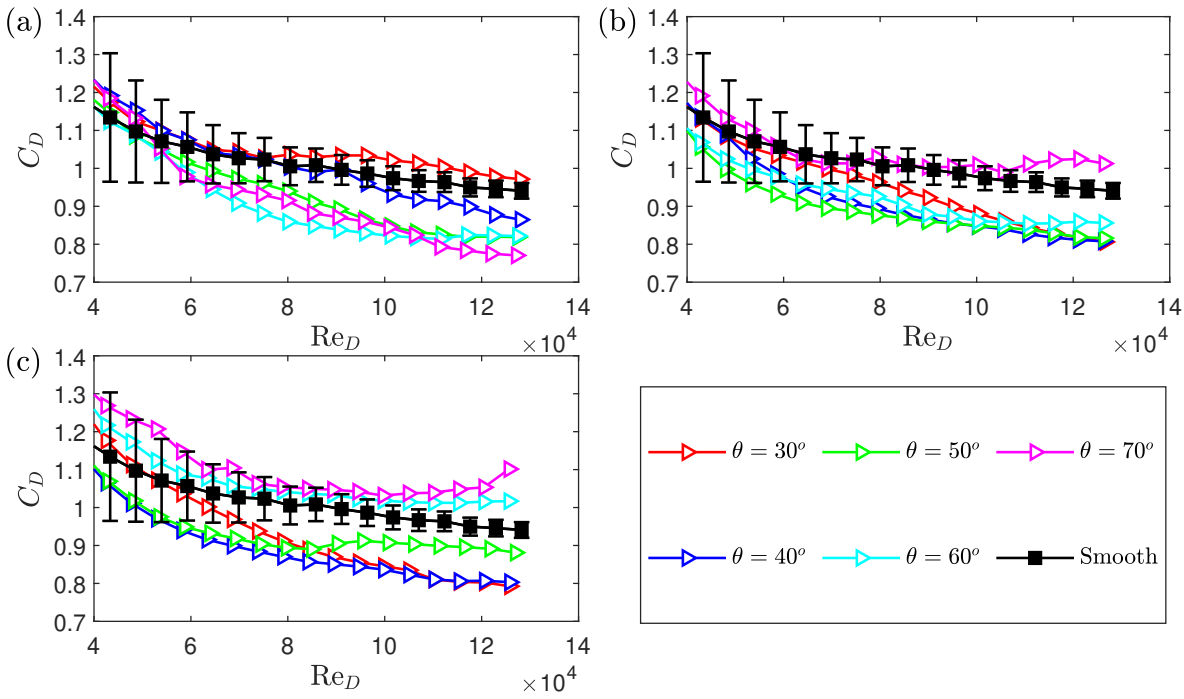


Figure 4.23: Variation of the drag coefficient at given Reynolds numbers for 2D tripwires with thicknesses of (a) 0.5 mm, (b) 1 mm and (c) 2 mm at angles of 30^o to 70^o from the stagnation point.

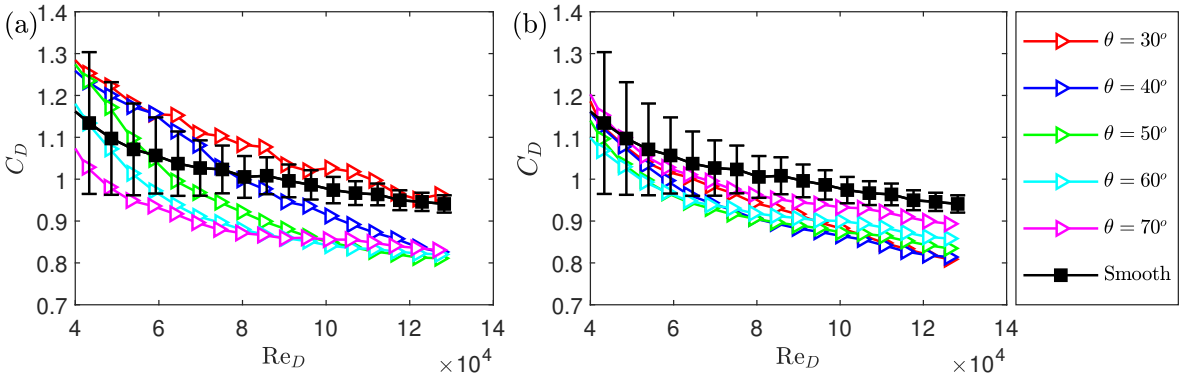


Figure 4.24: Variation of the drag coefficient at given Reynolds numbers for zigzag tripwires with $\lambda_{Re_D=60k}$ for (a) 0.5 and (b) 1 mm thickness at angles of 30^o to 70^o from the stagnation point.

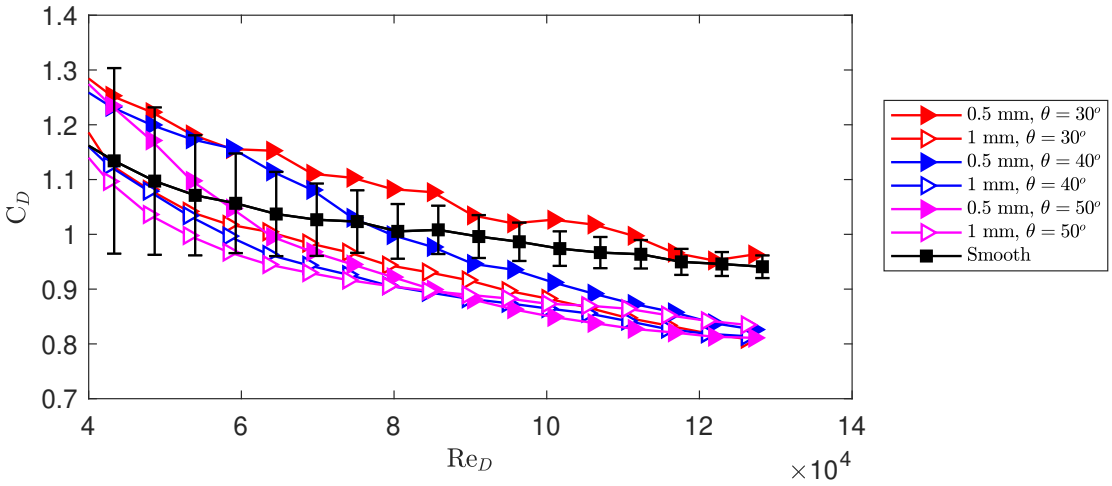


Figure 4.25: Variation of the drag coefficient at given Reynolds numbers for zigzag tripwires with $\lambda_{Re_D=60k}$ for 0.5 and 1 mm thickness at angles of 30^o, 40^o and 50^o from the stagnation point.

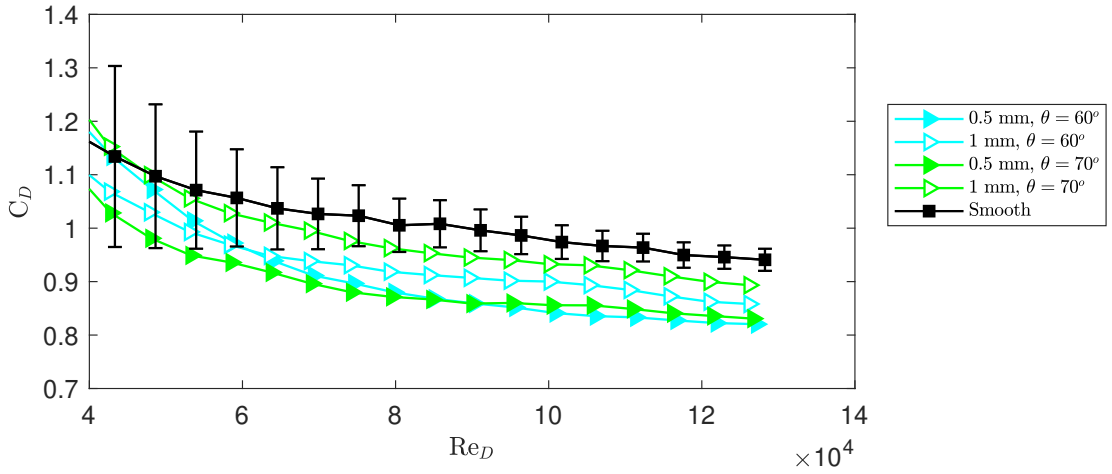


Figure 4.26: Variation of the drag coefficient at given Reynolds numbers for zigzag tripwires with $\lambda_{Re_D=60k}$ for 0.5 and 1 mm thickness at angles of 60^o and 70^o from the stagnation point.

In Figures 4.27(a) and 4.27(b), two different thickness values of 1 and 2 mm for the zigzag tripwires are compared at $\lambda_{Re_D=80k}$. An angle of 30° from the stagnation point is the most effective location for drag reduction for both thickness values at high Reynolds numbers. In Figures 4.27(b), 4.28 and 4.29, a 2 mm thick zigzag tripwire at $\lambda_{Re_D=80k}$ loses effectiveness at angles larger than 50° from the stagnation point, indicating permanent boundary layer separation.

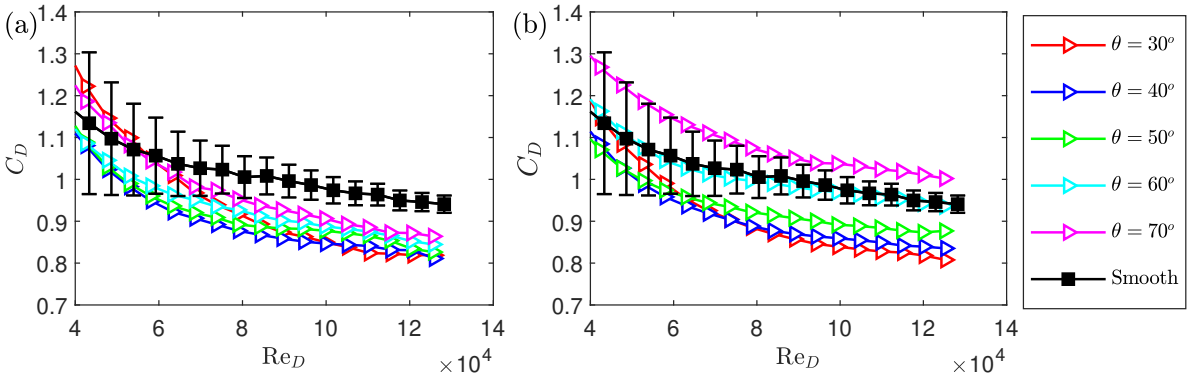


Figure 4.27: Variation of the drag coefficient at given Reynolds numbers for zigzag tripwires with $\lambda_{Re_D=80k}$ for (a) 1 and (b) 2 mm thickness at angles of 30^o to 70^o from the stagnation point.

At 30°, a 2 mm thick zigzag tripwire is more effective at reducing the drag coefficient at higher Reynolds numbers compared to a 1 mm thick zigzag tripwire with $\lambda_{Re_D=80k}$ from Figure 4.28. A 1 mm thick zigzag tripwire has a lower drag at larger angles of 40° to 70° from the stagnation point compared to a tripwire with a 2 mm thickness from Figures 4.28 and 4.29.

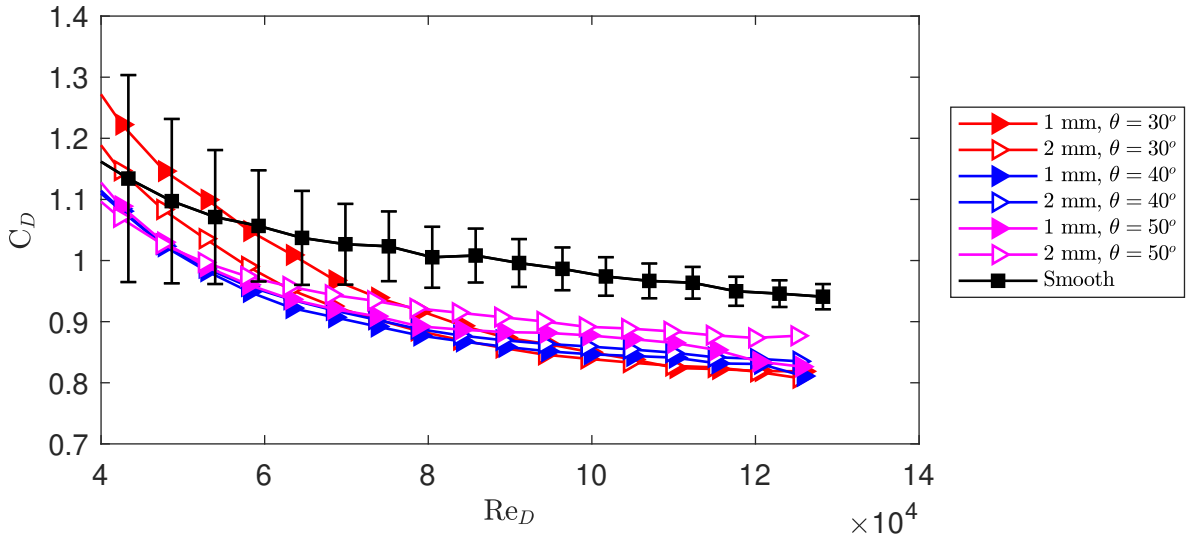


Figure 4.28: Variation of the drag coefficient at given Reynolds numbers for zigzag tripwires with $\lambda_{Re_D=80k}$ for 1 and 2 mm thickness at angles of 30^o, 40^o and 50^o from the stagnation point.

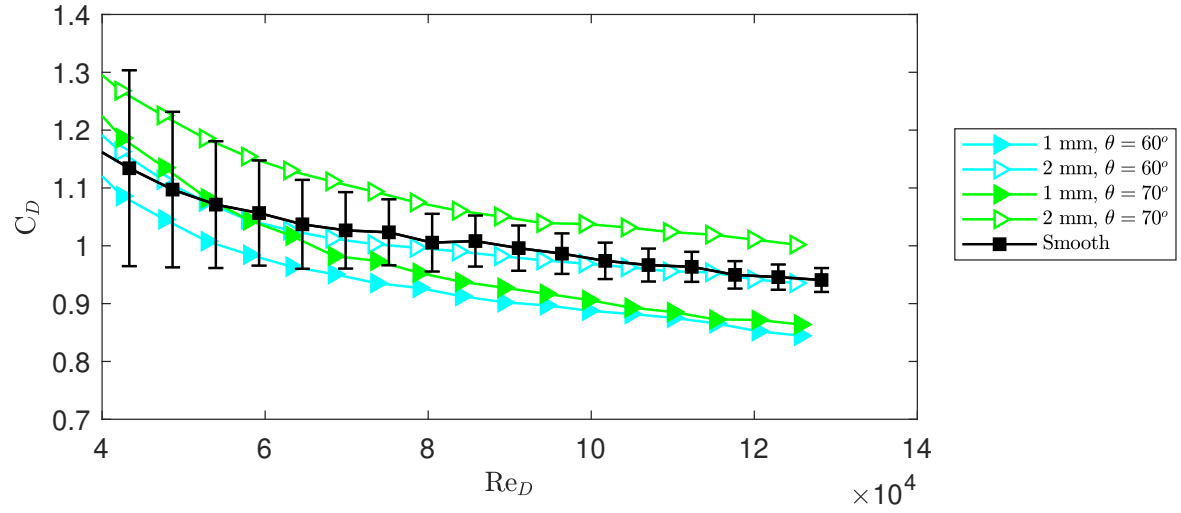


Figure 4.29: Variation of the drag coefficient at given Reynolds numbers for zigzag tripwires with $\lambda_{Re_D=80k}$ for 1 and 2 mm thickness at angles of 60^o and 70^o from the stagnation point.

4.4.3 Wavelength Comparison for Zigzag Tripwires

In Figure 4.30, two zigzag tripwires with different spatial wavelengths are compared at a given thickness of 1 mm. At angles of 30^o to 70^o from the stagnation point, the tripwire with lower spatial wavelengths, $\lambda_{Re_D=80k}$ has a lower drag compared to a tripwire with higher spatial wavelengths, $\lambda_{Re_D=60k}$ in Figures 4.31 and 4.32. There is a small variation in drag for both tripwires in Figure 4.31 past a Reynolds number of 1.0×10^5 when placed at angles of 30^o to 50^o from the stagnation point.

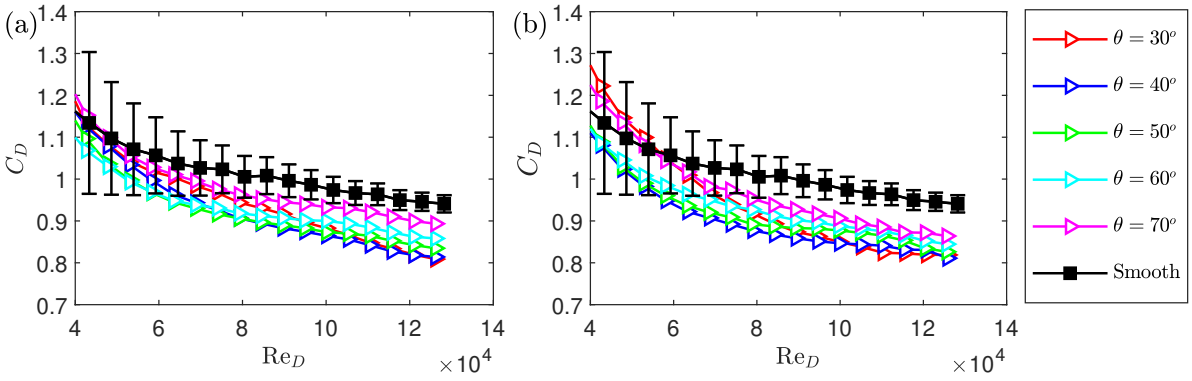


Figure 4.30: Variation of the drag coefficient at given Reynolds numbers for 1mm thick zigzag tripwires with (a) $\lambda_{Re_D=60k}$ and (b) $\lambda_{Re_D=80k}$ for angles of 30° to 70° from the stagnation point.

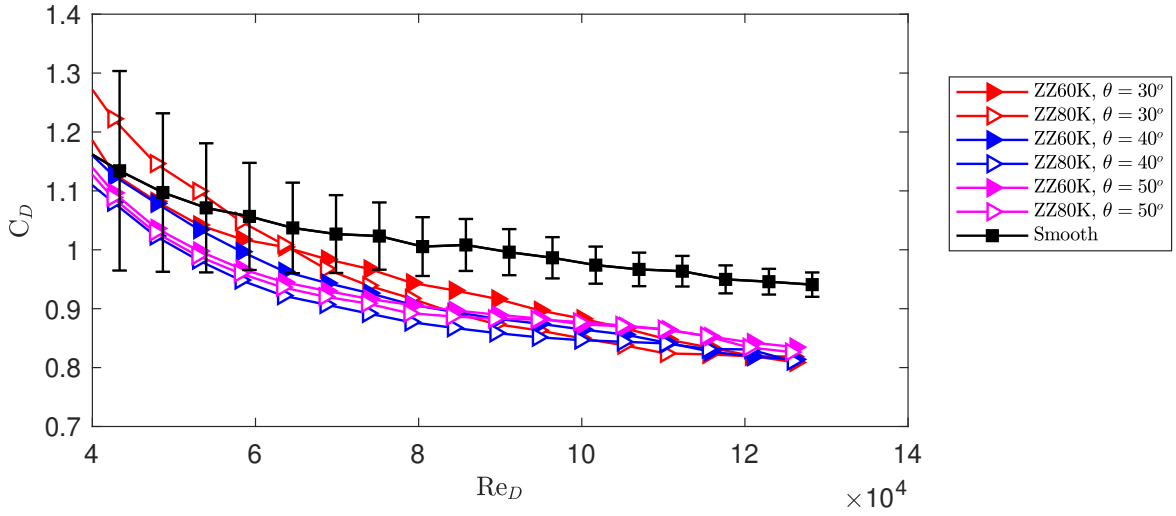


Figure 4.31: Variation of the drag coefficient at given Reynolds numbers for 1mm thick zigzag tripwires with $\lambda_{Re_D=60k}$ and $\lambda_{Re_D=80k}$ for angles of 30^o, 40^o and 50^o from the stagnation point.

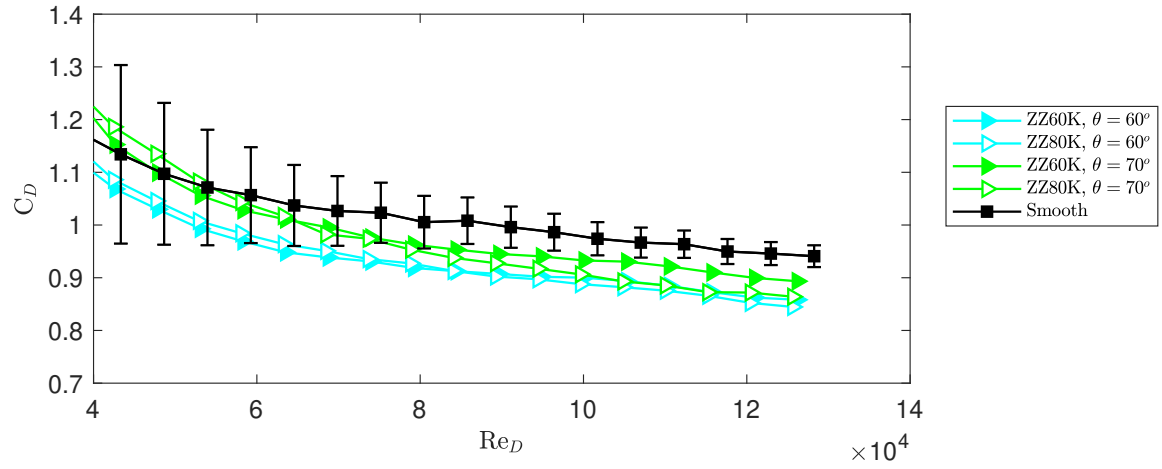


Figure 4.32: Variation of the drag coefficient at given Reynolds numbers for 1mm thick zigzag tripwires with $\lambda_{Re_D=60k}$ and $\lambda_{Re_D=80k}$ for angles of 60^o and 70^o from the stagnation point.

4.4.4 Optimal Tripwire Cases

The variation of the drag coefficient at given Reynolds numbers are obtained for 2D and zigzag tripwires with thickness values of 0.5, 1 and 2 mm at angles of 30° to 70° from the stagnation point in Figure 4.33. The boundary layer of a thick tripwire reattaches downstream of the cylinder surface at an angular range of 30° to 50° from the stagnation point by transitioning to turbulence, causing the shedding frequency and loading to be modified [22]. In Figures 4.34, 4.36 and 4.37, the variation of the drag coefficient and Strouhal number with Reynolds number has been obtained for 2D and zigzag tripwires with thicknesses of 1 and 2 mm at critical angles ranging from 30^o to 50^o from the stagnation point where drag reduction occurs. It is important to note that the boundary layer becomes permanently separated for larger tripwires with a thickness of 2 mm when placed at angles larger than 50° from the stagnation point. However, smaller tripwires with a thickness of 0.5 mm can remain attached to the cylinder at large angles up to 70° from the stagnation point. In Figure 4.35, the variation of the drag coefficient and Strouhal number with Reynolds number have been obtained for 2D and zigzag tripwires with a thickness of 0.5 mm at critical angles ranging from 50^o to 70^o from the stagnation point where drag reduction is evident.

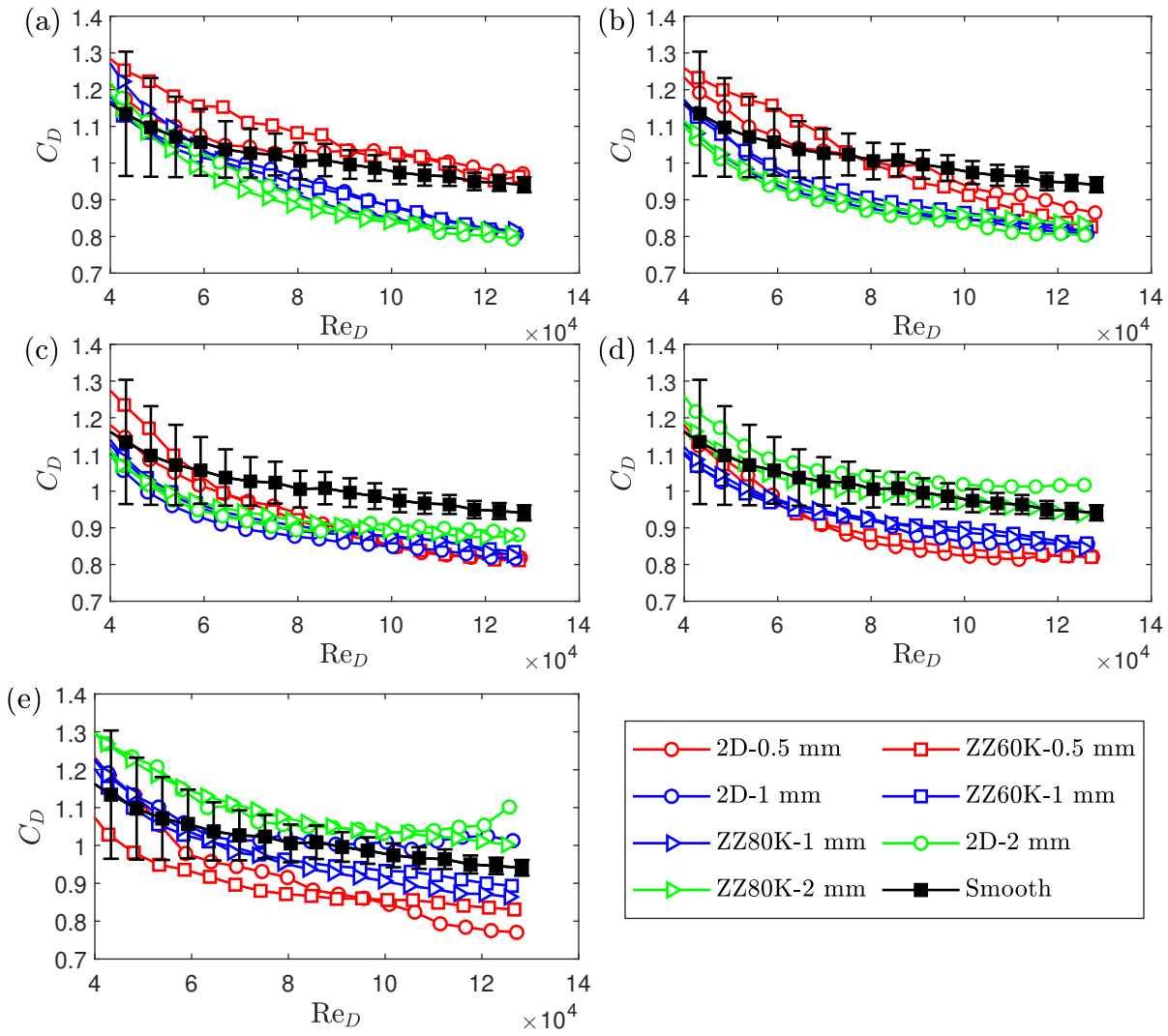


Figure 4.33: Variation of the drag coefficient with Reynolds numbers for all tripwires at angles of (a) 30^o, (b) 40^o, (c) 50^o, (d) 60^o and (e) 70^o from the stagnation point.

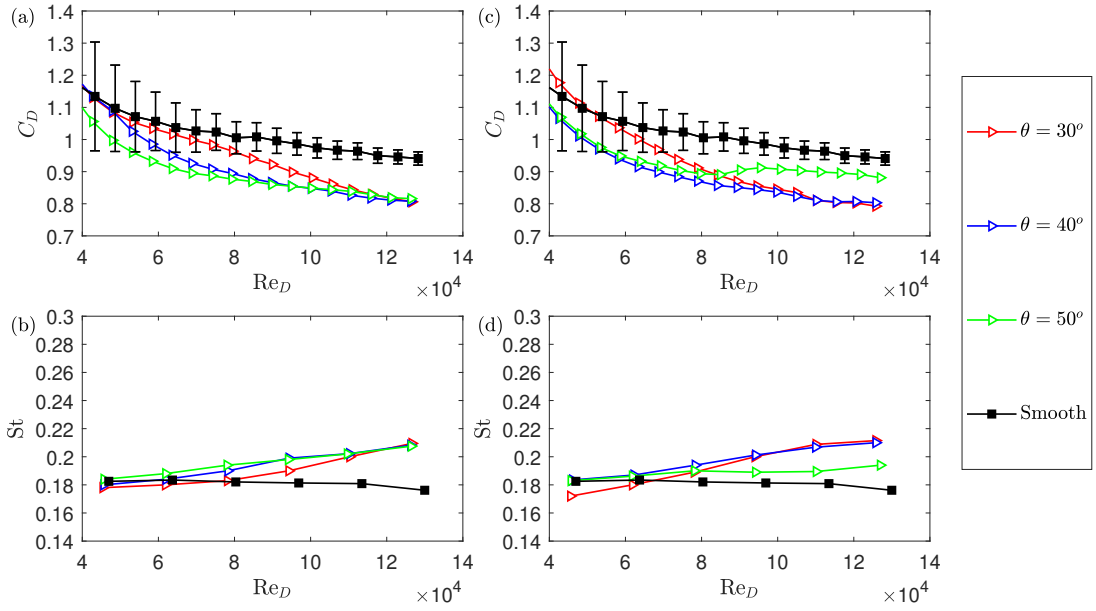


Figure 4.34: Variation of the drag coefficient and Strouhal number at given Reynolds numbers for 2D tripwires with thickness values of 1 mm (a), (b) and 2 mm (c), (d) at angles of 30^o to 50^o from the stagnation point.

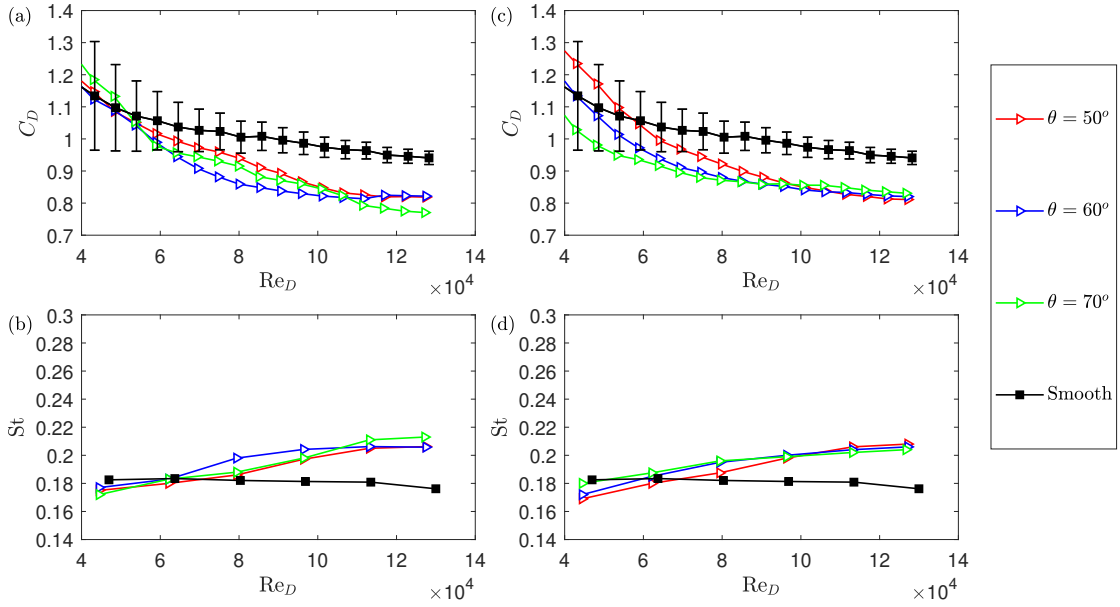


Figure 4.35: Variation of the drag coefficient and Strouhal number at given Reynolds numbers for 0.5 mm thick tripwires with 2D geometry (a), (b) and zigzag geometry with $\lambda_{Re_D=60k}$ (c), (d) at angles of 50^o to 70^o from the stagnation point.

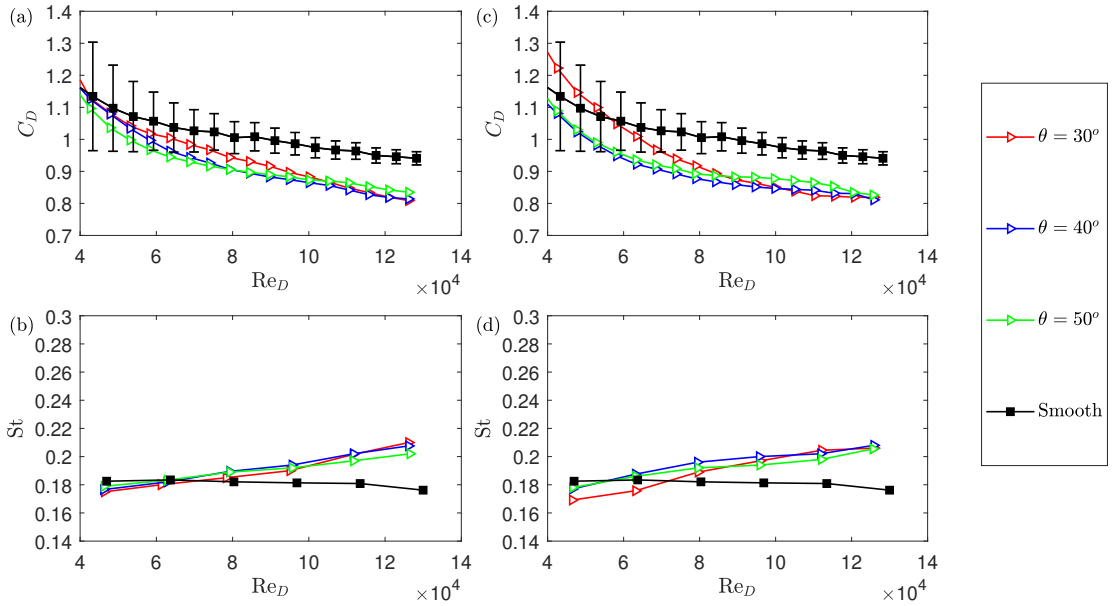


Figure 4.36: Variation of the drag coefficient and Strouhal number at given Reynolds numbers for 1 mm thick zigzag tripwires with $\lambda_{Re_D=60k}$, (a), (b) and $\lambda_{Re_D=80k}$ (c), (d) at angles of 30^o to 50^o from the stagnation point.

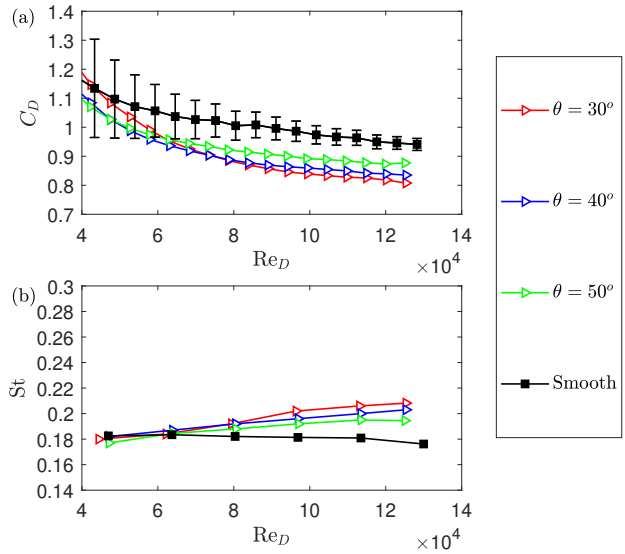


Figure 4.37: Variation of (a) drag coefficient and (b) Strouhal number at given Reynolds numbers for 2 mm thick zigzag tripwire with $\lambda_{Re_D=80k}$ for angles of 30^o to 50^o from the stagnation point.

The larger the thickness of tripwires, the more easily it can trip the flow to turbulence and decrease drag at lower angles from the stagnation point [45]. The effective angular range for tripwires with thickness values of 1 and 2 mm was 30° to 50° from the stagnation point. The effective angular range for 2D and zigzag tripwires with thickness of 0.5 mm is 50° to 70° from the stagnation point. When a tripwire is placed at an angular location smaller than the critical angle, the shear layer becomes reattached to the surface of the cylinder [26]. At the critical location where the minimum drag coefficient and maximum Strouhal number occurs, the shear layer experiences a bistable state in the cylinder cross-section by alternating between flow reattachment and separation patterns [26]. When a tripwire is placed at the respective critical angle, early development of shear layer instability is triggered in the wire shear layer. This increases the Strouhal number because it allows the mean recirculation bubble length to attain its maximum value in meeting the entrainment demands of the shear layer. On the other hand, the shear layer would always be separated if the tripwire is positioned at an angular location larger than the critical angle. For example, a 1 mm thick 2D tripwire effectively decreases drag at a high Reynolds number from a low angle of 30° to a maximum critical angle of 50° from the stagnation point where the shear layer is attached to the cylinder surface. Increasing the angular position beyond the critical angle of 50° such as 60° and 70° from the stagnation point causes the shear layer to permanently separate from the cylinder surface, leading to a larger drag. This causes the mean recirculation bubble length to contract, causing the Strouhal number to decrease.

The drag coefficient plotted as a function of Reynolds numbers found in Figure 4.38 shows the optimal cases where the given tripwire can effectively reduce drag at a specific angle from the stagnation point based on thickness and spatial wavelengths. In the optimal tripwire cases found below in Figure 4.38 and Table 4.4, the 2D tripwire with 0.5 mm thickness has the lowest average drag coefficient of 0.80 past a Reynolds number of 1.0×10^5 when placed 70^o from the stagnation point. The 2 mm thick tripwire with 2D and zigzag geometry at $\lambda_{Re_D=80k}$ has similar effectiveness past a Reynolds number of 8.0×10^4 when placed 30^o and 40^o from the stagnation point as shown in Table 4.4. It is observed from Figure 4.38 and Table 4.4 that there is a small variation in the drag coefficient for all optimal tripwire cases for Reynolds numbers greater than 8.0×10^4 except for a 2D tripwire with 0.5 mm thickness placed 70^o from the stagnation point. Overall, the maximum drag reduction of a tripwire relative to a smooth cylinder is approximately 20% when placed at its respective critical angle from the stagnation point.

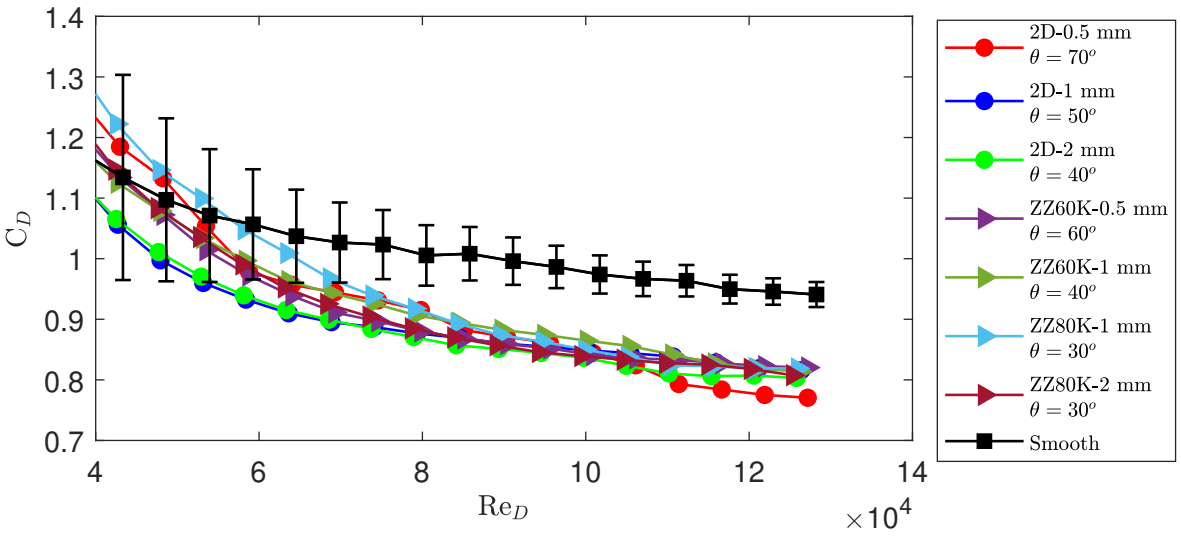


Figure 4.38: Variation of the drag coefficient with Reynolds number for the tripwire cases producing the lowest drag as previously identified.

Table 4.4: Average C_D values for optimal tripwire cases with 2D and zigzag geometry at a range of Reynolds numbers.

Type	$4.0 \times 10^4 < Re_D < 6.0 \times 10^4$ (6 - 10 m/s)	$6.0 \times 10^4 < Re_D < 8.0 \times 10^4$ (10 - 13 m/s)	$8.0 \times 10^4 < Re_D < 1.0 \times 10^5$ (13 - 15 m/s)	$Re_D > 1.0 \times 10^5$ (15 - 20 m/s)
2D-0.5 mm, $\theta = 70^o$	1.09	0.94	0.87	0.80
2D-1 mm, $\theta = 50^o$	0.99	0.89	0.86	0.83
2D-2 mm, $\theta = 40^o$	1.00	0.89	0.85	0.81
ZZ60K-0.5 mm, $\theta = 60^o$	1.05	0.91	0.86	0.83
ZZ60K-1 mm, $\theta = 40^o$	1.06	0.93	0.88	0.84
ZZ80K-1 mm, $\theta = 30^o$	1.13	0.96	0.87	0.82
ZZ80K-2 mm, $\theta = 30^o$	1.06	0.92	0.85	0.82

4.5 Effect of Single Tripwire on Fabric

In this section, a single tripwire is attached to fabrics with low, medium and high roughness to help support the design of skinsuits for a cyclist. The flow behaviour for fabric and tripwire combinations is compared to wrapping fabrics and mounting tripwires alone on a cylinder at angles of 30^o to 60^o from the stagnation point. This helps to explore the influence of the combined effects of surface roughness of fabrics, geometry and location of tripwires on the drag of a cylinder. The average drag coefficient values for Reynolds number ranges are tabulated for smooth, medium and rough fabrics with tripwires that are symmetrically placed at angles of 30^o to 60^o from the stagnation point.

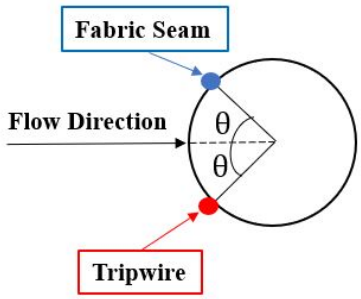


Figure 4.39: Schematic of a tripwire and a fabric seam placed symmetrically from the stagnation point.

4.5.1 Single Tripwire on a Smooth Fabric

In Figure 4.39, the fabric seam and the respective tripwire is placed symmetrically at an angle, θ, apart from the stagnation point. A single zigzag tripwire with 1 mm thickness and $\lambda_{Re_D=60k}$ is attached onto the smoothest fabric. In Figures 4.40 and 4.41, the variation of the drag coefficient with Reynolds number is compared for fabric 7 with one seam, 1 mm thick zigzag tripwire with $\lambda_{Re_D=60k}$ and when both are attached together in a symmetric orientation at angles of 30^o to 60^o from the stagnation point. At a low angle of 30^o from the stagnation point, fabric 7 with a 1 mm thick zigzag tripwire that has $\lambda_{Re_D=60k}$ attached in a symmetric orientation achieves the lowest minimum drag coefficient of approximately 0.77 at a critical Reynolds number of approximately 1.3×10^5 compared to using only fabric 7 and a tripwire separately from Figure 4.41(a). At 30^o, fabric 7 with a tripwire and the tripwire alone begins to have a similar flow behaviour at Reynolds numbers past 1.0×10^5. A 1 mm thick ZZ60K tripwire has a similar flow behaviour to the single seam of fabric 7 and the same zigzag tripwire placed symmetrically at angles of 40^o to 60^o from the stagnation point. They both have a lower drag coefficient compared to fabric 7 with one seam at a low angle of 30^o from the stagnation point. At higher angles of 40^o to 60^o from the stagnation point, fabric 7 with 1 seam has the lowest drag coefficient from Figures 4.41(b) to 4.41(d).

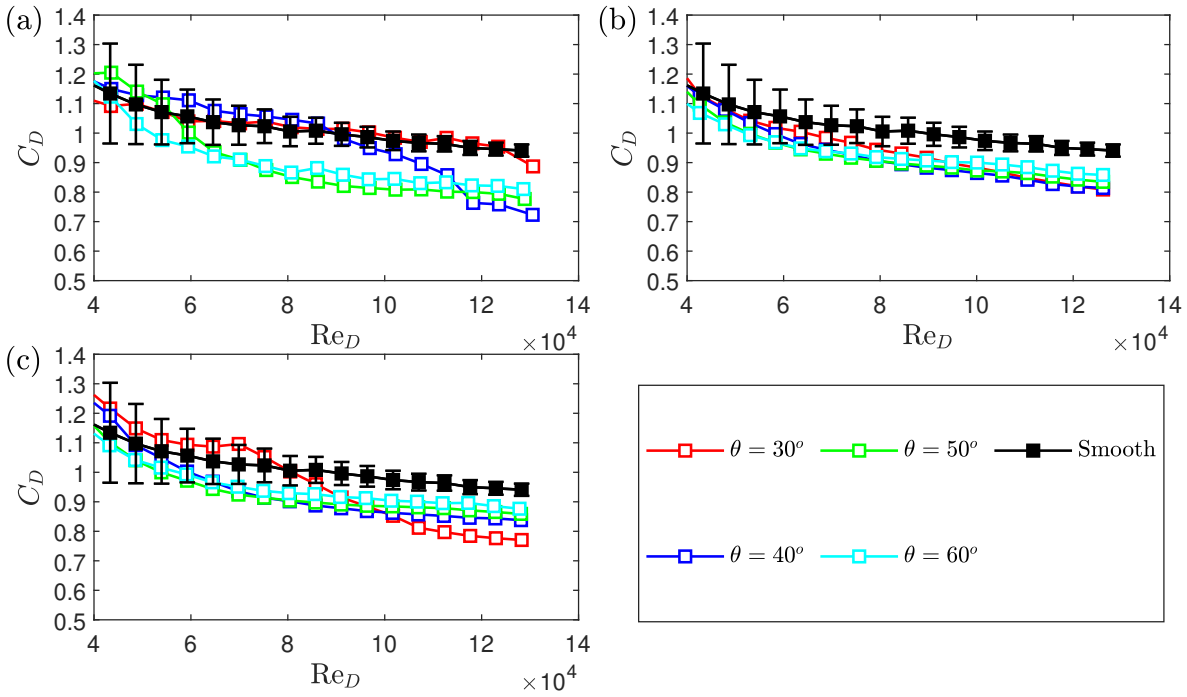


Figure 4.40: Variation of drag coefficient with Reynolds number at angles of 30^o to 60^o from the stagnation point for (a) fabric 7 with one seam, (b) 1 mm thick zigzag tripwire with $\lambda_{Re_D=60k}$, (c) fabric 7 with one seam and 1 mm thick zigzag tripwire with $\lambda_{Re_D=60k}$ that are placed symmetrically from the stagnation point.

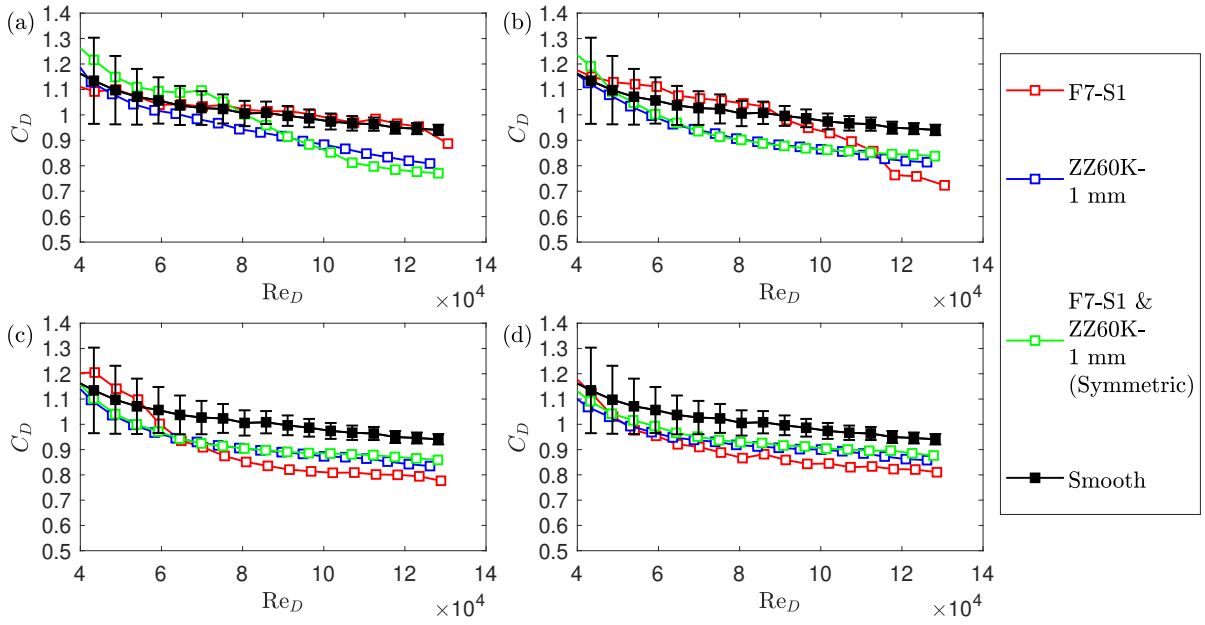


Figure 4.41: Variation of drag coefficient with Reynolds number for fabric 7 with one seam, a 1 mm thick zigzag tripwire with $\lambda_{Re_D=60k}$ and a combination where both are placed symmetrically at angles of (a) $\theta = 30^o$, (b) $\theta = 40^o$, (c) $\theta = 50^o$ and (d) $\theta = 60^o$ from the stagnation point.

4.5.2 Fabric and Tripwire Combinations for Medium and Rough Fabrics

Medium and rough fabrics have been attached with tripwires in three different orientations found in Figure 4.42 with respect to the incoming flow direction. T-S orientation means that the tripwire and fabric seam is 180^o apart with the tripwire facing first with respect to the incoming flow direction as shown in Figure 4.42(b). S-T orientation means that the tripwire and fabric seam is 180^o apart with the seam facing the incoming flow direction before the tripwire as shown in Figure 4.42(c).

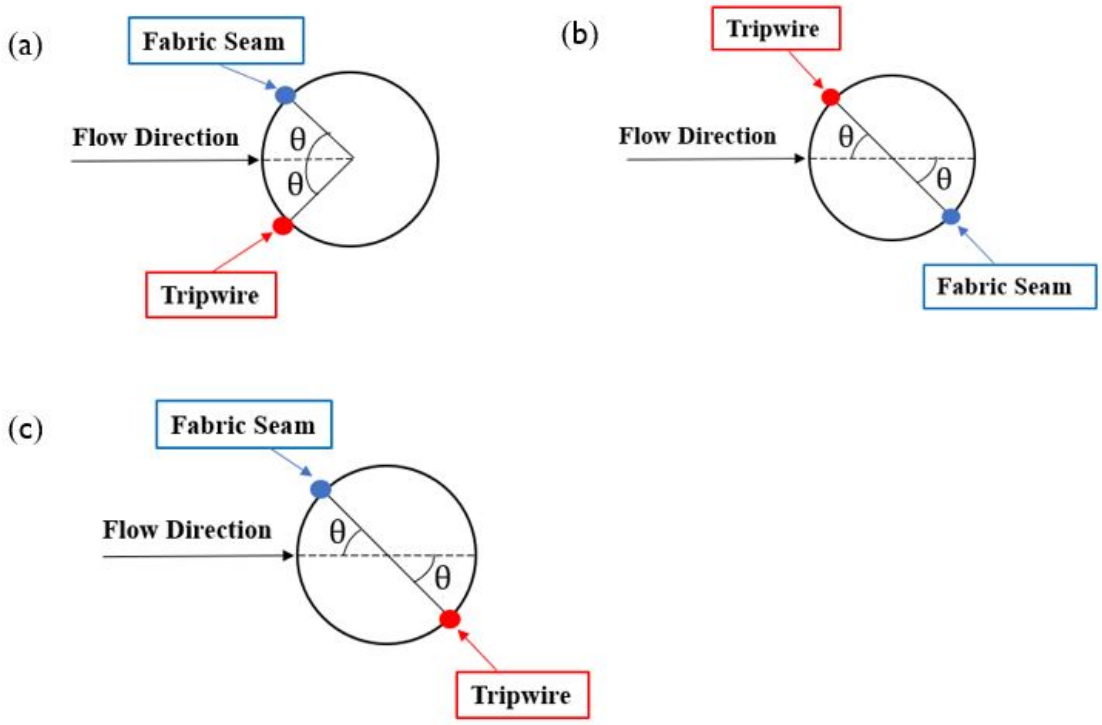


Figure 4.42: Fabric seam and tripwire that are (a) placed symmetrically from the stagnation point, (b) 180^o apart where the tripwire is facing the incoming flow direction before the seam in a T-S orientation and (c) 180^o apart where the seam of the fabric is facing the incoming flow direction before the tripwire in a S-T orientation.

4.5.2.1 Single Tripwire on a Fabric with Medium Roughness

A 2 mm thick 2D tripwire is attached on fabric 5 with one seam that has an intermediate roughness in three different orientations as previously shown in Figure 4.42. The flow behaviours for the multiple orientations of fabric 5 with one seam and a 2D tripwire with 2 mm thickness are compared to only placing fabric 5 with one seam and the tripwire separately at angles of 30^o to 60^o from the stagnation point in Figures 4.43 to 4.45. Similarly, a 2 mm thick zigzag tripwire with $\lambda_{Re_D=80k}$ is attached in three different orientations and compared to other cases found in Figures 4.46 to 4.48.

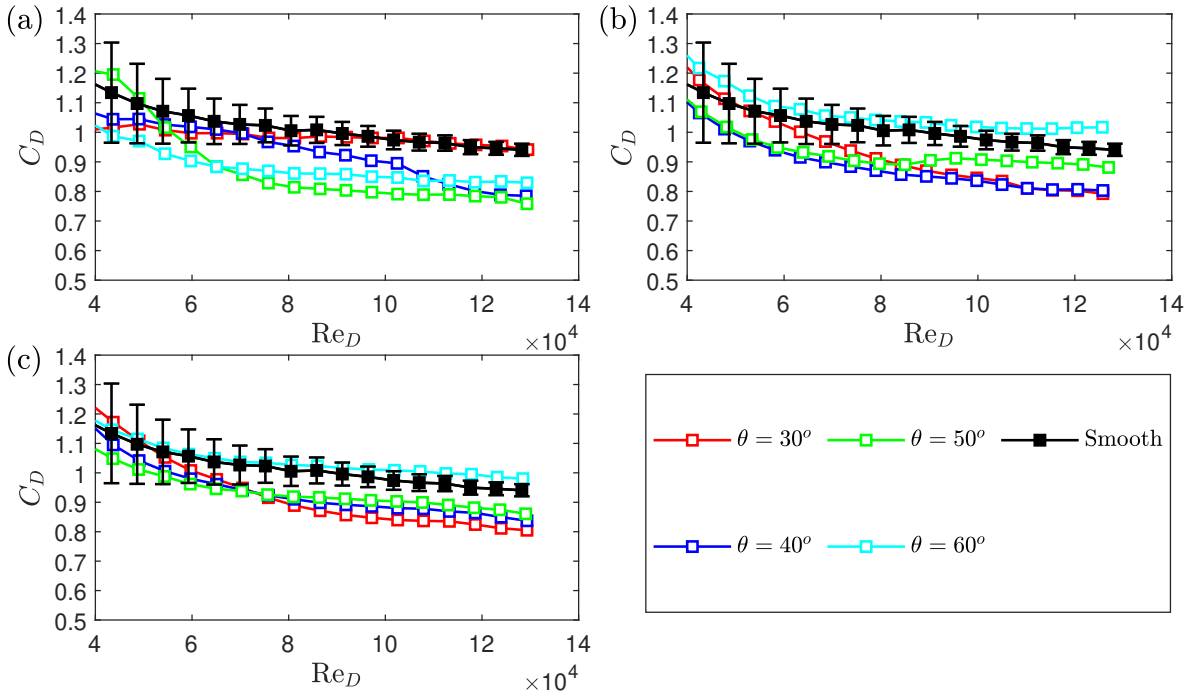


Figure 4.43: Variation of drag coefficient with Reynolds number at angles of 30^o to 60^o from the stagnation point for (a) fabric 5 with one seam, (b) 2 mm thick 2D tripwire (c) fabric 5 with one seam and 2 mm thick 2D tripwire that are placed symmetrically from the stagnation point.

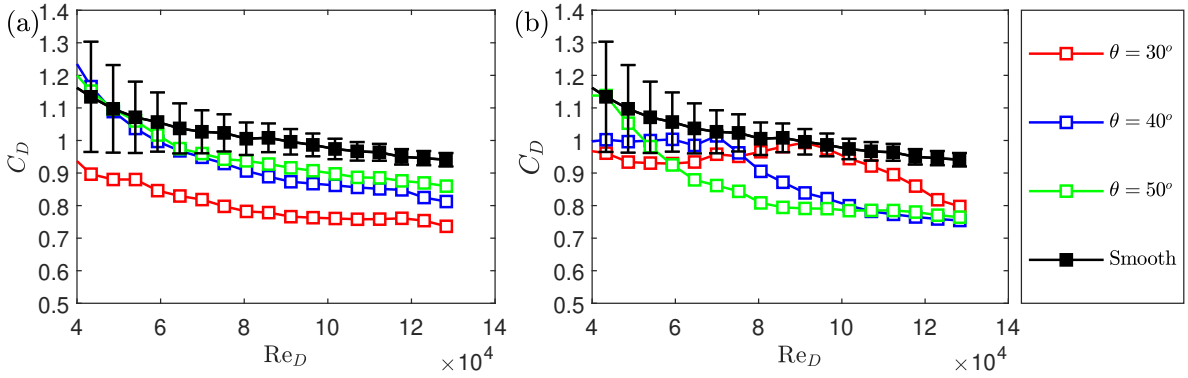


Figure 4.44: Variation of drag coefficient with Reynolds number at angles of 30^o to 50^o from the stagnation point for fabric 5 with one seam that is 180^o apart from a 2 mm thick 2D tripwire in (a) T-S orientation where the tripwire is facing the incoming flow direction before the fabric seam and (b) S-T orientation where the fabric seam is facing the incoming flow direction before the tripwire.

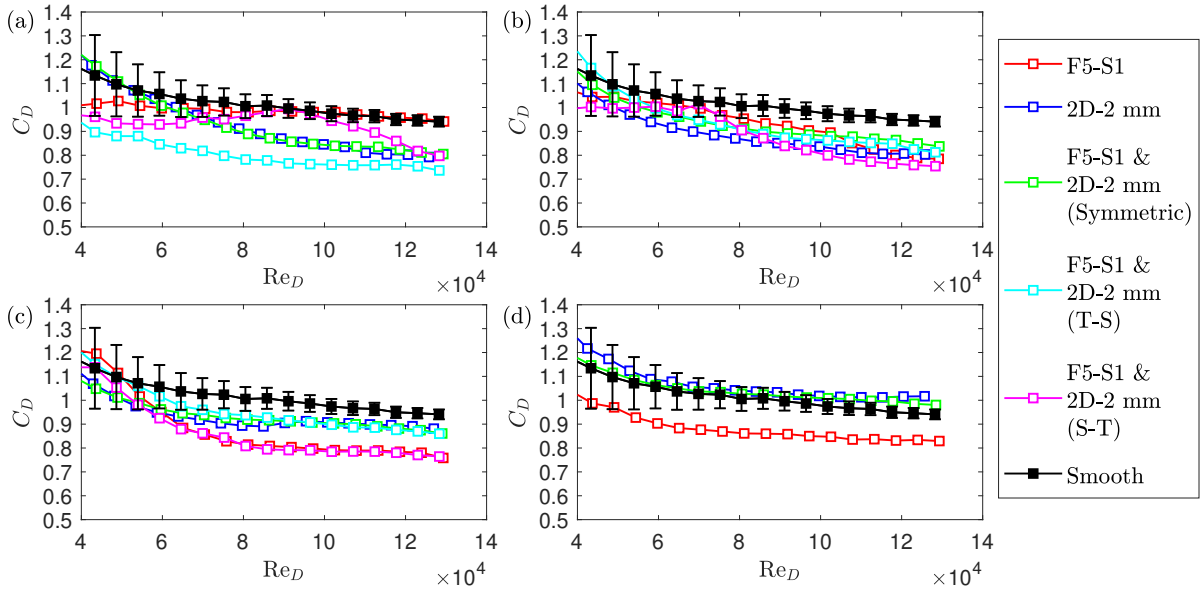


Figure 4.45: Variation of drag coefficient with Reynolds number for fabric 5 with one seam, a 2 mm thick 2D tripwire and a combination where both are placed symmetrically at angles of (a) $\theta = 30^o$, (b) $\theta = 40^o$, (c) $\theta = 50^o$ and (d) $\theta = 60^o$ from the stagnation point.

In Figure 4.43(a), fabric 5 with one seam has drag coefficient values close to a smooth cylinder when placed 30^o from the stagnation point. Fabric 5 with the 2 mm thick 2D tripwire attached in a T-S orientation is most effective at 30^o from the stagnation point compared to other cases with an average drag coefficient of 0.76 at Reynolds numbers of 8.0×10^4 and greater as shown in Figures 4.44(a) and 4.45(a). In Figure 4.44(b), fabric 5 with the 2 mm thick 2D tripwire attached in a S-T orientation are effective at Reynolds numbers greater than 1.0×10^5 in achieving an average drag coefficient value of approximately 0.77 when placed at angles of 40^o and 50^o from the stagnation point. The seam of fabric 5 and 2 mm thick 2D tripwire arranged in a symmetric orientation have a similar flow behaviour as placing a 2 mm thick 2D tripwire alone for majority of the angles from the stagnation point in Figure 4.45.

At $\theta = 50^o$, the 2 mm thick 2D tripwire alone and fabric 5 with symmetric and T-S orientations have similar drag coefficient values past a Reynolds number of 9.0×10^4 as shown in Figure 4.45(c). In Figure 4.45(c), fabric 5 with one seam only and with a 2 mm thick 2D tripwire attached in a S-T orientation has a similar flow behaviour past a Reynolds number of 6.0×10^4 at 50^o from the stagnation point with an average drag coefficient value of approximately 0.80. At 60^o from the stagnation point, fabric 5 with one seam has a lower drag coefficient than the other cases in Figure 4.45(d). Fabric 5 with one seam that is placed symmetrically from a 2 mm thick 2D tripwire and the same tripwire placed alone at an angle of 60^o from the stagnation point experiences a similar flow behaviour in having drag coefficient values greater than the smooth cylinder in Figure 4.45(d).

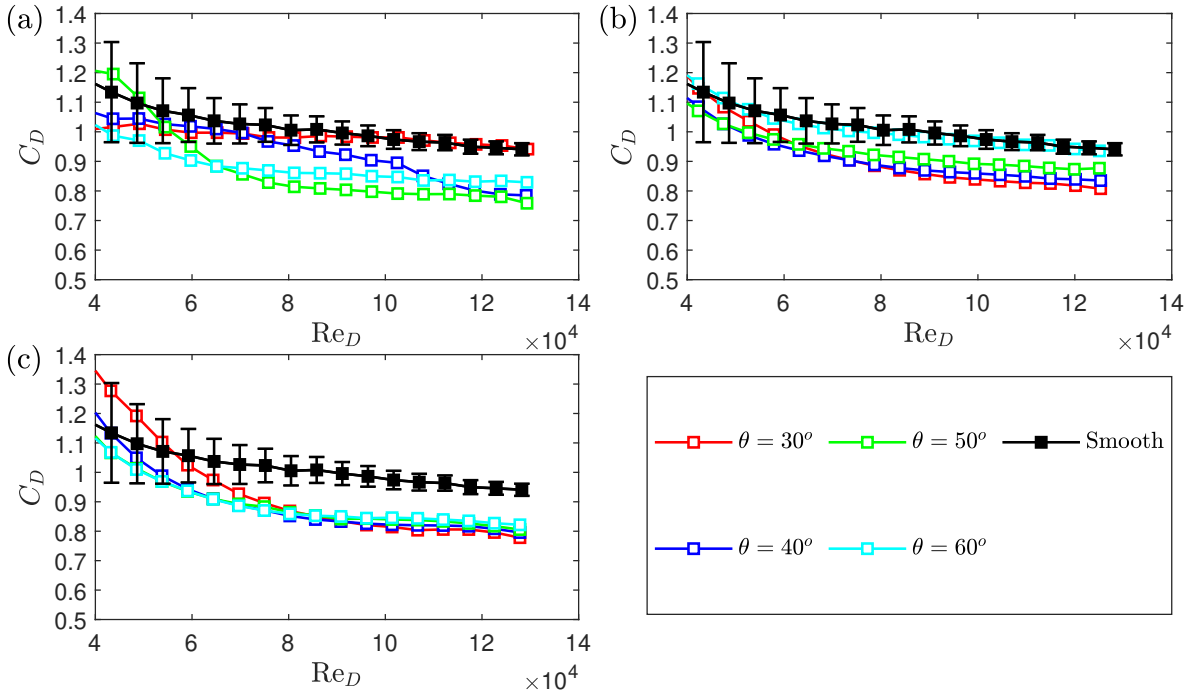


Figure 4.46: Variation of drag coefficient with Reynolds number at angles of 30^o to 60^o from the stagnation point for (a) fabric 5 with one seam, (b) 2 mm thick zigzag tripwire with $\lambda_{Re_D=80k}$, (c) fabric 5 with one seam and 2 mm thick zigzag tripwire with $\lambda_{Re_D=80k}$ that are placed symmetrically from the stagnation point.

At $\theta = 30^o$, fabric 5 with the 2 mm thick ZZ80K tripwire attached in a S-T orientation has a large drag coefficient up to a Reynolds number of 1.0×10^5 and decreases to a minimum drag coefficient value of 0.80 at a critical Reynolds number of approximately 1.3×10^5 as shown in Figures 4.47(b) and 4.48(a). The 2 mm thick ZZ80K tripwire placed 30^o from the stagnation point has a similar flow behaviour to the fabric 5 seam and the corresponding tripwire arranged in a symmetric orientation as shown in Figure 4.48(a). Fabric 5 with the 2 mm thick ZZ80K tripwire attached in a T-S orientation has maintained a low drag coefficient with an average value of 0.77 at Reynolds numbers starting from 6.5×10^4 and greater when placed 30^o from the stagnation point.

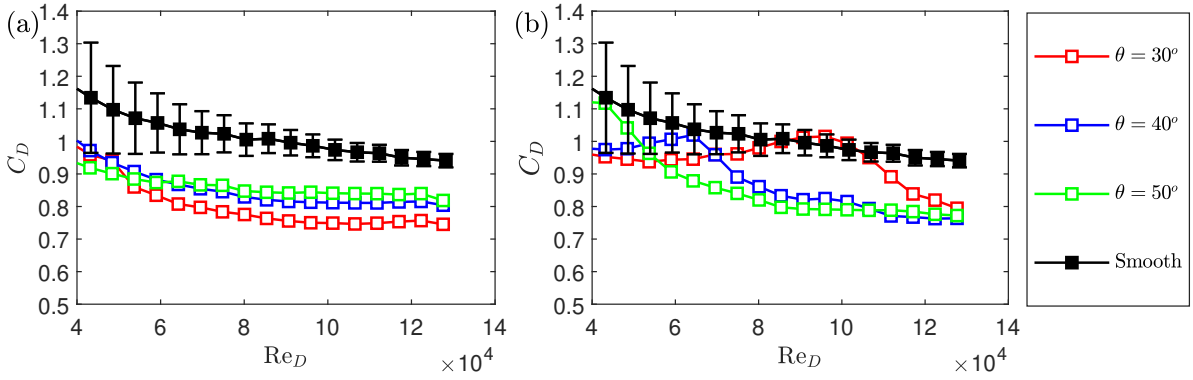


Figure 4.47: Variation of drag coefficient with Reynolds number at angles of 30^o to 50^o from the stagnation point for fabric 5 with one seam that is 180^o apart from the 2 mm thick zigzag tripwire with $\lambda_{Re_D=80k}$ in (a) T-S orientation where the tripwire is facing the incoming flow direction before the fabric seam and (b) S-T orientation where the fabric seam is facing the incoming flow direction before the tripwire.

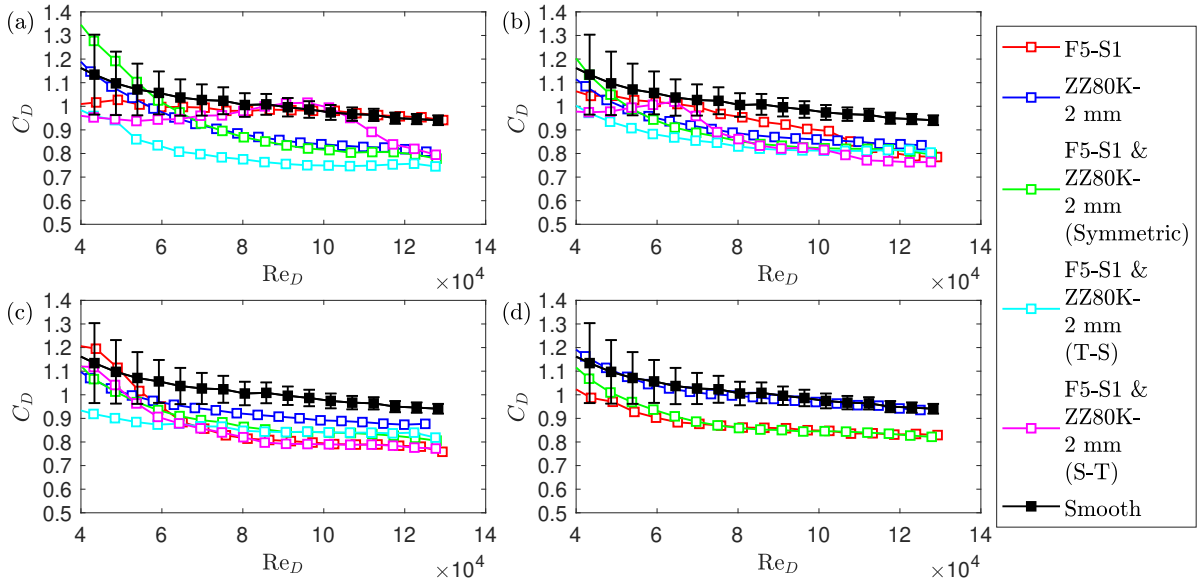


Figure 4.48: Variation of drag coefficient with Reynolds number for fabric 5 with one seam, a 2 mm thick zigzag tripwire with $\lambda_{Re_D=80k}$ and a combination where both are symmetrically placed at (a) $\theta = 30^o$, (b) $\theta = 40^o$, (c) $\theta = 50^o$ and (d) $\theta = 60^o$ from the stagnation point.

At $\theta = 40^o$, fabric 5 with the 2 mm thick zigzag tripwire attached in symmetric and T-S orientations have a similar flow behaviour at Reynolds numbers greater than 8.0×10^4 in Figure 4.48(b). Fabric 5 with the 2 mm thick ZZ80K tripwire attached in a S-T orientation

has the lowest drag coefficient with an average value of 0.78 past a Reynolds number of 1.0×10^5 compared to other cases placed 40^o from the stagnation point.

At $\theta = 50^o$, fabric 5 with the 2 mm thick zigzag tripwire placed in symmetric and T-S orientations also have a similar flow behaviour past a Reynolds number of 8.0×10^4 as shown in Figure 4.48(c). At $\theta = 50^o$, fabric 5 with one seam attached with a tripwire in a S-T orientation has a similar flow behaviour to using only fabric 5 with one seam in achieving the lowest drag compared to other cases regardless of the tripwire having a 2D or zigzag geometry from Figures 4.45(c) and 4.48(c). At $\theta = 50^o$ and 60^o, the 2 mm thick ZZ80K tripwire has large drag coefficients with values close to the smooth cylinder as shown in Figures 4.48(c) and 4.48(d). However, fabric 5 with one seam and a 2 mm thick ZZ80K tripwire arranged in a symmetric orientation share a similar flow behaviour to fabric 5 with one seam placed alone at an angle of 60^o from the stagnation point. Moreover, the symmetric orientation is found to be more effective than only using a 2 mm thick zigzag tripwire at angles larger than 30^o from the stagnation point.

Fabric 5 with one seam is more effective than placing only a 2D or zigzag tripwire with a thickness of 2 mm and $\lambda_{Re_D=80k}$ on a cylinder at angles of 50^o and larger from the stagnation point. Fabric 5 with a 2 mm thick zigzag tripwire having $\lambda_{Re_D=80k}$ arranged in a symmetric orientation has effectively decreased the drag coefficient at large angles of 50^o and 60^o from the stagnation point compared to having the fabric attached with a 2 mm thick 2D tripwire in the same orientation as shown in Figures 4.45(c), 4.45(d), 4.48(c) and 4.48(d).

At $\theta = 30^o$, attaching a 2D or zigzag tripwire with a thickness of 2 mm and $\lambda_{Re_D=80k}$ on fabric 5 has the lowest average drag coefficient of approximately 0.76 in a T-S orientation at Reynolds numbers greater than 8.0×10^4 as shown in Figures 4.45(a) and 4.48(a). At $\theta = 50^o$ in Figure 4.45(c), drag reduction is least effective when only a 2D tripwire, fabric and tripwire that are arranged in symmetric and T-S orientations are used because all drag

coefficient values are close to the flow behaviour of a smooth cylinder. On the other hand, drag reduction is effective in the Reynolds number range experienced by the upper arm region of a cyclist past 8.0×10^4 at large angles of 40^o and 50^o from the stagnation point when attaching a 2 mm thick tripwire with either 2D or zigzag geometry having $\lambda_{Re_D=80k}$ on fabric 5 in a S-T orientation.

4.5.2.2 Single Tripwire on Roughest Fabric

The roughest fabric, fabric 3 is attached with a 1 mm thick ZZ60K tripwire in three different orientations found in Figure 4.42. It is compared with other cases such as placing only a fabric and a tripwire separately on a cylinder at angles of 30^o to 60^o from the stagnation point. Fabric 3 with a 1 mm thick ZZ60K tripwire attached in a T-S orientation has the lowest drag coefficient of approximately 0.60 to 0.63 at all angles at a critical Reynolds number of approximately 1.3×10^5 in Figures 4.49(d) and 4.50. Overall, it has a lower drag than other cases at higher Reynolds numbers past 1.0×10^5 for angles ranging from 30^o to 50^o from the stagnation point. It is also shown to be effective for a large range of Reynolds numbers that occur from 6.0×10^4 to 1.30×10^5 when placed 60^o from the stagnation point. The roughest fabric (fabric 3) and smoothest fabric (fabric 7) with one seam that is placed symmetrically with a 1 mm thick ZZ60K tripwire relative to the stagnation point has a similar flow behavior to using the same tripwire alone on a cylinder at angles ranging from 30^o to 60^o from the stagnation point regardless of fabric roughness.

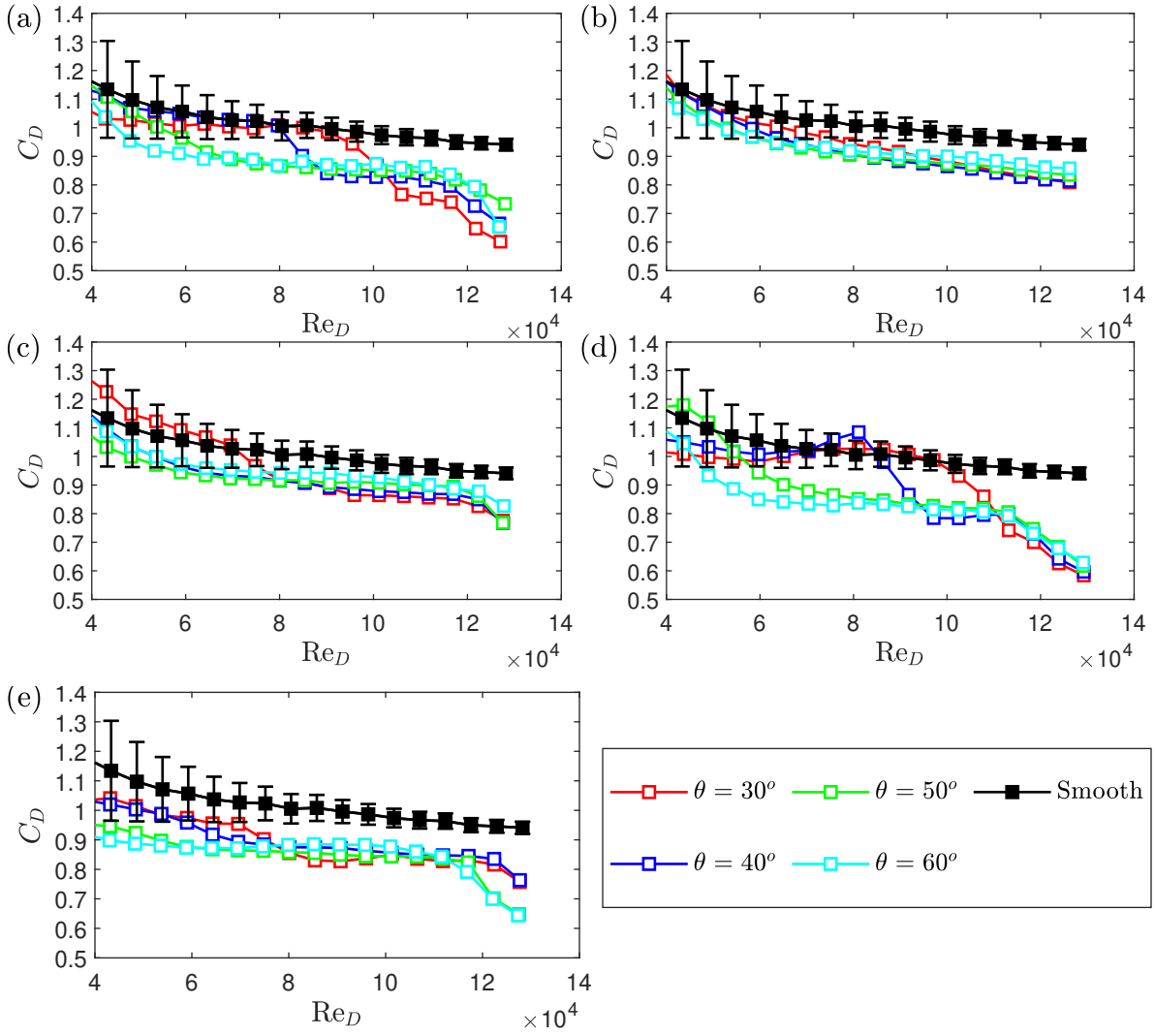


Figure 4.49: Variation of drag coefficient with Reynolds number at angles of 30^o to 60^o from the stagnation point for (a) fabric 3 with one seam, (b) 1 mm thick zigzag tripwire with $\lambda_{Re_D=60k}$, (c) fabric 3 with one seam and 1 mm thick zigzag tripwire with $\lambda_{Re_D=60k}$ arranged in a symmetric orientation, (d) fabric 3 with one seam that is 180^o apart from the 1 mm thick zigzag tripwire with $\lambda_{Re_D=60k}$ where the tripwire is facing the incoming flow direction first (T-S) and (e) fabric 3 with one seam that is 180^o apart from the 1 mm thick zigzag tripwire with $\lambda_{Re_D=60k}$ where the seam is facing the incoming flow direction first (S-T).

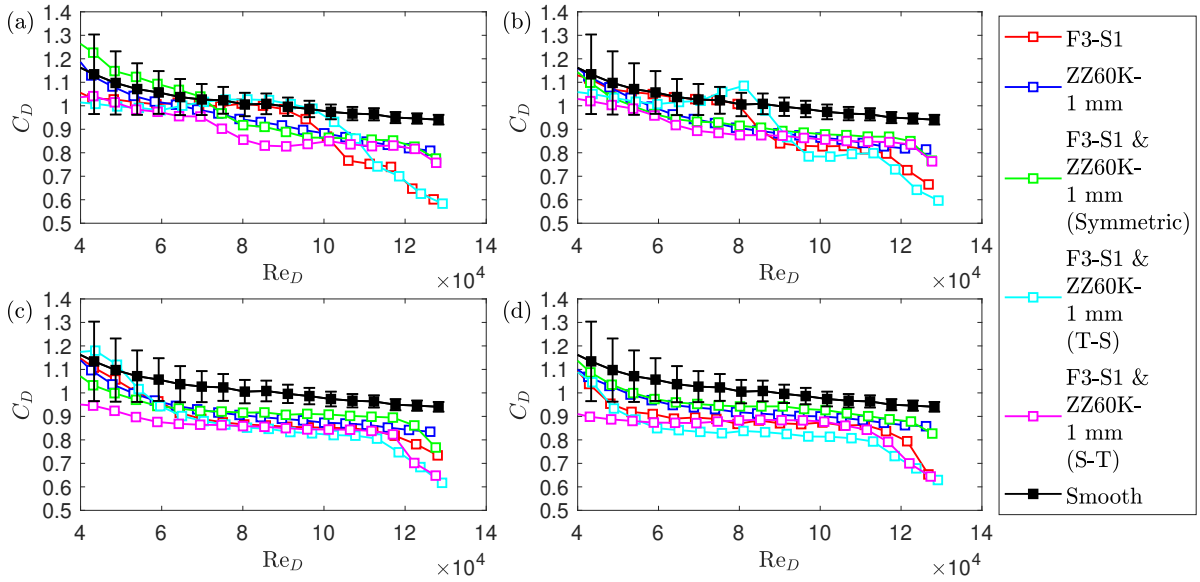


Figure 4.50: Variation of drag coefficient with Reynolds number for fabric 3 with one seam, a 1 mm thick zigzag tripwire with $\lambda_{Re_D=60k}$ and a combination where both are placed symmetrically at angles of (a) $\theta = 30^o$, (b) $\theta = 40^o$, (c) $\theta = 50^o$ and (d) $\theta = 60^o$ from the stagnation point.

4.5.3 Comparison of Fabrics and Tripwires Arranged in a Symmetric Orientation

In Figure 4.51, the drag coefficient is plotted as a function of Reynolds numbers when fabrics 3, 5 and 7 is attached with their respective tripwires in a symmetric orientation at angles of 30^o to 60^o from the stagnation point. It is observed that fabric 5 with a 2 mm thick ZZ80K tripwire has the lowest drag compared to fabrics 3 and 7 arranged in a symmetric orientation with other tripwires for a large range of Reynolds numbers when placed 40^o to 60^o from the stagnation point. Tables 4.5 to 4.8 shows the average drag coefficient values for a range of Reynolds numbers for fabrics 3, 5 and 7 with the respective tripwires attached in a symmetric orientation. In Tables 4.5 to 4.8 and Figure 4.51, fabrics 3 and 7 attached with the 1 mm thick zigzag tripwire in a symmetric orientation have a similar flow behaviour when placed at angles of 40^o to 60^o from the stagnation point for the entire range of Reynolds numbers from 4.0×10^4 to 1.30×10^5. Fabric 5 with the 2 mm thick 2D tripwire arranged in a symmetric

orientation is the least effective in reducing drag at an angle of 60^o from the stagnation point. Fabric 3 with the 1 mm thick ZZ60K tripwire arranged in a symmetric orientation has the lowest drag coefficient of 0.77 at a critical Reynolds number of approximately 1.3×10^5 when placed at angles of 40^o and 50^o from the stagnation point. The largest variation in the average drag coefficients for all cases in a symmetric orientation occurs at an angle of 60^o from the stagnation point compared to other angles past $Re_D = 6.0 \times 10^4$.

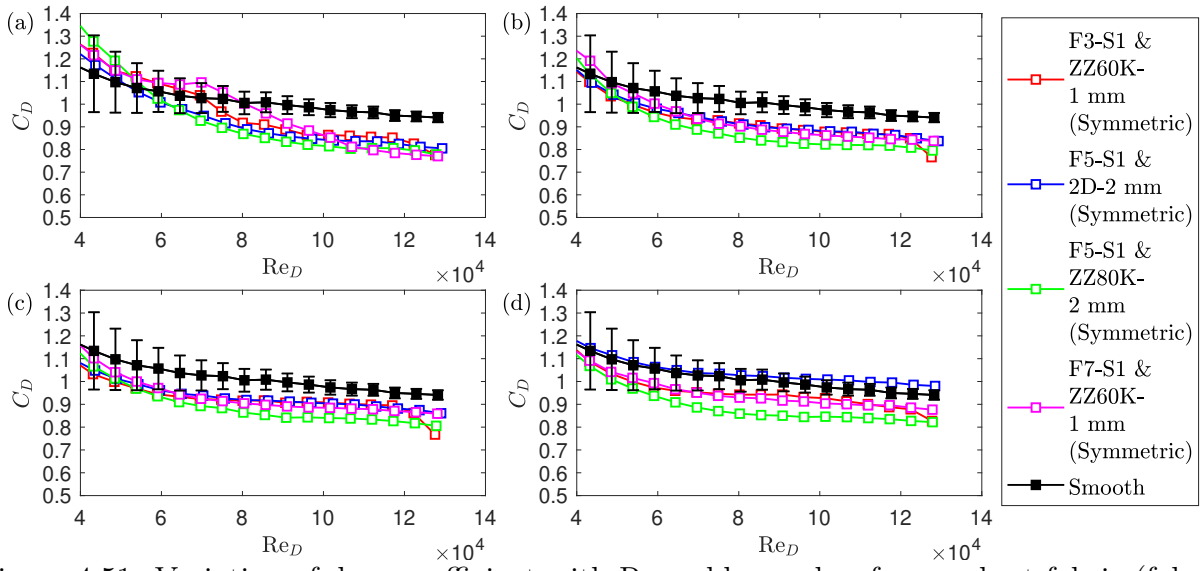


Figure 4.51: Variation of drag coefficient with Reynolds number for roughest fabric (fabric 3), smoothest fabric (fabric 7) and fabric with medium roughness (fabric 5) with tripwires arranged in a symmetric orientation at angles of (a) $\theta = 30^o$, (b) $\theta = 40^o$, (c) $\theta = 50^o$ and (d) $\theta = 60^o$ from the stagnation point.

Table 4.5: Average C_D values for smoothest fabric (fabric 7), roughest fabric (fabric 3) and fabric with medium roughness (fabric 5) with tripwires arranged in a symmetric orientation at a range of Reynolds numbers when placed 30^o from the stagnation point.

Type	$4.0 \times 10^4 < Re_D < 6.0 \times 10^4$ (6 - 10 m/s)	$6.0 \times 10^4 < Re_D < 8.0 \times 10^4$ (10 - 13 m/s)	$8.0 \times 10^4 < Re_D < 1.0 \times 10^5$ (13 - 15 m/s)	$Re_D > 1.0 \times 10^5$ (15 - 20 m/s)
F3-S1 & ZZ60K-1 mm	1.15	1.03	0.90	0.84
F5-S1 & 2D-2 mm	1.09	0.95	0.87	0.83
F5-S1 & ZZ80K-2 mm	1.15	0.93	0.84	0.80
F7-S1 & ZZ60K-1 mm	1.14	1.08	0.94	0.80

Table 4.6: Average C_D values for smoothest fabric (fabric 7), roughest fabric (fabric 3) and fabric with medium roughness (fabric 5) with tripwires arranged in a symmetric orientation at a range of Reynolds numbers when placed 40^o from the stagnation point.

Type	$4.0 \times 10^4 < Re_D < 6.0 \times 10^4$ (6 - 10 m/s)	$6.0 \times 10^4 < Re_D < 8.0 \times 10^4$ (10 - 13 m/s)	$8.0 \times 10^4 < Re_D < 1.0 \times 10^5$ (13 - 15 m/s)	$Re_D > 1.0 \times 10^5$ (15 - 20 m/s)
F3-S1 & ZZ60K-1 mm	1.02	0.93	0.90	0.85
F5-S1 & 2D-2 mm	1.03	0.94	0.90	0.86
F5-S1 & ZZ80K-2 mm	1.03	0.89	0.84	0.81
F7-S1 & ZZ60K-1 mm	1.08	0.94	0.88	0.85

Table 4.7: Average C_D values for smoothest fabric (fabric 7), roughest fabric (fabric 3) and fabric with medium roughness (fabric 5) with tripwires arranged in a symmetric orientation at a range of Reynolds numbers when placed 50^o from the stagnation point.

Type	$4.0 \times 10^4 < Re_D < 6.0 \times 10^4$ (6 - 10 m/s)	$6.0 \times 10^4 < Re_D < 8.0 \times 10^4$ (10 - 13 m/s)	$8.0 \times 10^4 < Re_D < 1.0 \times 10^5$ (13 - 15 m/s)	$Re_D > 1.0 \times 10^5$ (15 - 20 m/s)
F3-S1 & ZZ60K-1 mm	0.99	0.93	0.91	0.87
F5-S1 & 2D-2 mm	1.00	0.94	0.91	0.89
F5-S1 & ZZ80K-2 mm	1.00	0.90	0.85	0.83
F7-S1 & ZZ60K-1 mm	1.03	0.93	0.89	0.87

Table 4.8: Average C_D values for smoothest fabric (fabric 7), roughest fabric (fabric 3) and fabric with medium roughness (fabric 5) with tripwires arranged in a symmetric orientation at a range of Reynolds numbers when placed 60^o from the stagnation point.

Type	$4.0 \times 10^4 < Re_D < 6.0 \times 10^4$ (6 - 10 m/s)	$6.0 \times 10^4 < Re_D < 8.0 \times 10^4$ (10 - 13 m/s)	$8.0 \times 10^4 < Re_D < 1.0 \times 10^5$ (13 - 15 m/s)	$Re_D > 1.0 \times 10^5$ (15 - 20 m/s)
F3-S1 & ZZ60K-1 mm	1.02	0.95	0.94	0.89
F5-S1 & 2D-2 mm	1.10	1.04	1.02	1.00
F5-S1 & ZZ80K-2 mm	1.00	0.89	0.85	0.84
F7-S1 & ZZ60K-1 mm	1.04	0.95	0.92	0.89

Furthermore, varying the angular locations of fabric seams and tripwires from the stagnation point can effectively decrease the drag at Reynolds numbers experienced by the upper arm region of a cyclist. Drastic drag reduction mainly occurs for fabrics with three seams that are placed 60^o from the stagnation point. The drag reduction for a single tripwire placed at a critical angle from the stagnation point on a cylinder is similar to the literature with a minimum drag coefficient value of approximately 0.80 at high Reynolds numbers [45]. The influence of tripwires with a large thickness of 2 mm decreases the drag coefficient effectively at critical angles ranging from 30^o to 40^o from the stagnation point and permanently separate at larger angles. The separation of the reattached boundary layer is delayed at large angles up to 70^o from the stagnation point for smaller tripwires with a thickness of 0.5 mm. The overall relationship between the thickness and the critical angular location of the tripwire placed along the cylinder is in close agreement with previous literature findings [22, 32].

The results also provide an insight of how attaching a tripwire with the same thickness as a seam of the fabric in a symmetric orientation has a similar flow behaviour as attaching only a tripwire with 1 mm thickness regardless of the fabric roughness. The combination of fabrics and tripwires has a similar flow behaviour at specific angles compared to attaching only fabrics or tripwires onto a cylinder. Fabric 5 with an intermediate roughness attached with a 2 mm thick 2D tripwire in a symmetric orientation would reduce drag at a low critical angle of 30^o and have high drag at larger angles of 50^o and 60^o from the stagnation point similar to attaching the same tripwire alone on a cylinder. Moreover, attaching a 2D tripwire on a fabric with intermediate roughness that is thicker than the seam in a symmetric orientation would have similar flow attachment and separation patterns as placing the same tripwire alone on a cylinder for all angles. However, attaching a zigzag tripwire on a fabric with intermediate roughness would have different flow patterns than placing a zigzag tripwire alone at locations larger than the critical angle of the respective tripwire. For instance, a 2 mm thick zigzag tripwire placed alone on a cylinder has the same flow behaviour as fabric 5 with the same tripwire attached in a symmetric orientation when placed 30^o from the stagnation point. At

50^o and 60^o from the stagnation point, the drag coefficient values for a 2 mm thick zigzag tripwire placed alone on a cylinder increases, indicating a permanent boundary layer separation. However, fabric 5 with a 2 mm thick zigzag tripwire that is arranged in a symmetric orientation has maintained a lower drag coefficient at angles greater than 40^o from the stagnation point compared to placing only a 2 mm thick zigzag tripwire on the cylinder. This shows how a fabric with intermediate roughness attached with a tripwire that is thicker than the seam in a symmetric orientation has the same flow behaviour as the corresponding tripwire being placed alone on a cylinder at the same critical angle of a tripwire regardless of having a 2D or zigzag geometry. At locations larger than the critical angle of the zigzag tripwire attached, the fabric with the zigzag tripwire that is thicker than the seam is no longer under the influence of the respective tripwire but begins to share a similar flow behaviour as wrapping the cylinder with only a fabric of the same roughness that has a single seam. Furthermore, fabrics with an intermediate roughness attached with a zigzag tripwire that is thicker than the seam would have lower drag at locations larger than the critical angle of the same tripwire.

Fabric 5 with a 2 mm thick zigzag tripwire with $\lambda_{Re_D=80k}$ arranged in a symmetric orientation has the lowest drag compared to other fabric and tripwire combinations with the same orientation at angles of 30^o to 60^o from the stagnation point. An S-T orientation is the most effective at larger angles of 40^o and 50^o from the stagnation point for fabric 5 with a 2 mm thick tripwire that has 2D or zigzag geometry in producing an average drag coefficient value of 0.80 at Reynolds numbers greater than 8.0×10^4. Fabric 3 with a 1 mm thick zigzag tripwire with $\lambda_{Re_D=60k}$ in a S-T orientation is generally effective at angles of 30^o to 60^o in reducing the drag coefficient at Reynolds numbers ranging from 6.0×10^4 to 1.0×10^5. Fabric 3 with a zigzag tripwire arranged in a T-S orientation is effective for Reynolds numbers greater than 8.0×10^4 at large angles of 50^o and 60^o from the stagnation point. Moreover, these fabric and tripwire combinations can reduce drag by approximately 20% relative to a smooth cylinder at Reynolds numbers experienced by the upper arm region of a cyclist.

4.6 Potential Time Gains for Cyclists

Reducing the drag of a cyclist can help provide potential time gains with the same power input. The total drag area, C_DA of the cyclist and bicycle is 0.211 m^2 in a time trial position [3]. The most significant drag reductions occur along the upper arms and lower legs of a cyclist [8]. In a time trial position, the drag areas of the upper arms and lower legs contribute to 13% and 22% of the drag area of the cyclist, 0.134 m^2 [3, 47]. In 2022, female cyclist, Ellen van Dijk, and male cyclist, Filippo Ganna, had a record of cycling at average speeds of 13.68 and 15.78 m/s within an hour [48]. The records can be improved further by applying drag reductions up to 50% for the upper arms, lower legs and combined for each of the cyclists to increase potential time gains as shown in Figure 4.52. The potential time gains were calculated by assuming that the cyclists have the same drag force and power before and after drag reduction [49, 50]. It was observed from Figure 4.52 that the greatest potential time gains occur when drag reductions were applied on the upper arms and lower legs of both cyclists due to having a large increase in speed.

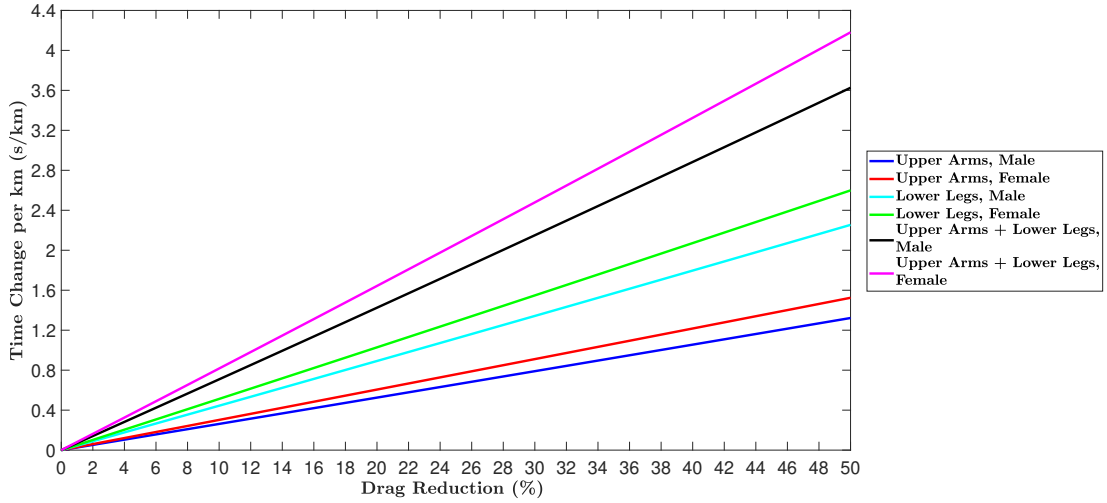


Figure 4.52: Variation of potential time gains when drag reduction is applied up to 50% for the upper arms and lower legs of cyclists with an hourly record in 2022.

Chapter 5

Conclusions and Future Work

The research objective of making design recommendations for skinsuits were implemented by attaching a tripwire onto fabrics with smooth, medium and high levels of roughness. The drag performance was compared to having only a fabric and tripwire placed separately on a cylinder at various angles from the stagnation point. Optimal cases of fabric and tripwire combinations were determined based on their flow behaviour in reducing drag at the Reynolds numbers experienced by the upper arm region of a cyclist. The hypothesis of the research has been met from the experimental campaign in proving that seams found in fabrics behave as tripwires when exposed to the oncoming flow of the wind. They both have an effect on the aerodynamic drag since it changes the flow regimes locally based on its' size and position relative to the incoming flow direction [6].

5.1 Benchmarking Experimental Setup

The current experimental setup that consists of a cylindrical model connected to two parallel mounted load cells was validated from previous literature in having similar drag coefficient values to a cylinder in subcritical flow. Strouhal number measurements were also conducted to assess the wake patterns when fabric seams and tripwires are placed on a cylinder.

5.2 Effects of Fabric Roughness and Seams

Fabric 3 with a highest roughness can decrease the drag coefficient at smaller critical Reynolds numbers while fabric 7 with the lowest roughness can decrease the drag coefficient at larger critical Reynolds numbers when the seam was placed 180^o from the stagnation point. Fabrics with three seams yielded a drastic drag reduction compared to having one, two and four seams when placed at an angle of 60^o from the stagnation point. Fabrics with four seams were able to decrease the drag coefficient values effectively near the Reynolds number range of the upper arm region of a cyclist from 6.0×10^4 to 1.0×10^5 at angles varying from 30^o to 45^o from the stagnation point. Moreover, adding more seams to a fabric allows the drag crisis to occur at a smaller critical Reynolds number.

5.3 Effects of 2D and Zigzag Tripwires

When a tripwire was placed at a critical angle from the stagnation point of a cylinder, a turbulent reattached boundary layer formed with a delayed final separation. The Strouhal number increased to a maximum value to indicate that there is maximum extension of the mean recirculation bubble length. When the tripwire was placed at an angular position past the critical angle, the Strouhal number decreased sharply to a minimum value. A separation bubble formed at the front of the tripwire but the flow behind it would be unable to reattach. This occurred from having a large spacing between the shear layers and vortices in the longitudinal direction. The vortex convection velocity decreased which subsequently led to a lower base pressure and a higher drag coefficient. Furthermore, boundary layer separation occurs when a tripwire is placed at an undesired angle such as placing thick tripwires at large angles and thinner tripwires at small angles from the stagnation point. It was also observed

that zigzag tripwires with varying spatial wavelengths and a nominal thickness of 1 mm was effective in decreasing the drag coefficient at high Reynolds numbers while a 2D tripwire with the same thickness increased the drag coefficient values greater than a smooth cylinder when placed 70^o from the stagnation point.

5.4 Effect of Single Tripwire on a Fabric

Fabrics with tripwires were attached to compare its effect on drag reduction compared to placing only fabrics and tripwires alone on a cylinder. It was observed that fabrics attached with tripwires that have the same thickness as a seam generally have a similar flow behaviour at all angles ranging from 30^o to 60^o from the stagnation point. Attaching a 2D tripwire onto a fabric with intermediate roughness that is thicker than a seam in a symmetric orientation experienced the same flow behaviour as attaching the same tripwire alone on a cylinder at all angles. For instance, fabric 5 with a 2 mm thick 2D tripwire that was arranged symmetrically from a 1 mm thick seam relative to the stagnation point had the same flow behaviour as having a 2D tripwire placed alone on a cylinder at angles ranging from 30^o to 60^o from the stagnation point. A fabric with an intermediate roughness that has a seam arranged in a symmetric orientation from a 2 mm thick 2D tripwire when placed on a cylinder would reduce drag at a low angle of 30^o and experience flow separation at angles larger than 40^o from the stagnation point similar to placing a 2 mm thick 2D tripwire alone on a cylinder. On the other hand, attaching a zigzag tripwire onto a fabric with intermediate roughness that is thicker than the seam experienced a different flow behaviour when placed beyond the critical angle of a tripwire. For example, fabric 5 with a seam that is arranged symmetrically from the zigzag tripwire with a thickness of 2 mm had the same flow behaviour at the critical angle of a tripwire of 30^o from the stagnation point. When placed at angles greater than 40^o, the boundary layer of the tripwire alone would permanently separate from the surface of the cylinder. However, the fabric with a seam that is arranged symmetrically from the 2

mm thick zigzag tripwire would begin to share a similar flow behaviour as wrapping only a fabric onto the cylinder at angles greater than 40^o from the stagnation point where they both experience drag reduction at high Reynolds numbers. Moreover, the use of tripwires and positioning of fabric seams are useful recommendations to consider for designing skinsuits because it can help provide potential time gains for cyclists.

5.5 Recommendations for Future Work

The pressure is high for body parts that act as stagnation points for the flow of a cyclist such as shoulders to arms and thighs to the feet because they are perpendicular to the oncoming flow of the wind. This causes the flow to collide and stop moving, leading to a larger pressure [51]. That is why it is recommended to place fabrics and tripwires on the upper arm and lower leg regions of a mannequin in a cycling position for future wind tunnel testing. The critical flow condition where the drag reduction occurs can be achieved on all limbs of a cyclist if rougher fabrics are used on the upper arms and lower legs while using smoother fabrics for the upper legs [8]. Decreasing the critical velocity of the upper arm using passive control methods such as surface roughness and trips are partly balanced by the increase in drag of the upper leg due to having a lower velocity deficit approaching it. A passive grid can also be installed upstream of the wind tunnel to help explore the wind gustiness effects that are commonly experienced by a cyclist in crosswind conditions.

Bibliography

[1] Fabio Malizia and Bert Blocken. Bicycle aerodynamics: History, state-of-the-art and future perspectives. *Journal of Wind Engineering and Industrial Aerodynamics*, 200:104134, 2020.

[2] Timothy N Crouch, David Burton, Zach A LaBry, and Kim B Blair. Riding against the wind: a review of competition cycling aerodynamics. *Sports Engineering*, 20(2):81–110, 2017.

[3] Thijs Defraeye, Bert Blocken, Erwin Koninckx, Peter Hespel, and Jan Carmeliet. Aerodynamic study of different cyclist positions: Cfd analysis and full-scale wind-tunnel tests. *Journal of Biomechanics*, 43(7):1262–1268, 2010.

[4] Wouter Terra, Andrea Sciacchitano, and Fulvio Scarano. A novel approach for skin suit aerodynamic optimization using local momentum deficit. *Multidisciplinary Digital Publishing Institute Proceedings*, 2(6):222, 2018.

[5] Arne Kilvik Skeide, Lars Morten Bardal, Luca Oggiano, and R Jason Hearst. The significant impact of ribs and small-scale roughness on cylinder drag crisis. *Journal of Wind Engineering and Industrial Aerodynamics*, 202:104192, 2020.

[6] Harun Chowdhury. Aerodynamic design of sports garments. *Applied Aerodynamics*, pages 21–41, 2012.

[7] Wei Jiang, Shijie Sun, Jun Qiu, Guoqiang Ma, Ding Weng, Mohan Hou, Lefan Guo, Jie Zhang, and Lifang Liu. Quantification of fabric morphology and prediction of drag crisis based on the fractal dimension. *Textile Research Journal*, page 00405175221118830, 2022.

[8] W Terra, A Sciacchitano, and F Scarano. Cyclist reynolds number effects and drag crisis distribution. *Journal of Wind Engineering and Industrial Aerodynamics*, 200:104143, 2020.

[9] Fabio Malizia and Bert Blocken. Cyclist aerodynamics through time: Better, faster, stronger. *Journal of Wind Engineering and Industrial Aerodynamics*, 214:104673, 2021.

[10] Lars Morten Bardal, Luca Oggiano, Olga Troynikov, and Inna Konopov. Influence of fabric structural attributes on their aerodynamic behavior. *Journal of Engineered Fibers and Fabrics*, 8(3):155892501300800314, 2013.

[11] Charles HK Williamson. Vortex dynamics in the cylinder wake. *Annual Review of Fluid Mechanics*, 28(1):477–539, 1996.

[12] XY Hsu, JJ Miau, JH Tsai, ZX Tsai, YH Lai, YS Ciou, PT Shen, PC Chuang, and CM Wu. The aerodynamic roughness of textile materials. *The Journal of the Textile Institute*, 110(5):771–779, 2019.

[13] Len Brownlie. Aerodynamic drag reduction in winter sports: the quest for "free speed". *Proceedings of the Institution of Mechanical Engineers, Part P: Journal of Sports Engineering and Technology*, 235(4):365–404, 2021.

[14] Jorgen Fredsoe and B Mutlu Sumer. *Hydrodynamics around cylindrical structures (revised edition)*, volume 26. Singapore: World Scientific, 2006.

[15] WM Chakroun, AA Abdel Rahman, and MMA Quadri. The effect of surface roughness on flow around a circular cylinder. *Wind Engineering*, pages 1–12, 1997.

[16] C Demartino and F Ricciardelli. Aerodynamics of nominally circular cylinders: A review of experimental results for civil engineering applications. *Engineering Structures*, 137:76–114, 2017.

[17] PW Bearman and JK Harvey. Control of circular cylinder flow by the use of dimples. *AIAA Journal*, 31(10):1753–1756, 1993.

[18] Elmar Achenbach. Influence of surface roughness on the cross-flow around a circular cylinder. *Journal of Fluid Mechanics*, 46(2):321–335, 1971.

[19] A Fage. The effects of turbulence and surface roughness on the drag of a circular cylinder. *Rep, Memo.*, 1283:1, 1929.

[20] Chuntai Zheng, Peng Zhou, Siyang Zhong, Xin Zhang, Xun Huang, and Raymond Chi-Hung So. An experimental investigation of drag and noise reduction from a circular cylinder using longitudinal grooves. *Physics of Fluids*, 33(11):115110, 2021.

[21] JJ Miau, HW Tsai, YJ Lin, JK Tu, CH Fang, and MC Chen. Experiment on smooth, circular cylinders in cross-flow in the critical reynolds number regime. *Experiments in Fluids*, 51(4):949–967, 2011.

[22] Tiago B Araújo, Christophe Sicot, Jacques Borée, and Robert J Martinuzzi. Influence of obstacle aspect ratio on tripped cylinder wakes. *International Journal of Heat and Fluid Flow*, 35:109–118, 2012.

[23] Suresh Behara and Sanjay Mittal. Transition of the boundary layer on a circular cylinder in the presence of a trip. *Journal of Fluids and Structures*, 27(5-6):702–715, 2011.

[24] Nando Timmer and Leo Veldhuis. The impact of skinsuit zigzag tape turbulators on speed skating performance. *Applied Sciences*, 11(3):988, 2021.

[25] Antrix Joshi and Alis Ekmekci. Correlation between single-wire and multi-wire tripping of the flow past a circular cylinder. *Fluid Dynamics Research*, 51(5):055506, 2019.

[26] Alis Ekmekci. Circular cylinders fitted with small-scale straight and helical wires: A comparative study on the wire-induced critical effects. *Experimental Thermal and Fluid Science*, 53:179–189, 2014.

[27] FS Hover, H Tvedt, and MS Triantafyllou. Vortex-induced vibrations of a cylinder with tripping wires. *Journal of Fluid Mechanics*, 448:175–195, 2001.

[28] Md Mahbub Alam, Y Zhou, JM Zhao, O Flamand, and O Boujard. Classification of the tripped cylinder wake and bi-stable phenomenon. *International Journal of Heat and Fluid Flow*, 31(4):545–560, 2010.

[29] Tamotsu Igarashi. Effect of tripping wires on the flow around a circular cylinder normal to an airstream. *Bulletin of JSME*, 29(255):2917–2924, 1986.

[30] M Pelacci, AG Robins, and S Szyniszewski. Drag reduction of a circular cylinder through the use of an architectured lattice material. *arXiv preprint arXiv:2102.08938*, 2021.

[31] Jose Luis Villafranca Nebres. *Wake similarity and vortex formation for two-dimensional bluff bodies*. University of Notre Dame, 1992.

[32] Tayfun Besim Aydin. *Controlling the near-wake of a circular cylinder with a single, large-scale tripwire*. University of Toronto (Canada), 2014.

[33] K Rengasamy and Alakesh Ch Mandal. Experiments on effective tripping device in a zero pressure gradient turbulent boundary layer. In *Journal of Physics: Conference Series*, volume 822, page 012016. IOP Publishing, 2017.

[34] Ryan Merrick and Girma Bitsuamlak. Control of flow around a circular cylinder by the use of surface roughness: A computational and experimental approach. In *4th International Conference Advances on Wind and Structures (A WAS08)*, 2008.

[35] Haecheon Choi, Woo-Pyung Jeon, and Jinsung Kim. Control of flow over a bluff body. *Annu. Rev. Fluid Mech.*, 40:113–139, 2008.

[36] JH Gerrard. The mechanics of the formation region of vortices behind bluff bodies. *Journal of Fluid Mechanics*, 25(2):401–413, 1966.

[37] Christoffer Norberg. Effects of reynolds number and a low-intensity freestream turbulence on the flow around a circular cylinder. *Chalmers University, Goteborg, Sweden, Technological Publications*, 87(2):1–55, 1987.

[38] RACM Slangen. Experimental investigation of artificial boundary layer transition: A comparison of different tripping devices. *M.S. Thesis, Delft Univ. of Technology, Delft, Netherlands*, 2009.

[39] M Kerkvliet. Numerical study of boundary layer transition behind a zigzag trip. *M.S. Thesis, Delft Univ. of Technology, Delft, Netherlands*, 2011.

[40] Michael Bishop and Serhiy Yarusevych. Mitigating blockage effects on flow over a circular cylinder in an adaptive-wall wind tunnel. *Journal of Fluids Engineering*, 133(8), 2011.

[41] GS West and CJ Apelt. The effects of tunnel blockage and aspect ratio on the mean flow past a circular cylinder with reynolds numbers between 104 and 105. *Journal of Fluid Mechanics*, 114:361–377, 1982.

[42] Sara Asghari Mooneghi, Siamak Saharkhiz, and S Mohammad Hosseini Varkiani. Surface roughness evaluation of textile fabrics: a literature review. *Journal of Engineered Fibers and Fabrics*, 9(2):155892501400900201, 2014.

[43] K Kleissl and CT Georgakis. Comparison of the aerodynamics of bridge cables with helical fillets and a pattern-indented surface. *Journal of Wind Engineering and Industrial Aerodynamics*, 104:166–175, 2012.

[44] Kevin Cooper. Bluff-body blockage corrections in closed-and open-test-section wind tunnels. *AGARD, AG-336, NTIS, Springfield, VA*, 6, 1998.

[45] David F James and Quan-Si Truong. Wind load on cylinder with spanwise protrusion. *Journal of the Engineering Mechanics Division*, 98(6):1573–1589, 1972.

[46] J Nebres and S Batill. Flow about a circular cylinder with a single large-scale surface perturbation. *Experiments in Fluids*, 15(6):369–379, 1993.

[47] Thijs Defraeye, Bert Blocken, Erwin Koninckx, Peter Hespel, and Jan Carmeliet. Computational fluid dynamics analysis of drag and convective heat transfer of individual body segments for different cyclist positions. *Journal of Biomechanics*, 44(9):1695–1701, 2011.

[48] Joseph Delves. What is the cycling hour record? `https://www.cyclist.co.uk/in-depth/cycling-hour-record`, 2022. Accessed: 2023-03-10.

[49] Bert Blocken, Thijs van Druenen, Yasin Toparlar, and Thomas Andrianne. Cfd analysis of an exceptional cyclist sprint position. *Sports Engineering*, 22:1–11, 2019.

[50] Bert Blocken, Stefanie Gillmeier, Fabio Malizia, and Thijs van Druenen. Impact of a motorcycle on cyclist aerodynamic drag in parallel and staggered arrangements. *Sports Engineering*, 24:1–11, 2021.

[51] Sungchan Hong and Takeshi Asai. Aerodynamics of cycling skinsuits focused on the surface shape of the arms. *Applied Sciences*, 11(5):2200, 2021.

Chapter 6

Appendix

6.1 Uncertainty Analysis of Drag Coefficient

Bias errors occur from pressure transducers when the value of the output signal does not correspond to the measured pressure. A hysteresis is a measurement error that occurs for load cells from the residual effects of previously applied loads. Offset compensation is the correction of errors that change the zero point of the readings of a load cell.

The average of 5 ramps were taken to obtain a single continuous curve that shows the variation of the drag coefficient with respect to Reynolds numbers. The squared difference was taken between each velocity value for an individual ramp and the corresponding mean velocity from the averaged curve. This was conducted for all the data points for each respective ramp. The standard deviation for velocity, δU of a smooth cylinder was obtained by dividing the sum of the squared differences between the individual velocities, U_i of each ramp and the corresponding mean velocity, U_M, i by 5 ramps and taking the square root as shown in Equation 6.1. The standard deviation of the drag coefficient of the smooth cylinder of each individual data point from the ramp was obtained from Equation 6.2. Equation 6.2 was simplified because there were negligible differences in the density measured and the frontal area of the cylinder was constant. The standard deviation of the

drag force that is measured from two SI-32-2.5 load cells was approximately 0.34 N for a full scale reading. The standard error of the mean, SEM was found in equation 6.3 by dividing the standard deviation of the drag coefficient, δC_D by the square root of the total number of ramps, N, performed. The error bar is twice the value of the standard error of the mean.

$$\delta U = \sqrt{\frac{\sum (U_i - U_M, i)^2}{N}} \tag{6.1}$$

$$\frac{\delta C_D}{C_D} = \sqrt{(\frac{\delta F_D}{F_D})^2 + (2\frac{\delta U}{U})^2} \tag{6.2}$$

$$SEM = \frac{\delta C_D}{\sqrt{N}} \tag{6.3}$$

The bias errors were more predominant in the force measurements of load cells with a standard deviation of $\delta F_D = 0.34$ N compared to pressure transducers with an average standard deviation of $\delta U_M = 0.017$ m/s. A larger drag force found at higher velocities decreased the standard deviation of the drag coefficient. This caused the error bars to decrease and approach closer to the averaged C_D value of a smooth cylinder as Reynolds numbers increase.